Cedre

Information Day 2016 Proceedings

Remote Detection & Maritime Pollution

Table of contents

Frédéric Périé,
President of Cedre's Strategy Committee

"Oil production at sea is one of the major uses of the ocean. To meet the technical challenges of this industry, it is our duty to preserve what is one of humanity's key resources. Total, as a leading light in responsible energy, examines and tests the latest advances geared towards minimising the impact of its activities on the natural environment.

To maintain sufficient safety levels so as to prevent accidental releases, to determine the response actions to be rapidly implemented in the event of an incident and to more fully understand the behaviour of oil at sea, Total depends on the research teams liable to support the scientific and technical developments identified so as to preserve the ocean and its ecosystems.

In order to maintain its remote sensing capabilities, Total deploys a research programme which encompasses recent developments and promotes exchanges between the different players in the field.

True to its commitment towards meeting the environmental challenges and preserving the environment wherever the Group operates, Total implements anticipatory measures and environmental protection actions against oil pollution. This commitment is illustrated by the support it provides to the activities conducted by Cedre, with which the Group enjoys close collaboration.

Cedre's portfolio of activities clearly positions it at the crossroads of the needs expressed by the different stakeholders and of the proposed solutions promoted by research players.

The Cedre Information Days are the chance to share, discuss and challenge these approaches in order to pinpoint progress opportunities or even new research projects. Naturally, as an industrial player, Total both benefits from and greatly contributes to these debates."

Stéphanie Cubier,
Head of the Marine Environment Office at the French Directorate of Water and Biodiversity Ministry of the Environment, Energy and the Sea

"The challenges related to the protection and preservation of marine ecosystems ranks among the priorities of the French Ministry for the Ecological and Inclusive Transition. Over the past years, our involvement has led, on a national level, to the development of the French law on reclaiming biodiversity which comprises several initiatives for the protection of the marine environment (recognition of the notion of ecological damage, creation of fishery conservation areas, requirement for ships travelling through the Pelagos and Agoa sanctuaries to be fitted with cetacean collision avoidance systems, supervision of the ballast water management of ships entering French waters, etc.).

On an international level, this involvement led to ocean protection being selected as a theme for the debates held during COP 21 in Paris in 2015 and its inclusion in the Paris Agreement.

The ministry's commitment towards preserving the quality of our oceans is also illustrated through the support provided to Cedre ever since its creation in 1979. This support is both financial and technical, in particular through regular, active participation in its different actions, as illustrated by this Information Day, which underscores Cedre's position at the interface between science and the operational aspects inherent to spill response at sea."

Stéphane Doll,
Director of Cedre

"Why choose the issue of remote sensing for this Information Day? Such systems have been frequently used by Cedre, in particular during the Prestige oil spill in 2002. Over and above operational aspects, it is also extremely useful for detecting deliberate discharge. In this context, strictly speaking Cedre does not conduct remote sensing, but rather works as a partner, in particular alongside the French Navy. We are involved in equipment trials and tests, as well as in analysing POLREPs and we have been organising aerial observation and remote sensing training courses for over twenty years. We also provide advice to the French and foreign authorities in charge of directing operations or of post-response legal aspects. The aim of this Information Day is to offer as broad a vision as possible of remote sensing in the field of marine spills."


1

Session 1

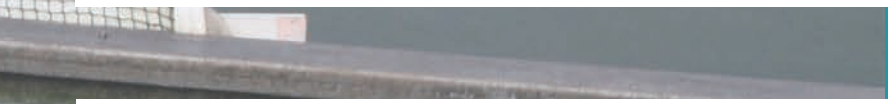

Remote sensing means

POLLUPROOF Project: PROOF improvement of HNS maritime POLLution by airborne radar and optical facilities - Experimental approach

S. Chataing[a], S. Angelliaume[b], P-Y. Foucher[c], E. Puckrin[d], S. Le Floch[a]

a) Cedre, Brest, France.

b) ONERA, Salon de Provence, France.

c) ONERA, Toulouse, France.

d) DRDC, Valcartier Research Centre, Canada.

Abstract

In case of maritime pollution by HNS (Hazardous and Noxious Substances), specific methods of identification and characterization are needed. The project POLLUPROOF (start January 2014 – End mid-2017) aims to test and validate the use of optical sensing methods, including hyperspectral and radar sensors, to detect, locate and classify 6 HNS. In this paper, the experimental approach followed during the project is detailed: the calibration of the optical sensors in meso-scale experiments and the validation of the optical and radar sensors in a realistic experiment at sea. The promising results obtained are specifically explained in other papers.

1- Introduction

Maritime shipping activities are responsible for about 20% of the pollution at sea. The pollutants discharged accidentally or deliberately can endanger the biodiversity and eco-balance of our oceans. Exhaust emissions and cargo mishaps associated with an increase in vessel traffic are sources of pollution which impact the marine environment (acidification, contamination of flora and fauna) and land (acid rain). This issue has become a priority at the national (Grenelle de la Mer) and regional (European - directives 2005/35 and 2005/33) levels as demonstrated by the implementation of several international conventions (e.g., OPRC-HNS Protocol (OPRC, 2000), MARPOL (MARPOL, 1973 completed in 1978)). Obviously the removal or drastic reduction of pollution resulting from maritime activities is a desirable objective. The magnitude of the problem is highlighted by the quantity of goods transported by sea: of an estimated 8,000 million tonnes (Mt) of chemicals transported worldwide, 350 Mt are transported via European waterways. It is estimated that there are more than 100 incidents per year involving the illegal discharge of noxious liquid substances in these waters. For over 25 years, French Customs (DGDDI) have deployed aircraft equipped with remote sensing instruments (radar and scanner IR/UV), to successfully prosecute ships involved in oil spill incidents. The effectiveness of this policy has been demonstrated through a significant reduction in oil pollution in the waters under French jurisdiction (during the period between 2006 and 2012, the number of ships caught polluting was reduced by three-fold).

This paper presents the POLLUPROOF project through its objectives and the experimental approach used to achieve them. Results from the experimental parts are beyond the scope of this paper and will be part of other presentations.

2 - POLLUPROOF project

2.1 - Objectives

The POLLUPROOF (PROOF improvement of HNS maritime POLLution by airborne radar and optical facilities) project would enhance the capabilities of French Customs to detect, locate and classify pollutants (other than hydrocarbons) originating from ship emissions (including particulates) in order to collect evidence for the prosecution of offenders while ensuring an effective intervention in the case of accidental discharge at sea.

The project is funded by ANR ECO-TECH 2013 and the members of the consortium have a recognized and complementary expertise in the field of aerial detection and marine pollution: ONERA, DGDDI, Cedre, CEPPOL, Agenium, AVDEF and DRDC. In addition to the consortium, Transport Canada (TC) acts as end-user and member of the steering committee. The project started in January 2014 and will end mid-2017.

The objectives of this project are:

1. Verify the capability to detect, locate and classify at least 3 of the 6 most noxious liquid substances transported by sea in Europe;
2. Achieve a reduction of spilled noxious liquid substances equivalent to the level for hydrocarbon emissions;
3. Develop a stronger policy to control the release of noxious gases within the sulfide emission control areas (SECA).

These objectives will be achieved by:

- Deployment of radar (SAR/SLAR) and optical sensing (hyperspectral cameras) capabilities for detecting liquid pollutants at sea;
- Evaluating the complementarity of optical and radar information;
- Identification of gaseous discharges of engine emissions and liquid pollutants using hyperspectral analysis.

To accomplish these activities, the POLLUPROOF project will analyze the needs of the French Customs regarding aerial detection and will proceed with:

- Calibration of optical measurements on liquid pollutants in mesoscale (test-tank) experiments located at Cedre;
- Airborne measurements of sea spills using hyperspectral optical and radar sensors, following the test-tank analysis;
- Algorithm development for detection, location and classification of pollutants. The consortium will then produce a data gathering evidence methodology. French Customs staff will evaluate the effectiveness and applicability of these advances using a human-machine interface.

2.2 - Hazardous and noxious substances

Six chemical substances have been chosen to evaluate the capability of remote sensing sensors: rapeseed oil, fatty acid methyl ester (FAME), toluene, heptane, xylene and methanol. These chemicals are among the most transported substances by maritime freight in Europe. Methanol and liquid chemicals represent 46% of the 165 million tonnes annually transported by chemical carriers while vegetable oil accounts for 29% (Olafsen, 2009). Some of these chemicals are classified as the most noxious substances in the IBC Code (IMO website), which provides an international standard for the safe carriage by sea of HNS in bulk. Those chemicals have already been involved in accidents at sea, e.g. Poona sank in 1971 with 600 T of rapeseed oil, Grape One sank in 1993 with 3000 T of xylene, Cape Horn carrying a cargo of 14,000 T of methanol was seriously damaged by an explosion in the port of Livorno in 2003 (Cedre, 2015), (Cunha et al., 2015). Rapeseed oil and FAME are part of the vegetable oil family; toluene, heptane and xylene are part of petrochemical products; methanol is part of the family of alcohols and derivatives. Their main properties are described below:

Rapeseed Oil: Rapeseed or colza oil is a vegetable oil obtained from crushed colza seeds. At ambient pressure and temperature, rapeseed oil is a viscous liquid with a specific gravity of 0.910. Rapeseed oil is insoluble in water and does not evaporate (vapor pressure below 0.01 kPa at 25 °C), these characteristics classify rapeseed oil as a floater F in the SEBC.

FAME: Fatty acid methyl esters are biofuel directly added to conventional fuels such as diesel. At ambient pressure and temperature, they are a liquid with a specific gravity of 0.888. This product is virtually insoluble in water (solubility of 0.023 mg.L-1 at 20 °C) and has relatively low evaporative potential (vapor pressure of 0.42 kPa at 25 °C) making it a floater F in the SEBC.

Toluene: Toluene, also named methylbenzene or phenylmethane, is an aromatic hydrocarbon that is commonly used as a chemical reagent or solvent, particularly in the industrial sector. Toluene is a liquid at ambient pressure and temperature and has a specific gravity of 0.867. Toluene is nearly insoluble in water (535 mg.L-1 at 25 °C) and tends to evaporate relatively easily (vapor pressure of 2.91 kPa at 20 °C). Considering the SEBC classification, toluene is a floating and evaporating FE substance.

Heptane: Heptane is the generic term to identify one of the 9 isomers of C7H16 and is a saturated hydrocarbon of the linear alkane family. This is a constituent of fuel and is used as an extraction solvent, a synthesis intermediate in the chemical industry and as solvent for glues, inks, rubbers and plastics. At ambient pressure and temperature, heptane is a volatile liquid (6 to 7.7 kPa at 20 °C) and nearly insoluble in water (< 2 mg.L-1 at 20 °C). With a specific gravity of 0.710, heptane is lighter than water and floats. According to the SEBC classification, heptane is considered as an evaporator E.

Xylene: Xylene or dimethylbenzene is a group of aromatic hydrocarbons with one methyl derivative on benzene. It is naturally present in oil and is observed in (diesel) engine exhaust gases, either as a residual oil chemical or formed during incomplete combustion. Xylene is also produced from oil in the petrochemical industry and is one

of the 30 most produced chemicals in the USA. It is used in the printing, rubber and leather industries mainly as a solvent. Xylene is an inflammable liquid with a pleasant fragrance. Chemical properties are similar from one isomer to another. Its specific gravity of 0.87 makes it float on water. Xylene is slightly soluble in water (solubility below 20 mg.L-1 at 20 °C) and is not likely to evaporate (vapor pressure of 0.89 kPa at 20 °C). Due to these characteristics, xylene is considered as an FE (floater and evaporator) in the SEBC classification.

Methanol: Methyl alcohol or methanol is the simplest alcohol of chemical formula CH3OH. At ambient temperature this polar liquid is used as antifreeze (for coolant for example), solvent or fuel (in aeromodelling for example). Methanol is not present in large amounts in nature and is industrially produced. Methanol is mainly used as basic material for chemical synthesis of more complex chemical products. Nearly 40 % of methanol is converted in formaldehyde to be then transformed in plastics, synthetic resins, paints, explosives or fabrics. Methanol is a light liquid (specific gravity of 0.791), volatile (vapor pressure of 12.3 kPa at 20 °C), miscible in water, inflammable and toxic with a characteristic odor. These properties enable the classification of methanol as DE, dissolving and evaporating substance.

3 - Experimental approach

The experimental approach is divided into two parts: first, the calibration of optical sensors on liquid pollutants in mesoscale experiments; second, airborne measurements of sea spills using hyperspectral optical and radar sensors.

3.1 - Calibration of optical sensors

The calibration of optical measurements on liquid pollutants has been realized in mesoscale (test-tank) experiments located at Cedre (Brest) in October 2014.

Three configurations have been tested, each one having specific objectives:

- Vertical configuration: comparison between clean water and water covered by a chemical;
- Horizontal configuration: detection of the gas cloud produced by the evaporation of the chemical;
- Tank: evaluation of the influence of the thickness of the slick.

o Vertical configuration

8 different HNS (benzene, toluene, xylene, diethyl ether (DEE), rapeseed oil, propanol, methanol, and heptane) were released into seawater inside a floating aluminum frame that was installed in the Cedre pool as presented in Figure 1. For each product, different spill volumes were used from 60mL up to 5L, and the sea water was thoroughly cleaned after each spill.

Figure 1: a) Aluminum frame installed in the Cedre pool. b) Aerial lift with the three hyperspectral cameras

Three different hyperspectral imaging systems from 0.4 to 12µm were used during this campaign: two reflective sensors (NEO HySpex cameras) from 0.4 to 1µm (VNIR) and from 1 to 2.5µm (SWIR), and a thermal longwave (LWIR) sensor from 8 to 12µm (Telops Hypercam). Hyperspectral imaging cameras were deployed inside an aerial lift at a height of 12m above the pool with a nadir looking geometry and a Bomem MR300 spectroradiometer was placed next to the edge of the pool. The three sensors were pointed towards the expected center of the slick.

The aim was to evaluate how hyperspectral sensors can contribute to the detection of pollutants in a nadir looking geometry.

o Horizontal configuration

The sensors used for this configuration were: two reflective sensors (NEO HySpex cameras) from 0.4 to 1µm (VNIR) and from 1 to 2.5µm (SWIR), an ASD Fieldspec camera from 0.4 to 2.5µm, a thermal longwave (LWIR) sensor from 8 to 12µm (Telops Hypercam), a Bomem MR300 spectroradiometer and a P-iCATSI (Polarized Improved Compact ATmospheric Sounding Interferometer).

Heptane, toluene, xylene, methanol, rapeseed oil, diethyl ether, silicone oil, unleaded gasoline and oil were released (volumes from 2 to 10L). Diethyl ether and methanol were discharged directly in the basin whereas the other products were released inside the floating aluminum frame.

Except for the interferometer, which was placed in an aerial lift several meters away from the basin, all the sensors were placed next to the edge of the pool.

o Tank

The aim of this test was to qualify the impact of the thickness of the slick on the measured spectra. For this configuration, the Bomem MR300 spectroradiometer and the ASD Fieldspec camera were used. Heptane, xylene and rapeseed oil were released at the surface of a black-painted metallic barrel full of seawater.

The cloud coverage during the trial didn't enable the realization of the initially planned measurements and supplementary measures must be realized in the ONERA laboratory.

3.2 - Evaluation of radar, optical and hyperspectral sensors at sea

o General presentation of the experiment

The experimentation took place in May 2015 over the French coast in the Mediterranean Sea at 2 locations: 42°46.8'N / 6°2.0'E for the first release and 42°45.5'N / 5°48.5'E for the second and third releases. One cubic meter of each of the six chemical products (presented in paragraph 2.b) was released at sea and imaged by radar and optical airborne sensors for their evaluation in real conditions.

HNS releases have been performed from the salvage, rescue and oil spill response vessel Ailette of the French Navy under the direction of CEPPOL (Centre of Practical Expertise in Pollution Response) and Cedre. Each chemical product was contained in a one cubic-meter tank, in HDPE (High Density PolyEthylene) for non-aggressive HNS (rapeseed oil, FAME, methanol) and in metal for reactive or corrosive HNS (xylene, heptane and toluene). Each tank was inserted in a metallic structure equipped with two 220L-floaters to ensure the floatability of the system and a lifting strap to manipulate the tanks with the on-board crane (Figure 2). The release of the HNS was performed from a dinghy by pulling a rope that activates the opening of the tank. Due to the difference of density between seawater and HNS, the chemicals spread at the sea surface.

In order to follow the drifts of the HNS slicks, two drifting buoys were implemented. Their GPS positions were transmitted by satellite every 15 minutes.

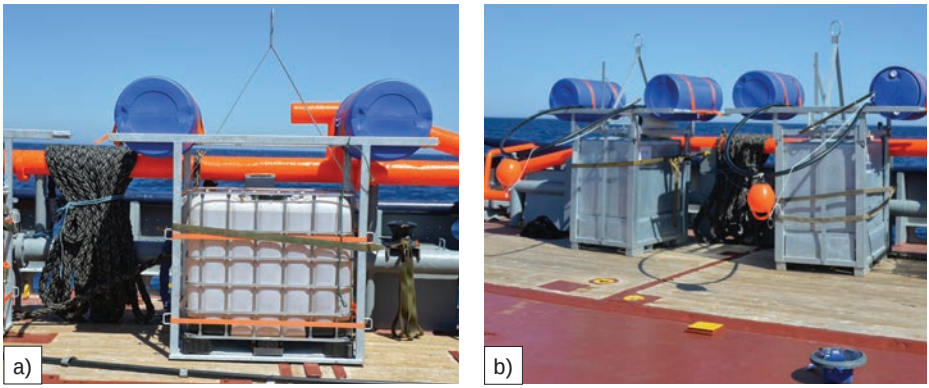

Figure 2: One cubic-meter tank a) HDPE b) Metal

Three aircraft imaged the HNS slicks:

- A Falcon 20 from AVdef company equipped with the experimental pod SETHI including the ONERA sensors: two radars (SAR) at X and L bands, full polarization (HH, HV, VH, VV), one SWIR hyperspectral camera (HYSPEX), one CamV2 camera (visible range);
- A Polmar aircraft from DGDDI equipped with IR sensor, UV sensor and SLAR radar at X-band;
- A Cessna C-303 chartered by DRDC equipped with an IR hyperspectral camera (TELOPS).

On board the Ailette two optical cameras were installed by DRDC: a MWIR hyperspectral camera and a Bomem MR304 LWIR and MWIR spectroradiometer.

In order to characterize the behavior of HNS once released at sea (evaporation, dissolution, emulsification…), sampling of the slicks, the water column and the atmosphere were planned.

o Experiment releases

HNS releases were planned to be performed two at a time, i.e. two HNS were nearly simultaneously released and imaged by the aircraft. The most dangerous HNS were first released (Heptane and Toluene), then Methanol and Xylene for the second release and finally FAME and rapeseed oil for the third release.

The methodology used to release HNS is ideally suited to good weather conditions and in particular for a sea state compatible with the lifting operations. The first release was performed as planned on the 18th of May thanks to good weather conditions. Then, a strong wind episode (19th to 21st May, force 8, 35 to 40 knots) forced us to re-plan the last two releases on the 22nd of May. Sea and weather conditions during experimentation are described in Table 1.

Date	Time (UTC)	Wind speed (m/s)	Wind direction (from-deg)	Wave height (m)	Wave direction (from-deg)
18 may 2015	17 : 00	8	255	0.5	240
22 may 2015	13 : 00	7	315	2	270
22 may 2015	16 : 00	7	315	1.75	270

Table 1: Environmental conditions

First release took place on the 18th of May, from 16:40 to 17:30 UTC. The sea was calm. Heptane and toluene were released from 2 semi-submersible 1 m^3 tanks at 16:30 and 16:35 UTC, respectively (Figure 3). Heptane and toluene were released at a fixed position (separated by about 100 m). No samplings were realized for this release due to the reactivity of these HNS. Two drifting buoys were deployed simultaneously with the releases.

The airborne sensors implemented for this release were:

- SETHI: radar (X + L quad-pol) and optical (SWIR) sensors
- DGDDI: SLAR and IR/UV.

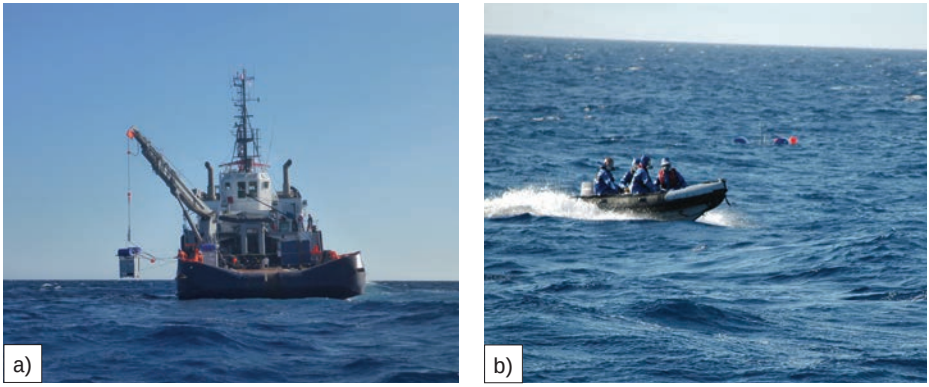

Figure 3: Releases of Heptane and Toluene

The positions of the two drifting buoys and the positions of the tanks at their opening and their recovery are given in Figure 4. Buoys and tank data show a WSW direction drift. Toluene and Heptane are highly volatile chemicals and their persistence at sea surface is limited (prediction of 30 minutes persistence with the software CHEMAP). However, drifting buoys are of interest during such experiments to get in situ information that enable one to readjust the prediction models.

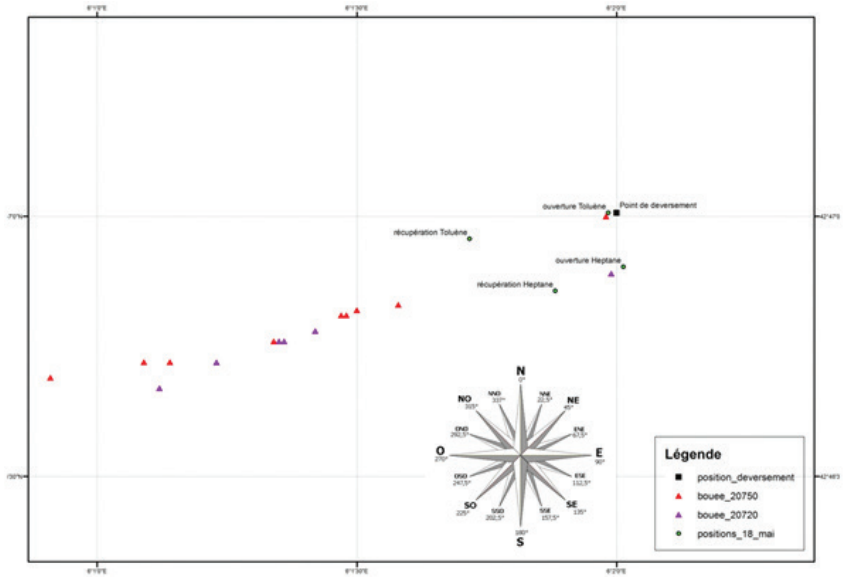

Figure 4: Tanks and drifting buoys positions map during the first release

Second release took place on the 22nd of May, from 13:25 to 13:55 UTC. There was a heavy swell, restricting any activity at sea; hence products were discharged directly from the back of the vessel (French Navy) advancing towards the east at a speed of 1 knot: methanol was released from 12:35 to 12:45 UTC and xylene from 12:55 to 13:25 UTC. The sea state made it impossible to use the dinghy, to deploy the drifting buoys and to sample the slick and water column.

The airborne sensors implemented for this release were:

- SETHI: radar (X + L quad-pol) and optical (SWIR) sensors
- DGDDI: SLAR and IR/UV
- DRDC: LWIR hyperspectral.

Third release took place on the 22nd of May, from 15:20 to 16:50 UTC. Because of the swell, products were also released directly from the back of the boat advancing towards the east at a speed of 1 knot: rapeseed oil was discharged from 15:00 to 15:30 UTC and FAME from 15:25 to 15:40 UTC (Figure 5). No samplings and no deployment of drifting buoys were possible due to the sea state.

The airborne sensors implemented for this release were:

- SETHI: radar (X + L quad-pol) and optical (SWIR) sensors
- DGDDI: SLAR and IR/UV
- DRDC: LWIR hyperspectral.

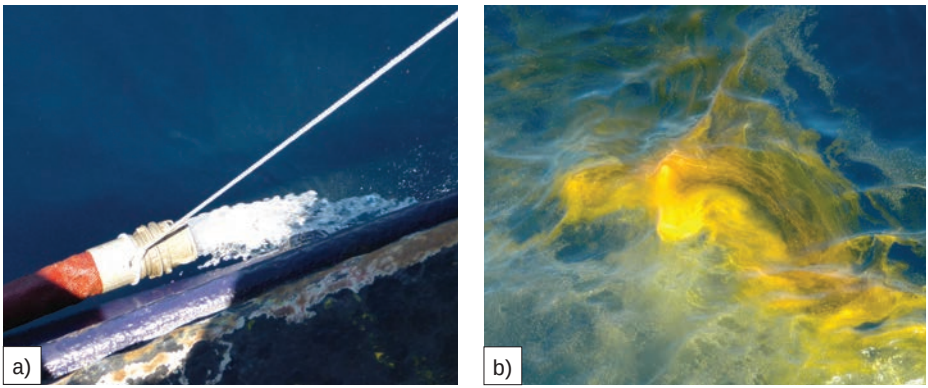

Figure 5: Releases from on board the Ailette (a) and rapeseed oil slick (b)

4 - Conclusions

The POLLUPROOF project aims to set-up a procedure for collecting evidence of illegal maritime pollution from noxious liquid substances using airborne sensors. To achieve this goal, an experimental approach divided into two parts has been realized. First, the optical sensors were calibrated in a mesoscale spill experiment. Then, optical and radar sensors were implemented in a realistic experiment at sea to image the slicks from noxious substances.

The optical and radar results obtained during these experiments are beyond the scope of this presentation and will be presented elsewhere. However, they are clearly promising and demonstrate how hyperspectral sensors are complementary to classic optical and radar sensors for the detection of chemicals at the sea surface.

Research presented in this paper is part of the POLLUPROOF research program (ANR-13-ECOT-007) funded by the French National Research Agency (ANR). Authors are very grateful to everyone involved in the experiment at sea (ONERA - Cedre - AVDEF - DGDDI - French Navy).

References

Cedre, 2015, Database for accidental spills of hydrocarbon and chemical products.

Cunha, I., S. Moreira, and M. M. Santos, 2015, Review on hazardous and noxious substances (HNS) involved in marine spill incidents-An online database: Journal of Hazardous Materials, v. 285, p. 509-516.

MARPOL, 1973 completed in 1978, International Convention for the Prevention of Pollution from Ships (MARPOL).

Olafsen, G., 2009, Chemical tanker trade: Chemical and Product Tanker Conference, Back to Fundamentals, 10 - 11 March 2009.

OPRC, 2000, OPRC-HNS Protocol: Protocol on preparedness, response and coordination to pollution incidents by hazardous and noxious substances.

Multifrequency radar imagery and characterization of hazardous and noxious substances at sea

S. Angelliaume[a], B. Minchew[b], S. Chataing[c], P. Martineau[a] and V. Miegebielle[d]

a) ONERA, France.

b) BAS, United Kingdom.

c) Cedre, France.

d) Total, France.

Abstract

The increase in maritime traffic, and particularly the transport of chemical products, necessitates enhancement of methods of prevention and intervention towards the spills of chemicals in the environment. Maritime pollution by chemical products occurs at much lower frequency than spills of oil, however the consequences of a chemical spill can be more wide-reaching than those of oil. While detection and characterization of hydrocarbons have been the subject of numerous studies, detection of other chemical products at sea using remote sensing has been little studied and is still an open subject of research. To address this knowledge gap, an experiment was conducted in May 2015 over the Mediterranean Sea during which controlled releases of hazardous and noxious substances were imaged by remote sensing systems. The aim of these experiments and subsequent analysis is to establish a procedure for collecting evidence of illegal maritime pollution by noxious liquid substances using airborne sensors.

In this paper we discuss the experimental procedure, which was carried out in collaboration with the French Navy and Customs, and report the main results from the airborne radar imaging campaign. We develop an accurate method for using multifrequency radar sensors to detect and quantify impact of chemical products at sea. We conclude by demonstrating the capability of radar imagery to distinguish two different substances within the same spill.

1 - Introduction

Airborne and spaceborne radar remote sensing is often used for oil slick detection over maritime surface (Brekke and Solberg, 2005; Girard-Ardhuin et al., 2005; Garcia-Pineda et al., 2009; Solberg 2012). In the oil and gas sector, oil slick detection using remote sensing is of great interest for exploration and environment program domains. In an operational context, oil slicks are usually detected using airborne and/or spaceborne synthetic aperture radar (SAR). Indeed, the oil layer on top of the sea surface damps the so-called “capillarity waves”, which are the origin of the sea surface roughness that significantly contributes to backscattered signal at high frequency (microwave domain). Once detected, the spill is characterized using optical imagery (Leifer et al., 2012).

Unlike hydrocarbons, there is limited research on the detectability of Hazardous and Noxious Substances (HNS) at sea using remote sensing. In that context, an experimental campaign of measurements (called POLLUPROOF) was conducted in May 2015 in

the Mediterranean Sea (off the French coast). Controlled release of six chemical and non-hydrocarbon oil products were carried out in collaboration with the French Navy and Customs. Polarimetric SAR (POLSAR) data were acquired at X- (9.75 GHz) and L-band (1.325 GHz) simultaneously by SETHI, the ONERA airborne SAR system (Bonin et al., 2009), over released products. Hyperspectral data (SWIR and LWIR) have also been acquired by ONERA and RDDC; French customs have also participated to the exercise at sea with their airborne surveillance system (X-band RAR, IR and UV imagery); but RAR (Real Aperture Radar) and optical remote sensing is beyond the scope of this paper.

The aim of this work is first to study the capability of high resolution multifrequency SAR imagery to detect HNS at sea and then to study the potential of radar imagery to quantify and characterize the spill: thickness or amount of product and distinction between different products.

This paper is organized as follows: Section 2 describes the experimental measurement campaign at sea; Section 3 presents the methodology for detecting and characterizing HNS; Section 4 presents some original results and demonstrates the relevance of radar imagery for monitoring non-hydrocarbon pollution over maritime surface.

2 - Experimentation at sea

2.1- Radar imagery

SETHI is the airborne remote sensing imaging system developed by ONERA, (Bonin et al., 2009). It integrates a new generation of radar and optronic payloads. It can operate over a wide range of frequency bands from UHF-VHF, to X-band including L-band with long range, very high resolution, polarimetric and interferometric capabilities. SETHI is a pod-based system operating onboard a Falcon 20 Dassault aircraft which is the property of the AvDEF company.

For the POLLUPROOF campaign, quad-pol SAR data have been acquired simultaneously at X- and Lband, with a resolution of 0.5 and 1.0 m, respectively. Images are generated with an azimuth resolution equal to the range resolution at both X- and L-band, which implies an integration time equal to 1.1 s at X-band and 4.1 s at L-band. Main characteristics of acquisition are summarized in Table 1.

Frequency	Bandwith	Polarization	Incidence angle	Swath
X	300 MHz (9.6-9.9 GHz)	Quad-pol (HH, HV, VH, VV)	45° (34-52°)	1500m (slant range)
L	150 MHz (1.25-1.4 GHz)	Quad-pol (HH, HV, VH, VV)	45° (34-52°)	1500m (slant range)

Table1: SETHI-Waveform

Incidence angle varies across the swath from 34° to 52°. Instrumental noise floor has been estimated using the method proposed in (Hajnsek et al., 2012) and the results

are shown Figure 1. The Noise Equivalent Sigma0 (NESZ) is very low, allowing sufficient Signal to Noise Ratio over the spill for efficient analysis.

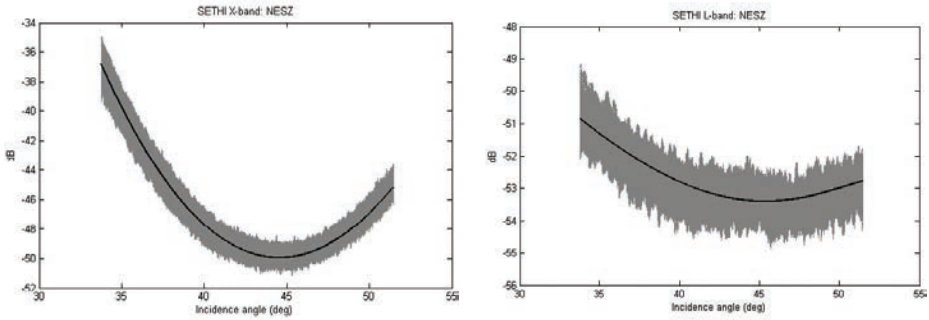

Figure 1: SETHI - Instrumental noise at X-band (left) and L-band (right)

2.2 - Chemical products

Six chemical substances have been chosen to evaluate the capability of remote sensing sensors. The choice was made to cover different chemical families and be as representative as possible of chemical products often transported by sea and classified as noxious substances. The chemical substances selected are the following:

- Category I : vegetal oil and fatty acid esters
  - o Rapeseed/colza oil
  - o Fatty Acid Methyl Esters (FAME)
- Category II : petrochemical products
  - o Toluene
  - o Heptane
  - o Xylene
- Category III : alcohols and derivatives
  - o Methanol

Toluene: Toluene, also named methylbenzene or phenylmethane is an aromatic hydrocarbon. This product is commonly used as chemical reagent or solvent, particularly in the industrial sector. Toluene is a colorless liquid at ambient pressure and temperature, with a specific gravity of 0.867 $g.cm^{-3}$. Toluene is nearly insoluble in water (0.535 $g.L^{-1}$ at 25 °C) and tends to evaporate relatively easily (vapor pressure of 2.91 kPa at 20 °C). Toluene vapors are 3.1 times heavier than air and are preferentially located next to the ground.

Heptane: Heptane is the generic term to identify one of the 9 isomers of C_7H_{16} and is a saturated hydrocarbon of the linear alkane family. This is a constituent of fuel and is used as extraction solvent, synthesis intermediate in chemical industry and as solvent for glues, inks, rubbers and plastics. At ambient pressure and temperature, heptane is a colorless liquid, volatile (6 to 7.7 kPa at 20 °C) and nearly insoluble in water

(< 2 $mg.L^{-1}$). With a specific gravity of 0.710 $g.cm^{-3}$, heptane is lighter than water and floats.

FAME: Fatty Acid Methyl Esters are biofuel directly added in conventional fuels such as diesel. At ambient pressure and temperature, they are a liquid with a specific gravity of 0.888$g.cm^{-3}$. This product is pretty much insoluble in water (solubility of 0.023$mg.L^{-1}$ at 20°C) and practically does not evaporate (vapor pressure of 0.42kPa at 25°C).

Methanol: Methyl alcohol or methanol is the simplest alcohol of chemical formula CH3OH. This is a colorless light liquid (specific gravity of 0.791 $g.cm^{-3}$), volatile (vapor pressure of 12.3 kPa at 20°C), miscible in water, inflammable and toxic with a characteristic odor. At ambient temperature, this polar liquid is used as antifreeze (for coolant for example), solvent or fuel (in aeromodelling for example). Methanol is not present in large amounts in nature and is industrially produced. Methanol is mainly used as basic material for chemical synthesis of more complex chemical products. Nearly 40% of methanol is converted in formaldehyde to be then transformed in plastics, synthetic resins, paints, explosives or fabrics.

Rapeseed Oil: Rapeseed or colza oil is a vegetal oil obtained from colza seeds crushing. This is the second most consumed food oil in France after sunflower oil. At ambient pressure and temperature, rapeseed oil is a viscous yellowish liquid with a specific gravity of 0.910 $g.cm^{-3}$. Rapeseed oil is insoluble in water and does not evaporate (vapor pressure below 0.01 kPa at 25 °C).

Xylene: Xylene or dimethylbenzene is a group of aromatic hydrocarbons with one methyl derivative on benzene. It is naturally present in oil, xylene is observed in (diesel) engine exhaust gases, either a residual oil chemical or formed during incomplete combustion. Xylene is also produced from oil in the petrochemical industry and is one of the 30 most produced chemicals in the USA. It is used in the printing industry, rubber and leather industries mainly as a solvent. Xylene is a colorless and very inflammable liquid with a pleasant fragrance. Chemical properties are similar from one isomer to another. Its specific gravity of 0.87 $g.cm^{-3}$ makes it float on water. Xylene is slightly soluble in water (solubility below 20 $mg.L^{-1}$) and is not likely to evaporate (vapor pressure of 0.89 kPa at 20 °C). Xylene vapors are heavier than air and tend to locate next to the ground.

These chemicals are part of the most transported substances by maritime transport in Europe and some of them are classified as the most noxious substances in the IBC Code (IMO). During the POLLUPROOF experiment, 1 m^3 of each of these six products was released at sea and imaged by airborne remote sensing sensors.

2.3 - Planning of measurements

Experimentation took place in May 2015. Three flights were performed, with two releases per flight:

- First flight took place on the 18th of May, from 16:40 to 17:30 UTC. The sea was calm. Heptane and toluene were released from 2 semi-submersible 1 m^3 tanks at 16:30 and 16:35 UTC, respectively (Figure 2). Heptane and toluene were released

at a fixed position (separated by about 100 m); SAR acquisitions began 10 min after the first release (heptane) and 5 min after the second release (toluene).

- Second flight took place on the 22nd of May, from 13:25 to 13:55 UTC. There was a heavy swell, restricting any activity at sea; hence products were released directly from the back of the boat (French Navy) advancing towards the east at a speed of 1 knot: methanol was released from 12:35 to 12:45 UTC and xylene from 12:55 to 13:25 UTC (Figure 3). SAR acquisitions began 40 min after the end of the first release (methanol) and at the end of the second release (xylene).
- Third flight took place on the 22nd of May, from 15:20 to 16:50 UTC. Because of the swell, products were also released directly from the back of the boat advancing towards the east at a speed of 1 knot: rapeseed oil was released from 15:00 to 15:30 UTC and FAME from 15:25 to 15:40 UTC (Figure 4). SAR acquisitions were synchronized with the release.

Sea and weather conditions during experimentation are described in Table 2 below.

Date	Time (UTC)	Wind (from)		Wave (from)	
		Speed (m/s)	Direction (deg)	Height (m)	Direction (deg)
18 May, 2015	17:00	8	255	0.5	240
22 May, 2015	13:00	7	315	2	270
22 May, 2015	16:00	7	315	1.75	270

Table 2: environmental conditions during experimentation at sea

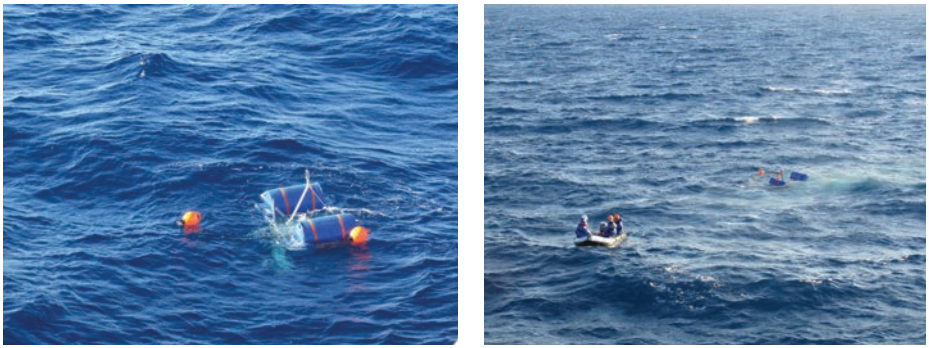

Figure 2 First flight: heptane and toluene release from semi-submersible tank

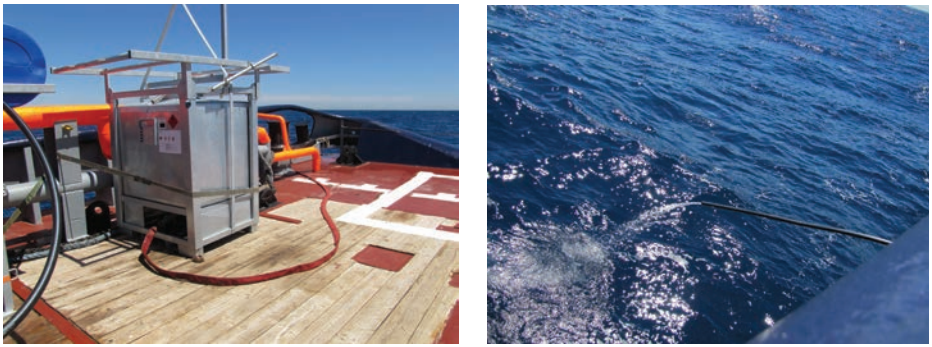

Figure 3 Second flight: methanol and xylene release from the boat

Figure 4 Third flight: rapeseed oil (left) and FAME (right) release from the boat

3 - Methodology

3.1 - Scattering from ocean surface

For the frequency bands mainly used in Earth Observation (X-, C- and L-band) and for incidence angles ranging from 30° to 60°, an ocean surface is a randomly rough surface where the radar backscatter is dominated by the Bragg scattering mechanism. As a consequence, the radar backscattered power, which is commonly defined by the normalized radar cross-section (NRCS), is greater in VV polarization than in HH and HV (e.g. Valenzuela, 1978). For each polarization, the NRCS is proportional to the spectral energy density of the sea surface waves with wavelength (λsea) that satisfies:

$$\lambda_{sea} = \frac{\lambda_{EM}}{2\sin(\theta_i)} \qquad (1)$$

where λ_{EM} and θ_i are the wavelength and the local incidence angle of the electromagnetic (EM) waves transmitted by the radar system, respectively. Ocean wavelengths corresponding to the Bragg wavelength are shown in Figure 5 for the three most common frequency bands (X-, C- and L-band). It is obvious that the carrier frequency has a crucial impact and using different data acquired at different frequencies over

the same area can provide additional information and improve our ability to characterize the imaged surface. While X- and C-band are relatively close, we can assume that the use of X- and L-band shall allow to obtain simultaneous information on different scales of the sea.

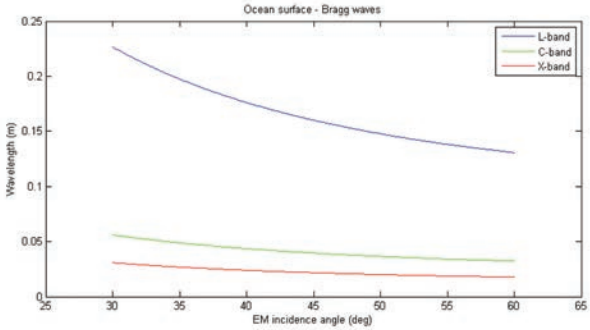

Figure 5: Ocean waves in resonance with the EM signal (Bragg mechanism)

Ocean surface is usually modeled as a composition of slightly rough tilted facets, each of which has superimposed small-scale surface roughness that creates a Bragg scatterer. Small-scale roughness is randomly distributed on the scattering surface and responds to the strength of local wind (i.e, gravitycapillarity waves). The tilt of the facet is caused by larger scale gravity waves on the ocean surface. The orientation of the facet normal in the radar reference frame is defined by two angles ψ and ξ. The resulting local incidence angle of the EM wave is:

$$\theta_i = \cos^{-1}[\cos(\theta + \psi)\cos\xi] \qquad (2)$$

where θ is the EM angle of incidence relative to local, un-tilted up.

Following this approach, the sea may be modeled as the superposition of two independent processes describing the small and large scale components. Two-Scales Model (TSM), based on a spectral description of the sea surface, has been proposed to formulate this composite-surface scattering (Elfouhaily et al., 1997; Soriano and Guérin, 2008). The NRCS is then given by (Valenzuela, 1978):

$$\sigma^0_{pp} = 4\pi\kappa^4_{EM}\cos^4\theta_I\Gamma_{pp}W \qquad (3)$$

where the subscript *p* denotes either H or V polarization, $k_{EM} = 2\pi/\lambda_{EM}$ is the EM wavenumber, *W* is the spectral density of the ocean surface roughness and Γ_{pp} is the reflectivity defined by:

$$\Gamma_{pp} = \left| \left(\frac{\sin(\theta+\psi)\cos\xi}{\sin\theta_i} \right)^2 \alpha_{pp} + \left(\frac{\sin\xi}{\sin\theta_i} \right)^2 \alpha_{qq} \right|^2 \qquad (4)$$

where the subscript q ($q \neq p$) denotes either H or V polarization. The reflectivity depends on the facet tilt, the EM wave incidence angle and the scattering coefficients such that (Valenzuela, 1978):

$$\alpha_{HH} = \frac{\cos\theta_i - \sqrt{\varepsilon - \sin^2\theta_i}}{\cos\theta_i + \sqrt{\varepsilon - \sin^2\theta_i}} \quad (5)$$

$$\alpha_{VV} = \frac{(\varepsilon - 1)(\sin^2\theta_i - \varepsilon(1 + \sin^2\theta_i))}{\left(\varepsilon\cos\theta_i + \sqrt{\varepsilon - \sin^2\theta_i}\right)^2} \quad (6)$$

The Bragg scattering coefficients only depend on the local incidence angle of the EM wave θ_i and the relative dielectric constant ε. Finally, for a given geometry of acquisition (fixed incidence angle) and assuming that the ocean surface is homogeneous over a sufficiently large area, the NRCS is only depending on the EM wavelength, the relative dielectric constant and the sea surface roughness.

In the case of an ocean surface covered by slicks, the product surface layer will dampen the capillarity waves, thereby attenuating the radar backscattered power by diminishing the surface roughness. The relative dielectric constant can also be modified in the case of a product which mixes with sea water. The resulting dielectric constant will be smaller than for pure sea water, because the relative dielectric constant of HNS is low compared to sea water (Minchew, 2012). The resulting NRCS will be lower for a product which mixes with water than for clean sea surface.

The starting point of this study is based on the assumption that in the case of a thin layer, only the short capillarity waves will be damped; when the layer gets thicker, longer capillarity waves will also be damped. These phenomena should be observable in the case of multifrequency SAR data acquired simultaneously over the same surface. Moreover, this should be enhanced when using EM wavelengths sufficiently apart (for instance X- and L-band radar frequencies) since the EM signal will simultaneously interact with hydrodynamic mechanisms of different scales (Figure 5).

3.2 - Detection and relative quantification

Many studies have suggested using polarimetric SAR (POLSAR) parameters to improve slicks detection capability (see review by Solberg, 2012). A comprehensive comparison of those parameters was undertaken by (Angelliaume et al., 2015). Following (Kudryatsev et al., 2013), (Angelliaume et al., 2015) quantitatively demonstrates the effectiveness of the Polarization Difference (PD=VV-HH in linear units) for slick detection on the ocean surface. The interest to use this parameter for a marine pollutant detection application is that PD is essentially proportional to the wave number spectrum taken at the Bragg frequency (Guérin et al., 2010). It is therefore very sensitive to small scale features of the ocean surface (damped by the slick) and quite insensitive to the larger scales, which rather drive the unpolarized contribution to the NRCS.

The main drawback of the Polarization Difference (PD) is that it is not normalized, making it difficult to define a threshold with which a detection map can be established. To overcome this limitation, we propose a normalized variant of PD. We note that PD ranges from a maximum value (PDmax) that occurs in the case of a clean sea surface and goes to 0 as the impact of the substance on the surface increases, since both VV and HH reflectivity tend to 0 over a perfectly smooth surface. Hence, we define the Normalized Polarization Difference (NPD) as:

$$NPD = \frac{PD_{max} - PD}{PD_{max}} \quad 0 \le NPD \le 1 \qquad (7)$$

NPD is equal to 0 in the case of a clean sea surface and goes to 1 as the impact of the substance on the ocean surface increases. PD_{max} is the polarization difference value in the case of a clean sea surface and can be estimated through a physical two-scale model (Soriano and Guérin, 2008; Angelliaume et al., 2014) or an empirical model (Gregers-Hansen and Mittal, 2012), using wind speed and wind direction information.

NPD can be interpreted as an indication of the presence and the impact of a substance on the ocean surface. It can be used directly or thresholded to produce a binary detection map.

3.3 - Oil/water mixing index

The basic premise of the oil/water mixing index (M_{dex}) is that radar backscattered power is diminished by oil slicks through mechanical damping of Bragg-wavelength capillary waves and reductions in the relative dielectric constant of the upper few centimeters near the sea surface (Minchew et al., 2012; Minchew, 2012). By decoupling the relative contribution to signal attenuation of surface waves mechanical damping and changes in dielectric constant, we can define the characteristics of the slick along a spectrum ranging from thin surface films to thicker emulsions. This information is critical for efficient cleanup operations.

In addition to the assumptions underlying the NRCS model, Eq.(3), the process of decoupling the mechanical and electromagnetic attenuation mechanisms requires us to assume that: (1) the longwavelength tilting of the sea surface [as described by angles ψ and ζ in Eq. (2)] is unaffected by the presence of an oil slick and (2) the dielectric constant of uncontaminated seawater is well-constrained. These assumptions allow for inferences of the long-wavelength tilting of the sea surface over the entire radar image (so long as the radar images ample areas of uncontaminated water), the dielectric constant of contaminated water, and the small-scale roughness spectrum of both contaminated and uncontaminated water. As described by (Minchew, 2012), the salient parts of the process of decoupling the mechanical and electromagnetic attenuation mechanisms can be summarized as follows:

1. Use the co-polarized ratio over uncontaminated seawater and an assumed value for the dielectric constant of pure seawater, ε_r^{water} , to infer the long-wavelength tilting of the ocean surface.

2. Calculate the short-wavelength roughness spectrum over uncontaminated water, W^{water}, by applying the tilt angles inferred in Step 1.

3. For each pixel of contaminated water, infer the local (effective) relative dielectric constant, ε_r^{oil}, from the co-polarized ratio and the inferred long-wavelength tilt angles deduced from Step 1.

4. Calculate the short-wavelength roughness spectrum over contaminated water, W^{oil}, using the dielectric constant inferred in Step 3 and the tilt angles obtained in Step 1.

M^{dex} values can then be calculated as follows:

$$M_{dex} = M_W - M_\alpha \quad (8)$$

$$M_W = \frac{W^{water} - W^{oil}}{W^{water}} \quad (9)$$

$$M_{dex} = \frac{|\alpha_{VV}^{water}|^2 - |\alpha_{VV}^{water}|^2}{|\alpha_{VV}^{water}|^2} \quad (10)$$

M_W is the *normalized damping factor* and M_α is the normalized power attenuation factor, both are ranging from 0 to 1. MW is a measure of how much the product will attenuate the sea surface roughness (0=no damping ; 1=total damping); M_α is a measure of how much the backscattered signal is attenuated due to a decrease of the relative dielectric constant (0=no attenuation ; 1=total attenuation).

M_{dex} is ranging from -1 to 1. Negative values indicate that the decreasing of the EM signal due to the presence of HNS on the ocean is more due to a decrease of the relative dielectric constant than to a decrease of the surface roughness; meaning that the product is mixed with the sea water. On the opposite, positive values indicate that the decreasing of the EM signal is mainly due to a smoothing of the ocean surface and thus we are in presence of a product that forms a film (more or less homogeneous) on the top of the sea surface. In an operational context, this information may be valuable to identify the behavior of the HNS and guide actions to achieve.

4 - Results and discussion

4.1 - Observation of Hazardous and Noxious Substances at sea

Heptane and Toluene: Both substances were never observed in SAR images, at X- and L-band; most likely because they are extremely volatile products, which do not impact the surface roughness. Remember that products (1 m^3 each) have been released only 5 and 10 minutes before acquisitions.

Methanol and Xylene: As methanol is an extremely volatile substance soluble in the water column and as SAR acquisition began 40 min after the end of the release, methanol was never observed in SAR images. On the other side, the impact of xylene is clearly observable on X- and L-band SAR imagery, without obvious influence of the

flight trajectory relative to the wind. Figure 6 shows illustrations of X-band VV polarization images acquired over xylene for upwind and crosswind observation. The size of the spill is about 1750 m x 200 m; the bright point just at the end of the spill is the ship (53 m length) from which releases were performed.

Rapeseed oil and FAME: FAME and rapeseed oil are two persistent substances; which are both clearly observable on SAR images acquired at X- and L-band during the 3rd flight. Figure 7 shows an illustration of VV polarized images acquired simultaneously at X- and L-band over the spill at 16:07 UTC. Rapeseed oil, having been released first, corresponds to the right part of the spill; FAME is on the left. From in situ information, we know that FAME is ranging from azimuth 4100 m to 5500 m, and that rapeseed oil is from azimuth 6000 m to 8500 m, and between we have a mixture of the two products. While it is not possible to visually distinguish the FAME and rapeseed oil, we observe a significant difference between L- and X-band acquisitions. Contrast between the spill and the clean sea surface is more significant at X-band than at L-band. Figure 8 shows an azimuth profile calculated by averaging from 3800 m to 3900 m in range (the spill is between azimuth 4800 to 5600 m and azimuth 6500 to 8200 m). While at X-band the spill seems homogeneous (Figure 7 top), at L-band (Figure 7 bottom) we observe strong variation of the EM signal into the spill with dark patches, due to a stronger impact of the HNS on the sea surface roughness at wavelengths corresponding to the L-band Bragg wavelength. This observation is particularly important: as previously demonstrated by (Wismann et al., 1998) or (Gade et al., 1998), it confirms that the EM signal backscattered by HNS is dependent on the wavelength and using different frequency bands should allow us to better characterize the spill.

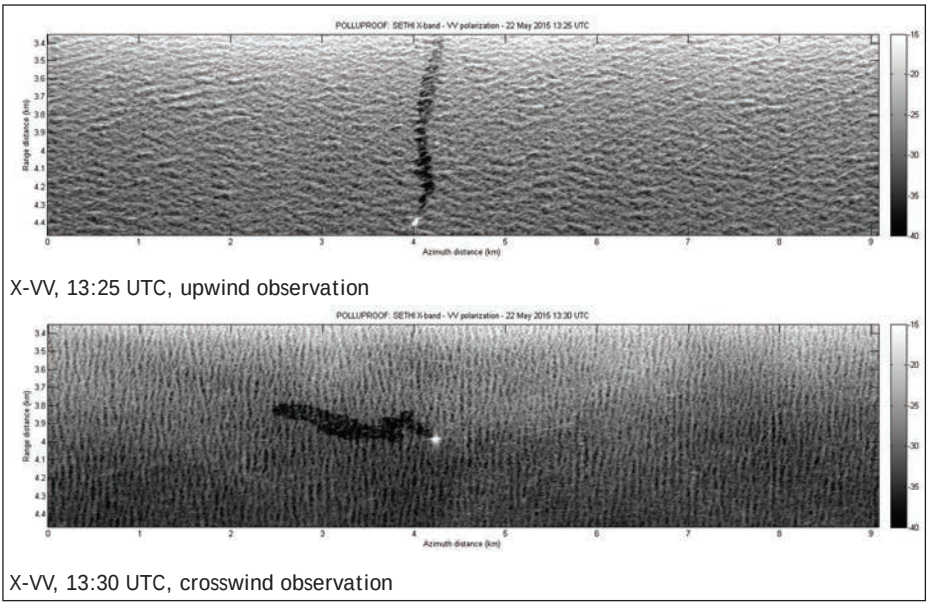

Figure 6: X-VV SAR images over xylene - upwind 13:25 UTC (top) and crosswind 13:30 UTC (bottom)

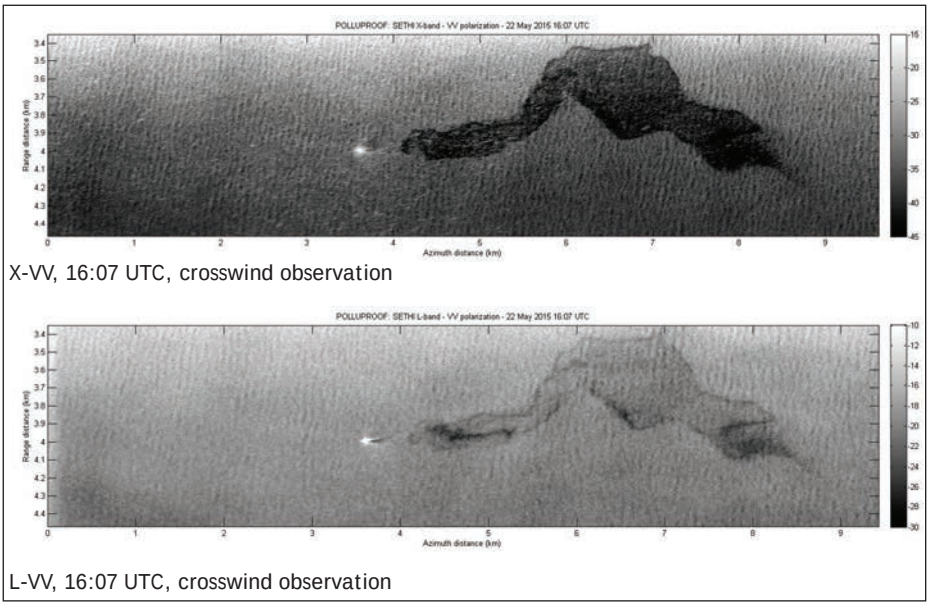

Figure 7: SAR images over rapeseed oil and FAME - X-VV (top) and L-VV (bottom) - 16:07 UTC

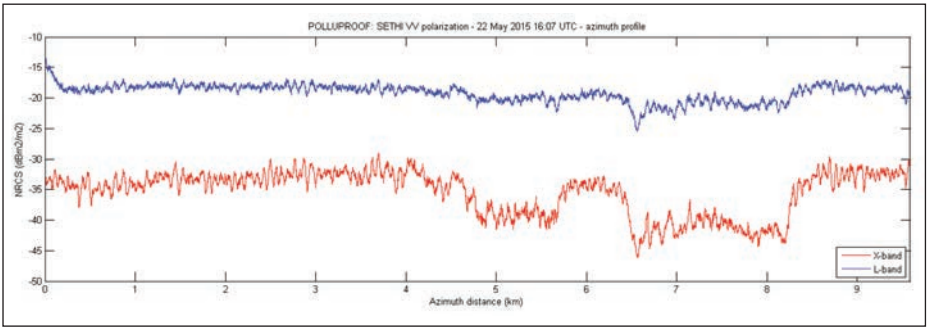

Figure 8: Range profile at X-band (red) and L-band (blue)

4.2 - Detection and quantification of impact on the ocean surface

As presented in paragraph *3.2, the Normalized Polarization Difference (NPD)* can be used for detection of HNS at sea and quantification of their impact on the ocean surface.

The proposed method is divided into 2 steps: as the contrast between the spill and ocean clean surface is more pronounced at X-band than at L-band, a detection mask is first calculated by thresholding the NPD map at X-band. Then, since we observe more variation of the signal into the spill at L-band than at X-band, the detection mask is applied to the NPD map computed at L-band.

Results are presented below: Normalized Polarization Difference map at X- and L-band,

thresholded for values greater than 0.7 at X-band, in the case of xylene (Figure 9) and FAME and rapeseed oil (Figure 10).

We can observe that, first the spill is well identified using this automatic method, then information provided by the two frequencies is effectively different. This observation is particularly conspicuous on the spill of the 3rd flight (FAME and rapeseed oil): at X-band values of NPD are almost always close to 1.0 (between 0.8 and 1.0); whereas at L-band much more fluctuations are observed. At X-band, response is saturated by the presence of the spill. This frequency is perfectly suited for detection but does not seem to provide information on the thickness. At lower frequency (L-band in our case), the EM signal backscattered by the slick fluctuates with the impact of the product on the sea surface. Hence, L-band can provide useful information for spill quantification and characterization.

Figure 11 shows two range profiles over xylene and FAME at X- and L-band. Clearly, NPD values at X-band are always ranging from 0.8 to 1.0, while the dynamic at L-band is greater. Over the FAME, NPD value at L-band reveals a stronger impact of the HNS on the sea surface in the center of the spill than at the extremities.

Information provided by Normalized Polarization Difference and simultaneous use of two frequency bands, allow us to detect HNS at sea and to quantify their impact on the ocean surface in terms of roughness. However, results shown Figure 10 do not enable us to distinguish between the two products that form the spill (rapeseed oil and FAME).

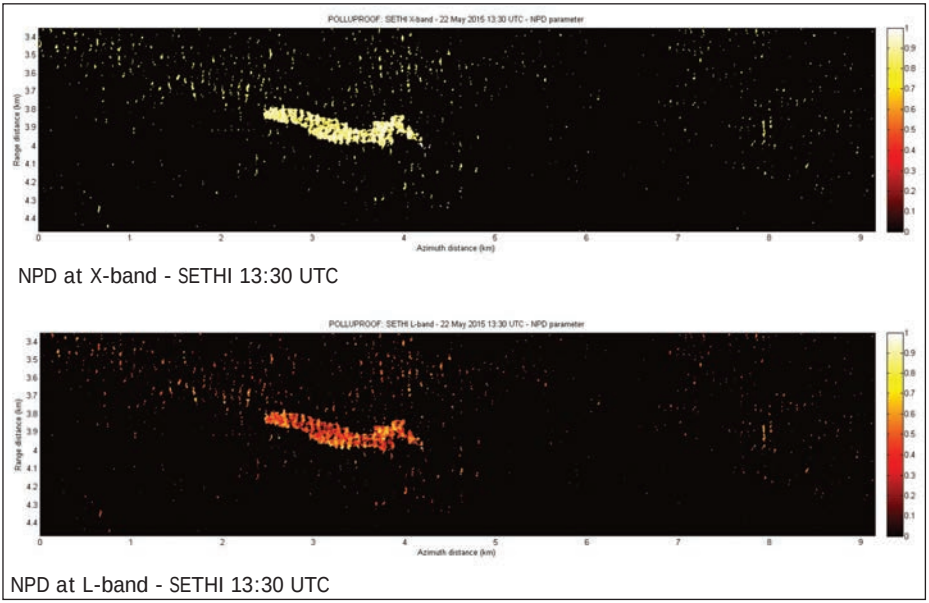

Figure 9: Normalized Polarization Difference (NPD) at X-band (up) and at L-band (down) - 13:30 UTC - xylene

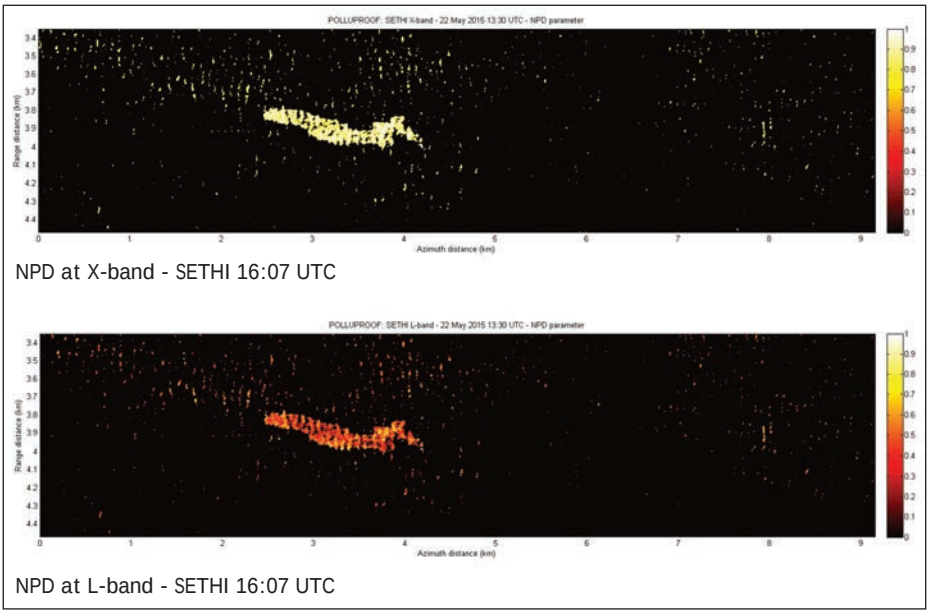

Figure 10: Normalized Polarization Difference (NPD) at X-band (up) and L-band (down) - 16:07 UTC - FAME and rapeseed oil

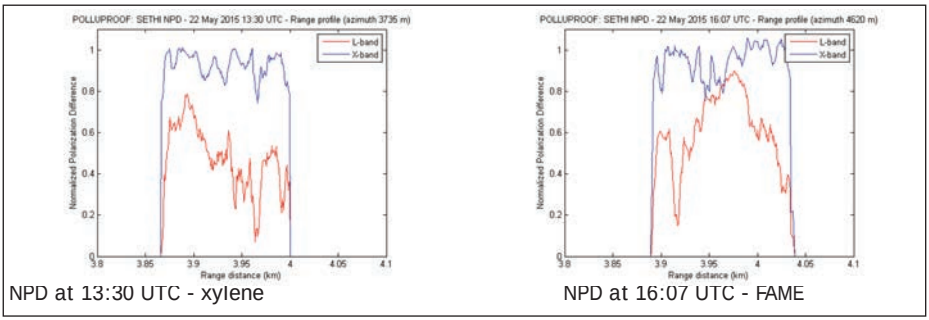

Figure 11: Normalized Polarization Difference (NPD) range profiles over xylene (left) and FAME (right) at X-band (blue) and L-band (red)

4.3 - Characterization

In the third exercise, spill is composed by rapeseed oil and FAME. The right part is rapeseed oil and the left part is FAME; in the middle there is a mixture of two. One can expect different behavior of each product on the sea surface: rapeseed oil is supposed to remain above the surface and produce a more or less homogeneous film. FAME will form a cloud in the water column composed by microdroplets. This is confirmed by observations made from the ship during the releases (Figure 12). These behaviors must be recovered by SAR imagery as they impact the ocean surface in different ways: damping of capillarity waves and/or modification of the dielectric constant by mixing with sea water.

FAME: 3D plume / mix between HNS and water

Rapeseed oil: discontinuous film on the surface

Figure 12: Photos taken from the ship during the release of the FAME (left) and the rapeseed oil (right)

Following results presented in paragraph 4.2; we focus on L-band data and compute M_W, M_α and M_{dex} parameters using the method presented in paragraph 3.3 and initially published in (Minchew, 2012). As for Normalized Polarization Difference map (see 4.2), a detection map has been used beforehand and values have been computed for each pixel detected as HNS using X-band data.

Figure 13 shows maps obtained over the full region of interest: the normalized damping factor (M_W), the normalized power attenuation factor (M_α) and the mixing index (M_{dex}). We clearly observed the separation between the two products constituting the spill (see Mdex Figure 13).

Figure 14 shows histograms (NPD at X- and L-band, M_W, M_α and M_{dex}) over xylene, rapeseed oil and FAME. Xylene and rapeseed oil have similar responses: Mα is close to 0, Mdex is greater than 0 and MW and NPD at L-band are equal; which corresponds to the presence of a film on the sea surface that damped the short waves. FAME has a different behavior: Mα is no longer negligible and thus Mdex is negative which means that, as expected, mixing is more present over FAME than over rapeseed oil and xylene. For the three products, NPD at X-band is always significantly high (greater than 0.9). Over the FAME, NPD at L-band allows us to distinguish two areas corresponding to two different concentrations, as it can be seen in Figure 10.

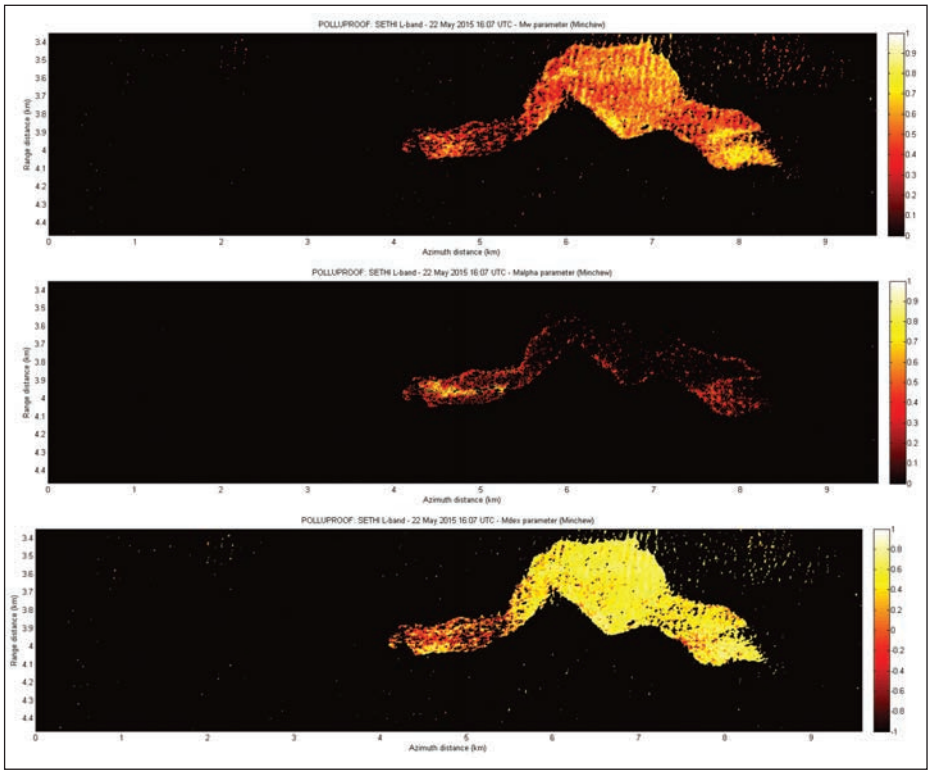

Figure 13: MW (top), Mα (middle) and Mdex (bottom) - L-band SAR acquisitions at 16:07 UTC - FAME and rapeseed oil

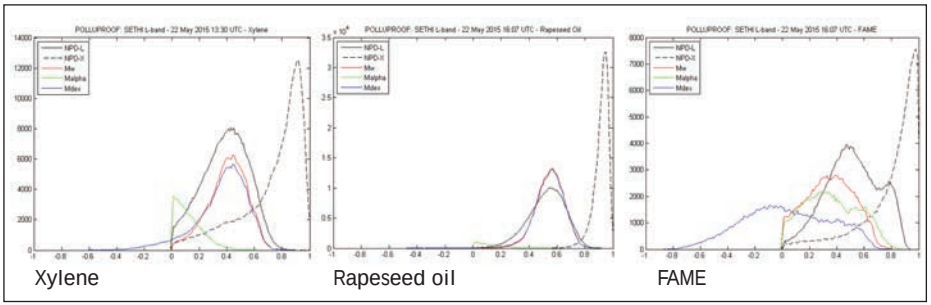

Figure 14: Histograms: NPD L-band (black), NPD X-band (dash black), MW (red), Mα (green) and Mdex (blue) over xylene (left), rapeseed oil (center) and FAME (right)

5 - Conclusion

Due to the increase of maritime transport of Hazardous and Noxious Substances (HNS), defined by the 2000 OPRC-HNS Protocol as substances other than hydrocarbon oil which, if introduced into the marine environment, is likely to create hazards to human health, controlling chemical pollution at sea becomes crucial. As for oil spill, remote sensing is of great interest for detecting, quantifying and characterizing chemical products that were discharged. However, our knowledge on the ability of remote sensing to achieve this is still limited.

An experimental campaign of acquisition (POLLUPROOF) has been conducted in May 2015 over the Mediterranean Sea during which controlled releases of hazardous and noxious substances have been realized; the aim being to establish a procedure for collecting evidence of illegal maritime pollution by noxious and hazardous liquid substances using airborne sensors.

Among the six products tested during this experimentation at sea, three have been detected without any ambiguity using SAR imagery: rapeseed oil, FAME and xylene. For the three others, the non-detectability can be caused either by a high volatility of tested products or by an impact into the water column that physically does not affect the backscattered signal at microwave frequency.

In addition, to demonstrate the ability of radar imagery to detect some HNS, two original results were presented in this paper: first an accurate method using X- and L-band radar imagery has been developed to detect and quantify the impact of chemical products at sea. X-band can easily detect the spills, even when the impact on the surface is limited; L-band is then used to quantify this impact. A Normalized Polarization Difference (NPD) parameter is then introduced for this purpose. We showed that, at L-band, the NPD parameter takes a wide range of values within the spill; this variation is related to the impact of the product on the ocean surface. Of course, this important result is only accessible to earth observation systems whose instrumental noise level is low enough. Then, we showed that the distinction between two HNS (with different thickness) within the same spill is possible with radar imagery only. We conclude that, using SAR data with the suitable wavelength can allow us to define the characteristics of the slick along a spectrum ranging from thin surface films to thicker emulsions. This information is critical for efficient cleanup operations.

As a future work, methods developed and tested on HNS will be tested on X- and L-band SAR data acquired by ONERA during the Norwegian oil spill experiment organized and managed by NOFO (Norwegian Clean Sea Association for Operating Companies) in June 2015.

6 - Acknowledgments

Research presented in this paper is part of the POLLUPROOF research program (ANR-13-ECOT-007) funded by the French National Research Agency (ANR).

Authors are very grateful to everyone involved in the experiment at sea (ONERA - Cedre - AVDEF - DGDDI - French Navy) and those who participated to SAR data processing. They are also very grateful to G. Soriano and C.-A. Guerin for GO-SSA modeling and to P. Dubois-Fernandez and H. Oriot from ONERA for successful discussions.

References

Angelliaume, S., P. Dubois-Fernandez, V. Miegebielle and D. Dubucq, "Polarimetric parameters for oil slicks detection using SAR data remote sensing — An evaluation," in Geoscience and Remote Sensing Symposium (IGARSS), 2015 IEEE International, pp. 3794-3797, 2015.

Angelliaume, S., V. Fabbro, G. Soriano and C.-A. Guerin, "The GO-SSA Extended model for all-incidence sea clutter modeling," in Geoscience and Remote Sensing Symposium (IGARSS), 2014 IEEE International, pp. 5017-5020, 2014.

Bonin, G., P. Dubois-Fernandez, O. Ruault-du-Plessis, S. Angelliaume, H. Cantalloube, H. Oriot, C. Coulombeix, "The new ONERA multispectral airborne SAR system in 2009," in Radar Conference, 2009 IEEE, pp. 1-3, 2009.

Brekke, C. and A.H.S. Solberg, "Oil spill detection by satellite remote sensing". Remote Sensing of Environment. ISSN 0034-4257. 95(1): 1- 13, 2005.

Elfouhaily, T., B. Chapron, K. Katsaros and D. Vandemark, "A unified directional spectrum for long and short wind-driven waves," J. Geophys. Res., 102(C7): 15 781–15 796, 1997.

Gade, M., W. Alpers, H. Hühnerfuss, H. Masuko and T. Kobayashi, "Imaging of biogenic and anthropogenic ocean surface films by the multifrequency/multipolarization SIR-C/X-SAR," J. Geophys. Res., 103(C9): 18 851–18 866, 1998.

Garcia-Pineda, O., B. Zimmer, M. Howard, W. Pichel, X. Li and I. MacDonald, "Using SAR images to delineate ocean oil slicks with a texture-classifying neural network algorithm (TCNNA)," Can. J. Remote Sens., 35(5): 411–421, 2009.

Girard-Ardhuin, F., G. Mercier, F. Collard and R. Garello, "Operational oil-slick characterization by SAR imagery and synergistic data," IEEE J. Ocean. Eng., 30(3): 487–495, 2005.

Gregers-Hansen, V. and R. Mittal, "An improved empirical model for radar sea clutter reflectivity". IEEE Transaction on Aerospace and Electronic Systems, 48(4): 3512–3524, 2012.

Guérin, C.-A., G. Soriano and B. Chapron, "The weighted curvature approximation in scattering from sea surfaces," in Waves in Random and Complex Media, 20(3):364–384, 2010.

Hajnsek, I., E. Pottier and S.R. Cloude, "Inversion of surface parameters from polarimetric SAR," in IEEE Transactions on Geoscience and Remote Sensing, 41(4): 727-744, 2003.

IMO, http://www.imo.org/en/OurWork/Safety/Cargoes/CargoesInBulk/Pages/IBC-Code.aspx

Leifer I., W. Lehr, D. Simecek-Beatty, E. Bradley, R. Clark, P. Dennison, Y. Hu, S. Matheson, C. Jones, B. holt, M. Reif, D. Roberts, J. Svejkovsky, G. Swayze, J. Wozencraft, "State of the art satellite and airborne marine oil spill remote sensing: Application to the BP Deepwater Horizon oil spill", in Remote Sensing of Environment, 2012.

Minchew, B., "Determining the mixing of oil and sea water using polarimetric synthetic aperture radar," in Geophys. Res. Lett., 39, L16607, 2012.

Minchew, B., C.E. Jones and B. Holt, "Polarimetric Analysis of Backscatter From the Deepwater Horizon Oil Spill Using L-Band Synthetic Aperture Radar," in IEEE Transactions on Geoscience and Remote Sensing, 50(10): 3812-3830, 2012.

Kudryavtsev, V.N., B. Chapron, A.G. Myasoedov, F. Collard, and J.A. Johannessen, "On Dual Co-Polarized SAR Measurements of the Ocean Surface," in Geoscience and Remote Sensing Letters, IEEE, 10(4): 761-765, 2013.

Solberg, AH.S., "Remote Sensing of Ocean Oil-Spill Pollution," in Proceedings of the IEEE, 100(10): 2931-2945, 2012.

Soriano, G. and C.-A. Guérin, "A Cutoff Invariant Two-Scale Model in Electromagnetic Scattering From Sea Surfaces," in Geoscience and Remote Sensing Letters, IEEE, 5(2): 199-203, 2008.

Valenzuela, G.R., “Theories for the interaction of electromagnetic and oceanic waves - a review,” in Boundary-Layer Meteorology, 13(1-4): 61–85, 1978.

Wismann, V., M. Gade, W. alpers, H. Hühnerfuss, “Radar signatures of marine mineral oil spills measured by an airborne multi-frequency radar,” in Int. J. Remote Sens., 19(18): 3607–3623, 1998.

Remote sensing of HNS using longwave infrared hyperspectral imaging

E. Puckrin[a], D. Duro[b], G. Gagne[b], A.-P. Bernier[b], L. Armstrong[c], S. Chataing[d]

a) DRDC - Valcartier Research Centre, Quebec, Canada.

b) AEREX Avionics, Quebec, Canada.

c) Transport Canada, Ottawa, Canada.

d) Cedre, Brest, France.

Abstract

A longwave infrared (LWIR) hyperspectral imager was deployed in support of the POLLUPROOF project for the detection and identification of HNS in a maritime environment. In October 2014, the Hyper-Cam sensor was installed on an articulated platform at a height of 12 m above a seawater basin at Cedre where several HNS were spilled. Several gases/liquids, including methanol, diethyl ether, xylene and toluene, were detected and identified from the exploitation of longwave infrared imagery using the Generalized Likelihood Ratio Test (GLRT). In May 2015, the Hyper-Cam was installed onboard a Cessna C-303 and flown at an altitude of 7500 ft above sea level in order to detect and identify spills of HNS in the Mediterranean Sea. The sensor was capable of detecting several slicks, such as colza oil and fatty acid methyl ester, but to date, it has not been possible to identify the chemical material forming the slick. It should be noted that hyperspectral remote imagers operating in other bands (e.g., reflective band at 0.4 – 2.5 microns) may be better suited for some HNS spills.

1 - Introduction

With ever increasing amounts of marine traffic involving vessels carrying larger quantities of hazardous and noxious substances (HNS) worldwide, it is important that techniques be developed to detect these chemicals in the event of maritime spills. Some of today's largest ocean-going chemical tankers can carry as much as 100,000 DWT in cargo, and any major mishap could result in an environmental disaster along coastal areas or at major ports. Several methods already have been developed for the detection of spills involving petroleum oil, which lies outside the definition of an HNS. These methods include Side-Looking Airborne Radar (SLAR) [1], and remote sensing methods based on IR and UV line scanner techniques [2]. It is equally important that effective detection methods be developed for HNS in a maritime environment.

In this paper, the deployment of a longwave infrared (LWIR) hyperspectral remote sensing imager during the POLLUPROOF project in 2014 and 2015 was examined to determine if it is feasible to detect some of the more important HNS threats in a maritime environment. The dependence of this technique to detect the unique spectral signature of a chemical may make it a useful technology for detecting and identifying a wide assortment of HNS. In the POLLUPROOF project, a small selection of HNS was chosen for investigation, including methanol, toluene and xylene, which have infrared signatures in the 8-12 micron longwave infrared band. Results of the detection and identification of these HNS are presented in the following sections.

2 - LWIR hyperspectral remote sensing capability

Most commercial-off-the-shelf LWIR hyperspectral imaging sensors are based on the dispersive push-broom type or an interferometer-based configuration. In this project, the Hyper-Cam sensor (Telops, Inc), which is based on the latter configuration, was used to detect HNS spills in a maritime environment. The sensor, shown in Figure 1, operates in the 8 – 12 micron thermal infrared region and incorporates a 320×256 pixel focal plane array detector based on cooled mercury-cadmium-telluride. In this work the sensor was configured with a 0.35 mrad spatial resolution and at a spectral resolution of 8 cm-1. The instrument has two integrated calibration blackbodies used to perform a radiometric calibration of the infrared measurements. The sensor also has advanced acquisition and processing electronics that offer the capability to convert the raw interferograms into spectra using a real-time discrete-Fourier transform. The sensor can be deployed either in a ground-based configuration, or mounted on a stabilization platform for integration in an aircraft. The Hyper-Cam has been used in several ground-based and airborne measurement campaigns previously (e.g., [3-5]).

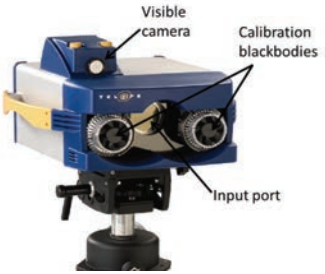

Figure 1: Photo of the Hyper-Cam LWIR imaging sensor

2.1 - Basin measurements at Cedre

During HNS spill experiments at the Cedre basin in October 2014, the Hyper-Cam was installed on a boom lift platform at a height of 12 m above ground level, as shown in Figure 2.

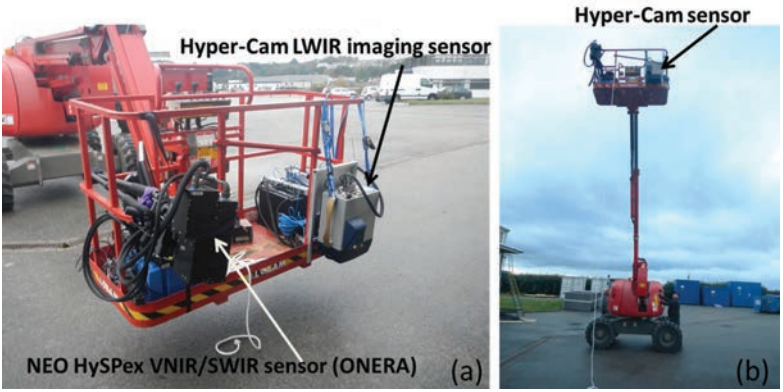

Figure 2: (a) Hyper-Cam LWIR imaging sensor installed on platform of a boom lift looking straight down. A HySpex hyperspectral imager covering the 0.4 – 2.5 micron region was also installed and operated by personnel from ONERA. (b) Hyper-cam installed on boom lift 12 m above ground

A sequence of hyperspectral measurements were made of the spill area, shown in Figure 3, that started before the spill began and continued for a period of several minutes after the spill occurred to determine the behaviour of the resulting gas plume/slick. Details of the spill releases at the Cedre basin can be found in a companion reference [6].

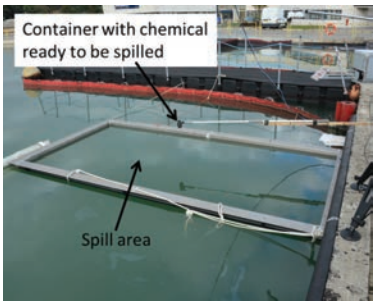

Figure 3: Region of the spill area viewed by the Hyper-Cam, and the container with the chemical to be spilled into the seawater by Cedre personnel

2.2 - Sea measurements

The Hyper-Cam has been successfully used previously [4] in an airborne configuration onboard a fixed-wing aircraft using a stabilization platform. The complete system is shown in Figure 4.

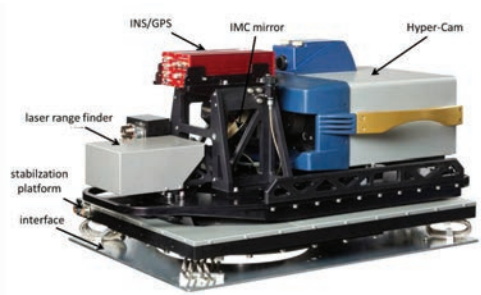

Figure 4: Airborne platform for flying the Hyper-Cam instrument in a fixed-wing aircraft [4]

The airborne configuration includes a stabilization platform, the Hyper-Cam instrument, an Image Motion Compensation (IMC) mirror, an INS/GPS unit, a laser range finder and one visible boresight camera. All these modules are rigidly mounted on a high-stiffness base plate. The IMC mirror is used to compensate the airplane pitch, roll and forward motion, while the stabilization platform is used to reduce the airplane vibrations and to compensate the airplane yaw. The IMC mirror is controlled by the navigation module which receives and uses the information from a laser range finder, for altitude determination, and a GPS/INS unit. The GPS/INS also enables ortho-rectification and geo-referencing of the collected data. In the airborne configuration, the Hyper-Cam performs a step-and-stare measurement, as shown in Figure 5, where the pointing mechanism sweeps in order to provide a constant ground field-of-view (FOV),

i.e. a staring mode. The pointing mechanism then returns to its original position in order to be ready to observe the next ground FOV. A percentage of the FOV is used for overlap between two consecutive ground FOVs to ensure no ground area is missed. An interferometer-based imager, such as the Hyper-Cam, requires the measured scene to be stable during the full measurement of the interferogram, which usually requires about 1 s, depending on the size of the region being imaged.

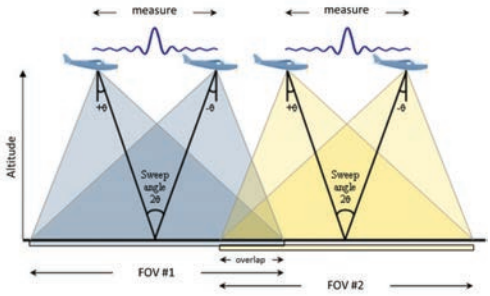

Figure 5: Step-and-stare airborne measurement configuration for an interferometer-based imager [4]

Airborne measurements of chemical spills carried out in May 2015 in the Mediterranean Sea off the cost of Toulon were performed with this system configuration installed onboard a Cessna C-303 aircraft, as shown in Figure 6. Details of the spill releases at sea can be found in another reference [6].

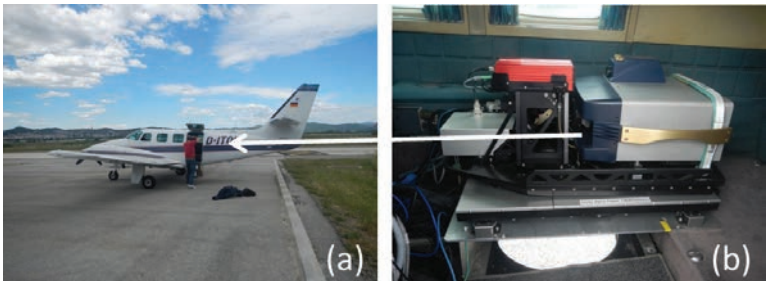

Figure 6: (a) Cessna C-303 aircraft deployed with (b) Hyper-Cam airborne system installed inside looking down through an open hole

3 - Detection and identification of HNS using LWIR Hyperspectral Sensing

The results of the detection of HNS is divided into two parts; the results obtained at the Cedre basin from Hyper-Cam measurements made in October 2014, and results obtained from the HNS spills in the Mediterranean Sea in May 2015.

3.1 - Detection phenomenology

There are two potential observables that may be detected and identified in the hyperspectral remote sensing of chemical spills. One observable consists of the infrared signature corresponding to the gas plume emanating from the spilled material in the

water. For the gas plume to be detected, there must be a sufficient concentration of the gas and the existence of a sufficient temperature difference between the plume and background scene. An expression [7] that approximates the difference in the radiance (δL) associated with a gas plume (having transmittance τ_{gas}) and a clear scene without gas present (L_{clear}) is given by,

$$\delta L = (1 - \tau_{gas})\left(\mathrm{B}(T_{gas}) - \mathrm{L}_{clear}\right),$$

where $B(T_{gas})$ is the Planck radiance at the temperature of the gas. The first term in the expression shows the dependence of the radiance on the transmittance of the gas, and the second term shows the dependence on the difference in temperature between the gas and background. Figure 7 shows the absorbance spectra of some of the gas signatures used in the experiments at Cedre. These include signatures for methanol, xylene and toluene; however, other liquids including diethyl ether were also spilled to test the detection procedure. The absorbance intensity of the signatures varies by an order of magnitude between toluene and methanol, and with different vapour pressures, these chemicals provide interesting test cases for the detection capability.

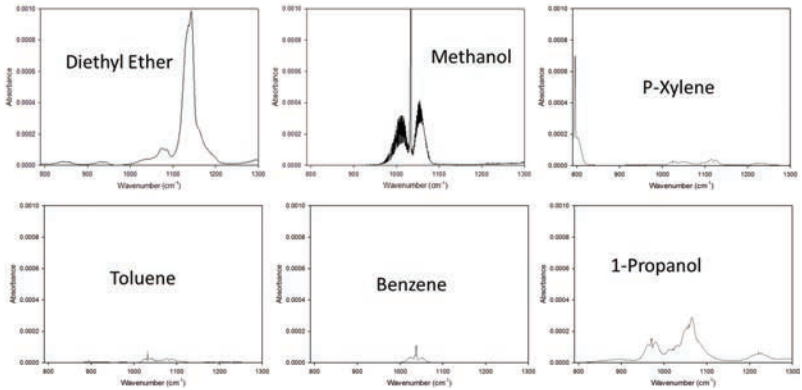

Figure 7: Absorbance signatures of various chemicals spilled at the Cedre basin

The second possible observable, which consists of a thin liquid film on the surface of the water, requires the use of the Fresnel equations to describe the detection phenomenon [8].

3.2 - Detection algorithm

For both the basin and sea measurements, the hyperspectral images were exploited using the Generalized Likelihood Ratio Test (GLRT). A detailed description of the detection method is given in a previous work [9]. The GLRT detection algorithm was used to identify the gas plumes (or slicks) originating from the chemical spills in the water. Essentially, the GLRT is described mathematically by:

$$\mathrm{GLRT}\quad \frac{m^T P_B^{\perp} m}{m^T P_{BS}^{\perp} m} = \frac{(P_B^{\perp} m)^T (P_B^{\perp} m)}{(P_{BS}^{\perp} m)^T (P_{BS}^{\perp} m)} = \frac{\left\| P_B^{\perp} m \right\|^2}{\left\| P_{BS}^{\perp} m \right\|^2}$$

where the numerator represents the squared norm of the measurement, m, projected out of the background space, B, and the denominator represents the squared norm of the measurement projected out of the background + signature space, S. If the measurement does not contain the signature of interest, the result of the GLRT is approximately one. If the does contain the signature of interest, the GLRT will produce a value greater than one.

3.3 - Basin measurements at Cedre

In this section, results of the detection of spills at the Cedre basin in October 2014 are presented. Figure 8 shows the detection and identification of a 10 L spill of methanol with the hyperspectral sensor mounted at a height of 12 m above the spill. The water's surface was warmed by about 2oC as a result of the spill. Figures 8(a,b) show the colour and infrared images, respectively, measured with the Hyper-Cam. The unpolluted region denoted with the blue dots to the right of the spill zone in Figure 8(b) was used for determining the background in the GLRT algorithm. The region of the plume measurement was confined to the space within the metal frame of the spill zone. The detection of the methanol vapour is illustrated by the red pixels in Figure 8(c) and the strength of the detection is indicated by the white intensity level in Figure 8(d). The calibrated spectrum for one pixel with a positive detection is shown by the blue spectrum in Figure 8(e). This is compared to the reference spectrum of pure methanol vapour (from Figure 7). It is clear that even in the unfiltered measurement, the presence of methanol is evident from the spectral features. Figure 8(f) shows the filtered spectral output of the GLRT detector. Essentially the projected measurement result agrees with the projected methanol signature (taking into account a phase shift of 180 degrees in the display).

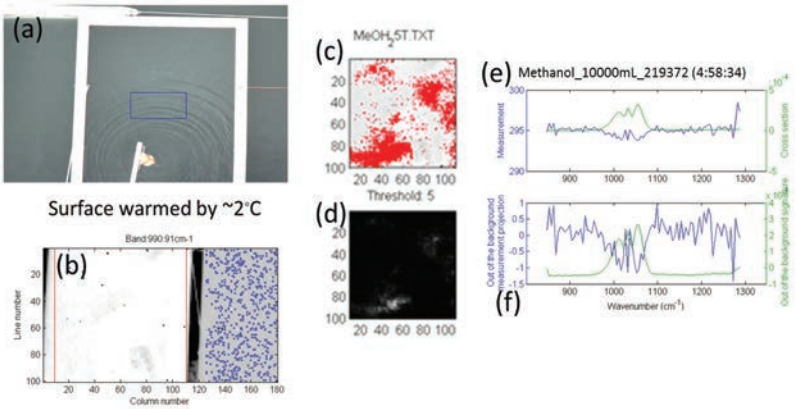

Figure 8: (a) Visible image of the spill confinement zone, (b) Hyper-Cam infrared image of confinement zone immediately after spill, (c) red pixels indicate spill vapour detections within the spill zone, (d) the detection plane shows the strength of the detection (stronger detections are shown by brighter pixels), (e) the Hyper-Cam measurement (blue) for one pixel in the spill zone and the methanol reference signature (red), and (f) the projected results from the GLRT detector

Figure 9 shows the detection of a 5 L spill of diethyl ether for two different times. In this case the surface of the water was cooled by about 2°C. Figure 9(a) displays a similar series of graphs as described for Figure 8. The diethyl ether is clearly observed as indicated by the red pixels detected by the GLRT algorithm. An analysis of another hyperspectral image about 2.5 min later indicates that the diethyl ether is still present, but starting to subside from the spill zone. Again, it is clear that even in the unfiltered spectral measurement in the right side of the panels, the presence of diethyl ether is evident from the spectral features. The filtered spectral output of the GLRT detector also shows very good agreement between the projected measurement result and the diethyl ether signature.

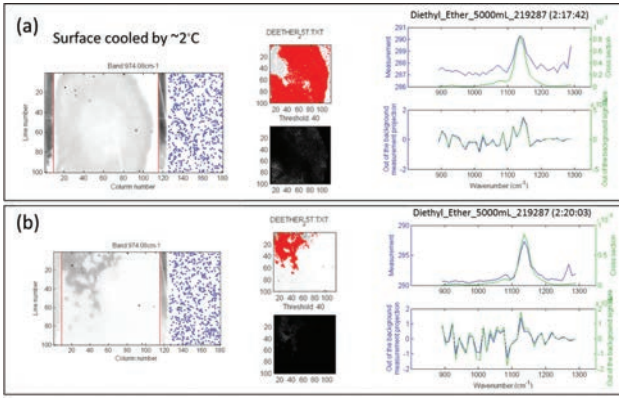

Figure 9: (a) Detection results from a 5 L spill of diethyl ether, similar to that discussed for methanol in Figure 8. (b) A subsequent detection result after a time delay of 2.5 min

Figure 10 shows the detection of a 5 L spill of p-xylene. Using a similar analysis as discussed for Figure 8, it appears that the vapour from the p-xylene spill is also detected, as shown in Figure 10(c), although it is clear that the level of agreement in the filtered results of Figure 10(f) is less satisfactory than for the other spills.

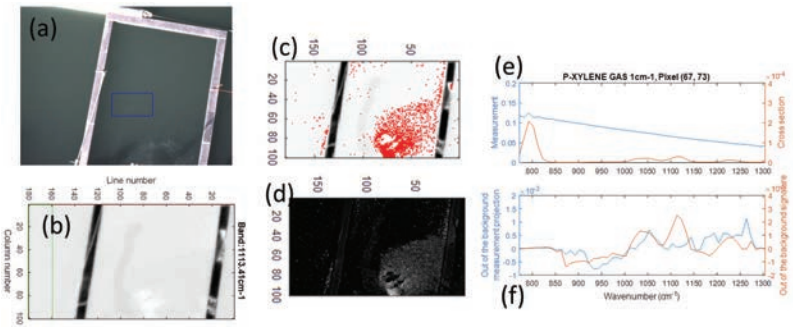

Figure 10: (a) Visible image of the spill confinement zone, for p-xylene (b) Hyper-Cam infrared image of confinement zone immediately after spill, (c) red pixels indicate p-xylene vapour detections within the spill zone, (d) the detection plane shows the strength of the detection (stronger detections are shown by brighter pixels), (e) the Hyper-Cam measurement (blue) for one pixel in the spill zone and the p-xylene reference signature (red), and (f) the projected results from the GLRT detector

Figure 11 shows the detection of a 5 L spill of toluene. In Figure 11(a) the mechanism to release the spill is visible in the image. Using a similar analysis as discussed for Figure 8, it appears that the vapour from the toluene spill is detected, as shown in Figure 11(c).

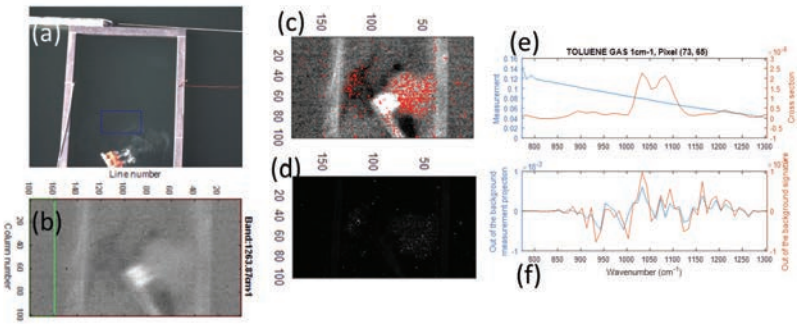

Figure 11: (a) Visible image of the spill confinement zone, for toluene (b) Hyper-Cam infrared image of confinement zone immediately after spill, (c) red pixels indicate toluene vapour detections within the spill zone, (d) the detection plane shows the strength of the detection (stronger detections are shown by brighter pixels), (e) the Hyper-Cam measurement (blue) for one pixel in the spill zone and the toluene reference signature (red), and (f) the projected results from the GLRT detector

For all of the detection results in Figures 8 -11, it is possible that the signature of the liquid spill is also contributing to a positive detection result. This is especially possible for spills involving xylene that exhibit low vapour pressures and where the liquid signature may be the only observable present to be detected. In general, the infrared signatures that correspond to liquid features are similar to their gaseous counterparts, although they may be shifted spectrally by a few wavenumbers and may exhibit a somewhat different lineshape. The effect of refraction by the thin liquid film may also impact the detection, but generally for films of thickness less than 2 microns these effects are not large. Additional work is being undertaken to fully understand the contribution of vapour and liquid signatures on the detection results of these spills.

3.4 - Sea measurements

Hyper-Cam images for the third release consisting of colza oil and Fatty Acid Methyl Ester (FAME) that took place on 22 May 2015 from 15:20 to 16:50 UTC were exploited with the GLRT detector. Two infrared images for colza oil and FAME are shown in Figure 12. The images were collected with the sensor installed in a Cessna C-303 flying at an altitude of 7500 ft above the water.

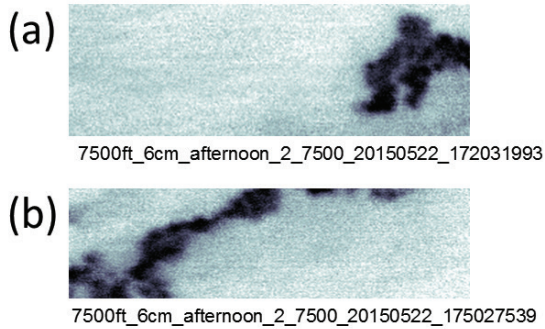

Figure 12: (a) Infrared image of a colza oil slick measured at 15:20 UTC (17:20 LT) and (b) a FAME slick measured at 15:50 UTC (17:50 LT)

The results of the GLRT detection are shown in Figure 13. In this case there is confusion between the identities of the slicks. Either the colza or the FAME is detected for both slicks, which is probably due to the weak signatures of these materials in the LWIR region. Work on detecting the xylene slick that was released earlier in the afternoon is currently being investigated.

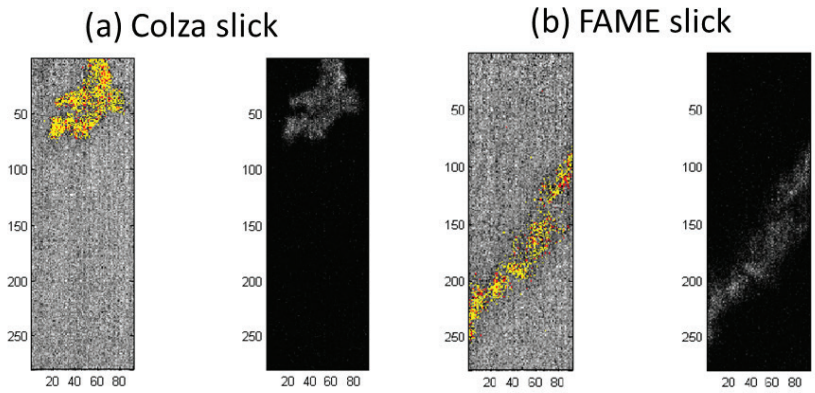

Figure 13: GLRT detection results of (a) colza oil slick and (b) FAME slick. The slicks are detected but not successfully identified in the LWIR band

4 - Conclusions

Longwave infrared hyperspectral remote sensing of HNS using the Hyper-Cam sensor in both a ground-based and airborne configuration was undertaken during the POLLUPROOF project during October 2014 (Cedre basin) and May 2015 (Mediterranean Sea). The hyperspectral images of the spills of several different materials at Cedre were analyzed with the GLRT detector. Several gases/liquids were detected including methanol, diethyl ether, xylene and toluene. Other materials such as colza were much more difficult to detect and identify in the longwave infrared band due to the lack of a strong spectral signature. It should be noted that hyperspectral remote sensing in other bands (e.g., reflective 0.4 – 2.5 microns) may be better suited for some HNS spills.

Exploitation of colza oil and FAME spills in the Mediterranean Sea showed that the slicks may be detected, but not yet identified with the Hyper-Cam sensor. Additional work is being performed to understand the spectral signatures of these chemicals and the exploitation methodology.

References

[1] Wagner, P., Hengstermann, T. and Zielinski, O., MEDUSA: an airborne multispectral oil spill detection and characterization system, SPIE Proceedings, Vol. 4130, Infrared Technology and Applications XXVI, 2000.

[2] Oil Spill Science and Technology: Prevention, Response and Clean-Up, edited by Mervin Fingas, Elsevier, 2011.

[3] Farley, V., Chamberland, M., Lagueux, P., et al., Chemical agent detection and identification with a hyperspectral imaging infrared sensor, Proceedings of SPIE Vol. 6661, 66610L (2007).

[4] E. Puckrin ; C. S. Turcotte ; P. Lahaie ; D. Dubé ; V. Farley, et al. Airborne infrared-hyperspectral mapping for detection of gaseous and solid targets, Proc. SPIE 7665, Chemical, Biological, Radiological, Nuclear, and Explosives (CBRNE) Sensing XI, 766516 (May 05, 2010).

[5] Turcotte, C.S., Puckrin, E., Aubé, F., Farley, V., Savary, S. and Chamberland, M., Novel compact airborne platform for remote sensing applications using the Hyper-Cam infrared, SPIE Proceedings Vol. 8713-15, Airborne Intelligence, Surveillance, Reconnaissance (ISR) Systems and Applications X, D. J. Henry, ed., Baltimore (2013).

[6] Chataing, S., Angelliaume, S., Foucher, P-Y., Puckrin, E., POLLUPROOF Project: PROOF improvement of HNS maritime POLLution by airborne radar and optical facilities – Experimental approach, Sea Tech Week – Sea and digital technologies, 10-14 October 2016, Brest.

[7] Lavoie, H., Puckin, E., Theriault, J.-M., Bouffard, F., Passive Standoff Detection of SF6 at a Distance of 5.7 km by Differential Fourier Transform Infrared Radiometry, Applied Optics, 59, 1189 (2005).

[8] Born, M. and Wolf, E., Principles of Optics: Electromagnetic Theory of Propagation, Interference and Diffraction of Light, 7th edition, Cambridge University Press (1999).

[9] Manolakis, M., Marden, D. and Shaw, G.A., Hyperspectral image processing for automatic target detection applications, Lincoln Laboratory Journal, Vol. 14, 79 (2003).


2

Session 2

Remote sensing to support marine surveillance service

Custom's expertise in remote sensing

L. Buignet, French Customs, France

Introduction

In order to contribute to the mission of surveillance and law enforcement in marine pollution, the French Customs have two dedicated aircraft for remote sensing of marine pollution (F406 POLMAR III). These air assets are in charge of collecting surface information with their airborne remote sensing tools.

Primarily, these specific remote sensing equipments were developed to observe oil release.

The crew members were trained including by Cedre, to detect, identify and characterize marine pollution. This observation alone is enough to recognize pollution and determine the legality or illegality of a leakage.

1 - The aircraft

French Customs have two dedicated aircraft for remote sensing of marine pollution:

- A Reims-Aviation F406 POLMAR III, fitted with a Side Looking Airborne Radar (SLAR), a Scanner (infra Red / U.V. and Visible optical) and an MX10 Camera. The F-ZBGD is based at Lorient Lann-Bihoué Air Base.

Figure 1: The F406 POLMAR III

- A Reims-Aviation F406 POLMAR II (retrofitted in POLMAR III), fitted with a Side Looking Airborne Radar (SLAR), a Scanner (infra Red / U.V. and Visible optical) and a Micro Wave Radar. The F-ZBCG is based at Hyères Air Base. This aircraft is fitted with a specific micro wave Radar: the micro wave radar is able to determine the thickness of the wake pollution (by comparing the difference in temperature with the sea).

Figure 2: The F406 POLMAR II

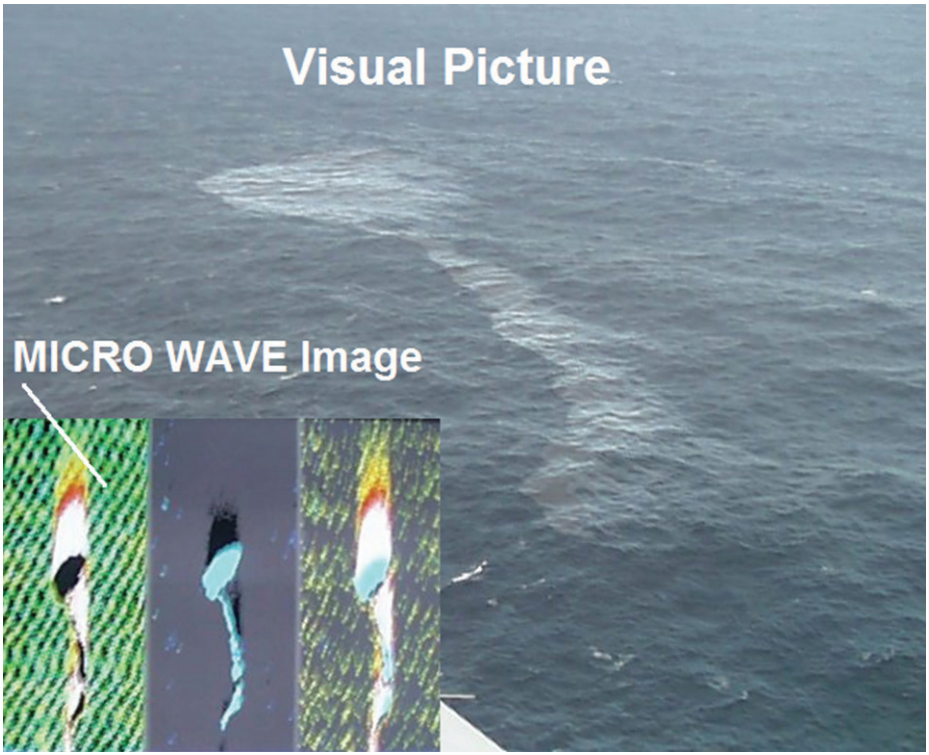

Figure 3: Comparison between visual picture and microwave images

2 - The equipment

Inside the two F406 POLMAR III, we find only one computer with a 17 inch screen, which brings together the different functions: remote sensing images, MAP, Photos and video processing, and the draft reports.

Figure 4: Computer inside the F406 POLMAR III

3 - Airborne remote sensing processing

Due to the specific Radar "SLAR", the flight profile must be stable and straight. The SLAR coverage is efficient between 2 Nm and 20 Nm (width depending on the flight height/level). The sensor hole in the plane is offset by the Scanner coverage (IR / UV / visible).

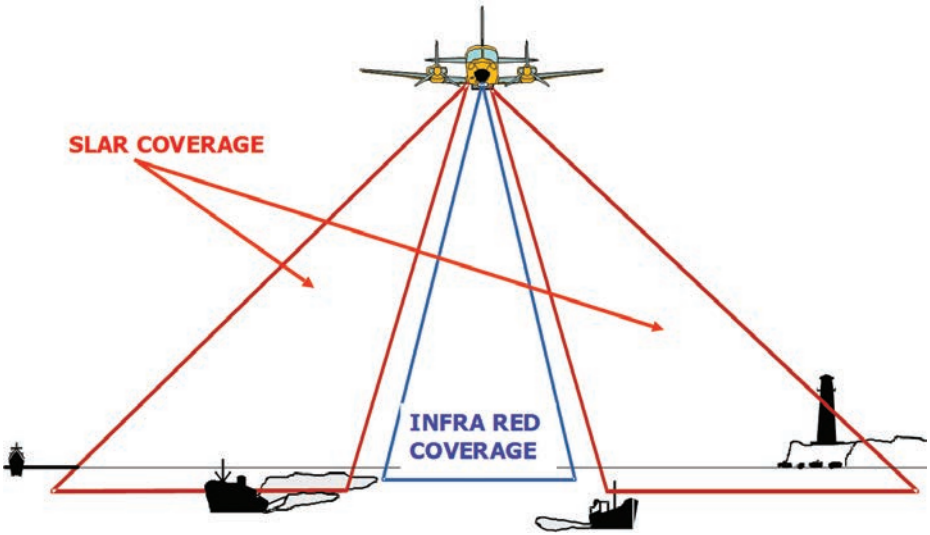

Figure 5: SLAR and IR coverage

4 - Side Looking Airborne Radar processing (SLAR)

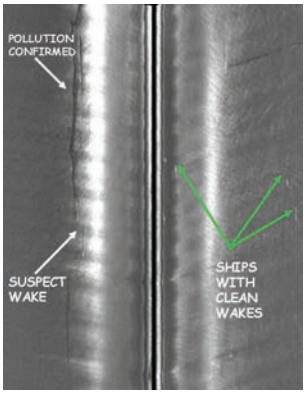

This radar detects sea surface abnormalities, due to an oil or HNS (Hazardous and Noxious Substances) product which removes the wave capillarity at the surface of the water.

This system has some sea limitations which are: 0/1<SEA CONDITIONS<4/5

Figure 6: SLAR image

5 - Infra Red and Ultra-Violet line scanner

The IR detects infrared radiation with a wavelength in the band of 8-12 micrometers emitted from the oil. These layers of oil radiate more slowly than the surrounding clear sea and show up as variations in grey levels (or in defined colours). Thicker layers (greater than about 0.5 millimetres) will absorb sunlight more rapidly than the surrounding sea and show white on the display.

An ultraviolet scanner is a passive device detecting reflected ultraviolet with a wavelength of about 0.3 micrometers.

6 - Standard detection and investigation

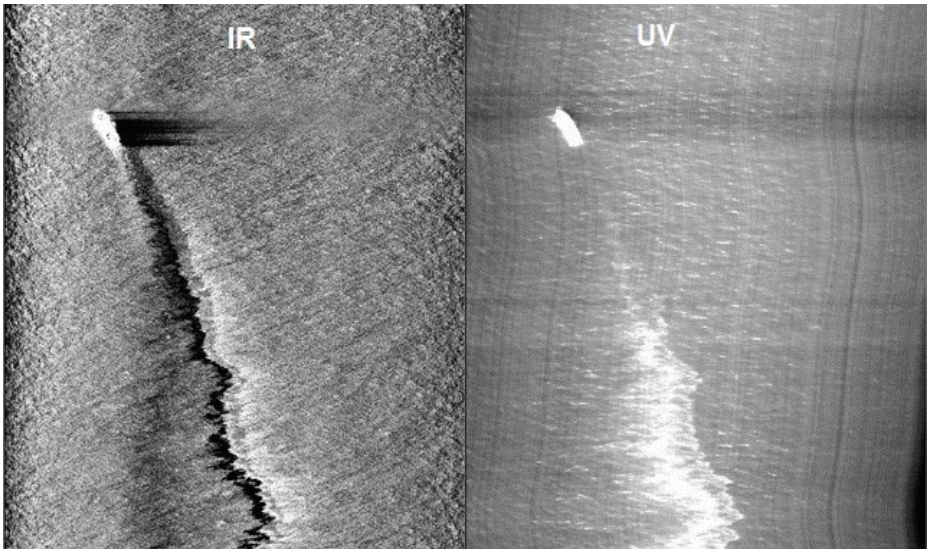

Figure 7: IR and UV images

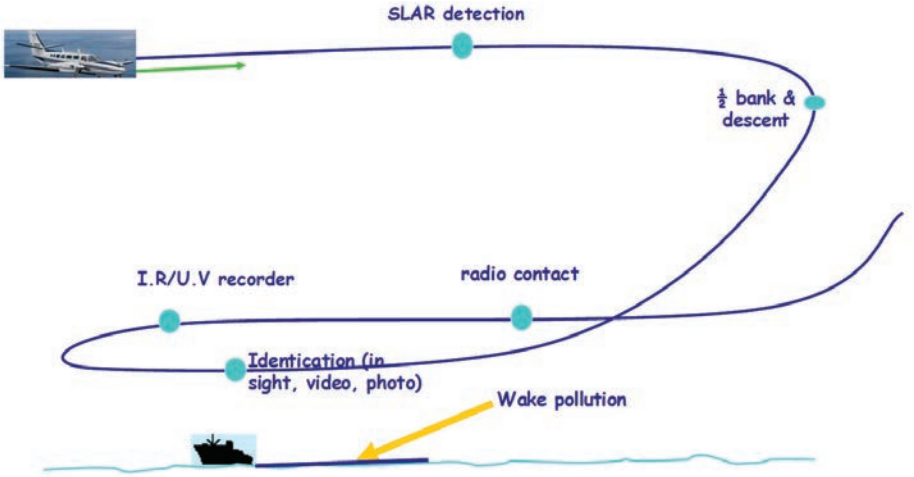

Figure 8: Standard detection process

In flight, our mission is to closely monitor, detect, investigate, identify and report any illegal discharges from suspected polluters, in compliance with national and MARPOL regulations, in order to collect evidence and prosecute.

7 - The future, a new multimission aircraft

Figure 9: The new maritime patrol aircraft in development

French Customs are developing a new maritime patrol “KA350ER-FC” aircraft with conventional surveillance systems (panoramic OM400 Radar and InfraRed multispectral camera) and with a Side Looking Airborne Radar (SLAR), a Scanner (infra Red / U.V. and Visible optical) for remote sensing of marine pollution.

Remote sensing as evidence in court

Y. Rabuteau, ALLEGANS Network, UMR AMURE, Université de Bretagne Occidentale, Brest, France

Warning

This paper is based on an oral presentation made by the author at the Cedre Information Day on 16th October 2016 and should therefore not be considered as an article on legal doctrine, which would call for more substantial bibliographical references together with references to past cases. The conclusions of this paper are based solely on the experience and analysis of the author, an operational legal expert and research associate. The complex question of the future use of remote sensing equipment to provide evidence in court requires, in our opinion, a comprehensive, in-depth study in comparative, international and European law in order to obtain actionable conclusions.

This paper is divided into four parts: first an introduction to the issue of "remote sensing and evidence", then a section presenting the legal frameworks of offences and of evidence in terms of operational discharge at sea (I), followed by a section on remote sensing, how it is considered by the courts and questions and advances observed in this field (II), and finally some conclusions and recommendations. This paper focuses solely on the question of detecting and gathering evidence of illegal, deliberate discharge of polluting substances from ships, with regard to French law.

1 - Introduction

From a legal point of view, the question of remote sensing and its use to provide evidence calls for the definition and clarification of terms and notions relating to the technology, how it is implemented and its purpose. The first point of clarification required is no doubt to determine what is the purpose of remote sensing in general terms. In this respect, we understand that remote sensing is a means of detecting, measuring and acquiring information remotely, using instruments, systems, whether active or passive, without systematic or direct human involvement in implementing the equipment or observing the target. This initial point is of particular importance as it draws attention to the predominant role of the technological equipment in relation to direct observation "by the human eye".

Now, the equipment itself must be addressed. The wide range of remote sensing technologies and measurement instruments (applicable to marine pollution) is striking: whether it be SLAR, UV scanners, FLIR cameras, satellite imagery or even digital videos and photographs, the variety is such that all the expected information can be made available, yet expertise is essential to interpret the information gathered in terms of evidence…

In this respect, what information is liable to be provided by remote sensing? We know that the existing solutions can be used to both detect and characterise discharges at sea. This is a fundamental point as the information on the type of spill observed, whether it is oil or another substance, an estimation of the surface area and thickness

of the slick and the concentration of pollutant in the discharge are expected elements in terms of evidence, but are also called for by the trial court and the parties to the criminal proceedings to gauge its severity.

Finally, it is important to clarify the notion of "evidence" itself in the field of deliberate discharge at sea. In French law, illegal discharge of oil or other polluting substances at sea from a ship (see section I) constitutes a punishable offence. It is therefore governed by criminal law (definition, sanctions, jurisdictional rule), meaning that evidence of both the material element AND the intentional element of the offence must be provided to condemn the offender. In terms of illegal discharge, these two points are of significant importance. Providing evidence of the material element implies here demonstrating the reality of the discharge in hand which is in violation of the rules of the Marpol Convention: for instance, demonstrating that the concentration of a reported discharge is indeed in excess of the 15 ppm concentration limit, in the case of a substance covered by Annex I of the convention. The intentional element, on the other hand, means that the deliberate nature of the discharge observed must be proven in order to distinguish it from an incident or accident.

If these two elements are demonstrated, the offence is constituted and criminal liability may be sought.

2 - Legal framework of the offence and the evidence:

2.1 - What the texts say:

We know that discharging polluting substances from a ship into the sea in violation of the rules of the Marpol Convention constitutes an offence according to French law: a deliberate marine pollution offence. Today, all the annexes of the Marpol Convention have been transposed into the French Environmental Code, as a basis for incrimination, hence:

- Article L.218-11: "Committing a discharge of a polluting substance in violation of the provisions of rules 15 and 34 of Annex I, relating to the prevention of pollution by oil, or an infringement of the provisions of rule 13 of Annex II, relating to the control of pollution by noxious liquid substances in bulk, of the Marpol Convention is punishable, for any captain of a French ship, by a fine of 50,000 Euros.
- Article L.218-14: Releasing harmful substances transported in packages in violation of the provisions of rule 7 of Annex III of the Marpol Convention is punishable, for any captain of a French ship, by seven years of imprisonment and a fine of 1 million Euros.
- Article L.218-15: I. Committing one of the offences described in the provisions of rule 11 of Annex IV and of rules 3, 4 and 5 of Annex V of the MARPOL Convention is punishable, for any captain of a French ship, by one year of imprisonment and a fine of 200,000 Euros.

  II. Committing one of the offences described in the provisions of rules 12, 13, 16 and 18 of Annex VI of the MARPOL Convention, as well as in the provisions of I to IV of article L. 218-2, is punishable, for any captain of a French ship, by one year of imprisonment and a fine of 200,000 Euros."

It is also interesting to note that the level of monetary sanctions has evolved to reach a maximum fine of €15 million, since the law on environmental liability in 2008, for a discharge in violation of Annex I of the Marpol Convention (see article L.218-12 of the French Environmental Code).

Thus the stakes are high and the question of evidence is taking on growing importance, in particular in light of the diversion, detainment and bond payment procedures which are implemented following the observation of a discharge and the drafting of the official report by the agent.

The definition of the offence is therefore part of a global procedure and must be in compliance with international law, but no specific information is provided as concerns the evidence accepted for such offences. What do the texts say in this respect? To determine the legal specifications concerning evidence, we turn to general criminal law.

In criminal law, the choice of evidence is said to be "free". Under article 427 of the French Code of Criminal Procedure: "Except where the law provides otherwise, offences may be established by any type of evidence and the judge shall decide based on his personal conviction. The judge shall base his decision solely on the evidence presented to him during the debates and discussed by the parties before him".

In other words, in the absence of express provisions on the type of evidence required and how it is adduced – which is the case of illegal discharge – evidence can be provided by all appropriate means. This provision would a priori appear to open the way to remote sensing but does not constitute the sole legal framework to be taken into consideration. Indeed, over and above this general provision as concerns evidence, an important point of clarification elucidated by the criminal system relating to ship-source discharge. This point relates to the value of the official report drawn up by the agent who observed the offence. The French Environmental Code states (in article L.218-28) that: "The official reports drawn up by the agents mentioned in article L. 218-26 shall be valid until proven otherwise. They shall be immediately submitted to the Chief Prosecutor by the agent who reported the violation (...)".

The report has probative value and is therefore recognised and protected by law. The defendant must there provide evidence that the observations mentioned in the report are inaccurate.

Nevertheless, these two points (freedom of evidence and value of the report) are the only elements specified by the texts.

2.2 - What legal precedents have been set?

In the absence of other legal provisions, many useful clarifications have been provided in terms of evidence of the offence by legal precedents in criminal cases of illegal discharge at sea.

In this respect, reference should be made to the "Traquair" case and the decision of the Rennes Court of Appeal on 18th March 1996. Without going into the details of this case of operational discharge, it is important to remember that 20 years ago (1996) court practice in this field was no doubt not as advanced as it is today, and the question of evidence of the material element of the illegal nature of the discharge

remained to be clarified. In this respect, the decision of the Rennes Court of Appeal is noteworthy in that it makes explicit reference to the Bonn Agreement and its Oil Appearance Code. The Court stated that "Given that a sample is not required by law as **evidence of the offence, which can also be provided by direct visual observation from aircraft (...) corroborated by colour photographs** (...) However, given that various experimentations (...) have demonstrated

- That no discharge with an oil content less than or equal to 15 mg/l has ever been detected visually,

- That discharges with an oil content (...) of between 15 and 100 mg/l cannot be observed from an aircraft (...) given that they never form continuous films of over a few decimetres long".

It can hence be concluded that if the discharge can be detected visually, it is necessarily a violation of Annex I of the Marpol Convention, as it exceeds the maximum authorised concentration. Since this legal precedent was set, further cases have followed and the elements expected to support observations have been clarified: photographs to support references to the Bonn Agreement, showing the sea conditions, the source of the discharge, the identity of the ship, etc. All these elements provided by photographs corroborate the direct visual observation by the agent in charge of drawing up the report.

According to case law, the intentional element, i.e. the deliberate nature of the observed discharge, is established based on the elements provided by the enquiry, the inspection of the ship, the hearing of the defendant and the different witnesses, as well as a "body of concurring evidence" (French Supreme Court, "Fast Rex" case, 18/03/2014).

3 - Remote sensing: Questions and advances

3.1 - Does the verdict of the "Traquair" case exclude recourse to remote sensing?

This is the first question to be addressed from a legal point of view as, while this decision legitimised the use of the Bonn Agreement Oil Appearance Code, it also underlined the importance of direct visual observation... So what happens if the discharge cannot be directly and visually observed to be compared with this appearance code? If the discharge is only determined to be in excess of the concentration limit by remote sensing? If the discharge is observed at night? All these questions appear to be at odds with the requirements established by the "Traquair" case.

Nevertheless, other cases open the way to a broader approach towards forms of evidence. The French Supreme Court stated that, in this matter, the principle of freedom of evidence fully applies (Supreme Court, "Concordia I" case, 13/03/2007), and that photographs are not mandatory (Marseille High Court, "Cimil" case, 06/09/2004), the sovereign discretion of the judges being the fundamental principle.

3.2 - What answers and advances have been observed?

While the reference used in the case of direct visual observation must necessarily be the Bonn Agreement Oil Appearance Code, the development of the use of remote

sensing technology as well as certain recent decisions highlight certain advances. The "Carthage" case is of particular interest. The Aix-en-Provence Court of Appeal recognised (verdict on 08/02/2016) the reality of an operational discharge initially detected at night by SLAR, then confirmed by IR, together with the identification of the ship's position through AIS data, recorded in a regularly established report. There is therefore a shift towards a conviction based on "(...) the cross-comparison of different pieces of information from different sources". Mention can also be made of examples of advances observed, such as the decision by Truro Magistrates Court in the United Kingdom on 4th October 2013, in the "Maersk Kiera" case, in which evidence of the ship's position at the time of the discharge was ultimately provided by satellite imagery (EMSA operated satellite), thus confirming that the ship was in the territorial waters under the UK's sovereignty (condition required to allow legal action).

4 - Conclusion

The use of evidence obtained by remote sensing technologies, without direct visual observation, does not go against the principle of freedom of evidence presented above.

We know that the different technologies which exist can be used to detect operational discharge in ships' wakes, to characterise the type of pollutant and to provide the information required as concerns the materiality of the discharge, as well as the identity or position of the ship. Each remote sensing technique provides a share of the data that can be measured according to the technology used (temperature, concentration, etc.) without any risk of confusion. If direct observation is not possible, all the techniques and information available (SLAR, IR, UV, AIS data, satellite imagery) should therefore be considered together without exception, to corroborate the report and the observation made by the agent using the means available to him at that time.

To encourage court practices to evolve in this field, a reasonable approach would consist in raising magistrates' awareness of the existing technologies. In the future, the systematic inclusion of data obtained by remote sensing in reports of discharges detected in daylight, in addition to aerial photographs, would appear to contribute to this initiative.

Moreover, to consolidate the interpretation of this data and its probative nature, it would appear fundamental to have a reference comparable to the Bonn Agreement Oil Appearance Code but dedicated to remote sensing images. The aim is to enable the trial court to draw upon internationally recognised experimentation which will serve as a reference for training agents in charge of drafting the report. The examination of this data during the trial hearing would be a useful complement to the report and the account of the agent, as has been the case of aerial photographs for over 20 years. The judicial handling of remote sensing evidence can only evolve through the practices of our specialised courts.

We can thus expect and indeed hope for an evolution of the methods of observing, collecting evidence of and judging cases of operational discharge given the reality of this form of pollution which, as we know, has been adapted in response to our criminal policy.

Long term surveillance and monitoring of natural events in coastal waters

F. Gohin, Ifremer, Plouzané, France

Introduction

In the last decades, satellite observations have been largely used in operational oceanography (Le Traon et al., 2015). Satellite-derived mineral Suspended Particulate Matter (SPM, related to the turbidity and the light regime within the surface waters) and Chlorophyll-a (related to the abundance of phytoplankton) are major products obtained from the Ocean Colour imagery (Gohin, 2011). At the European and global levels, these products are available through the CMEMS (Copernicus Marine Environment Monitoring Service). In situ data, model outputs and gridded products derived from satellite observation are provided freely by CMEMS. These data are used for validating biogeochemical models and for the long term surveillance, as this required by the European Marine Strategy Directive for the eutrophication risk in coastal waters. They not only bring unique information on the seasonal cycle of turbidity and phytoplankton at the scale of the continental shelf but also provide daily observations of exceptional events that may affect the ocean colour, as coccolithophore blooms, harmful algal plume, river plumes or resuspension of SPM after storms.

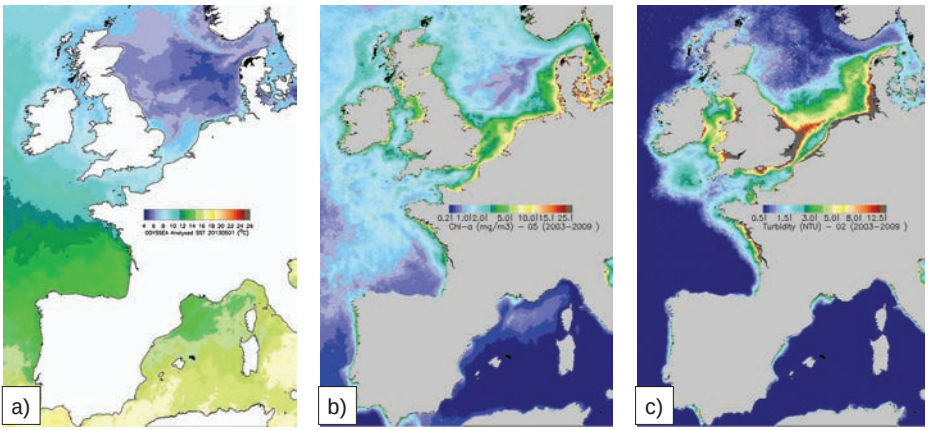

Figure 1: Typical map for long-term surveillance

a): SST on May 1st 2013 (infra-red data)

b): Mean Chlorophyll-a in May (Ocean Colour data)

c): Mean Turbidity in February (Ocean Colour data)

1 - The satellite products for the long-term surveillance

Sea Surface Temperature (SST) is derived from infra-red sensors. Turbidity and Chlorophyll-a are derived from Ocean Colour sensors (Fig. 1). These quantities are tightly related to the climate variability and the evolution of the fluxes of nutrients in the river plumes. The effect of the neap/spring tidal cycle and waves on resuspension of

sediment visible on the Ocean Colour images has been studied in details in Gohin et al. (2015). Fig. 2 shows contrasted situations of SPM in March 2008 and March 2014. In March 2008 a late storm, occurring in time of spring tide, results in a considerable increase in SPM in the surface waters on March 12th whereas in 2014, the last storms highly affect SPM at the beginning of March. Anticyclonic conditions after the 8th of March 2014 are followed by a fast decrease of the SPM concentration at the surface on March 12th.

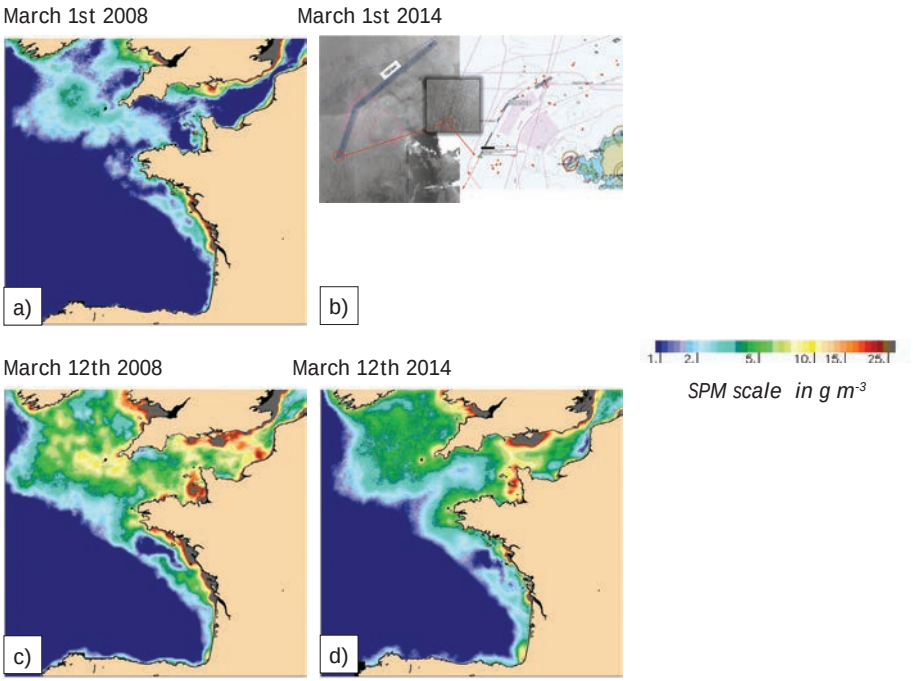

Figure 2: Variability in the non-algal SPM at the beginning of March 2008 and 2014. (a) March 1st 2008; (b) March 1st 2014; (c) March 12th 2008; (d) March 12th 2014

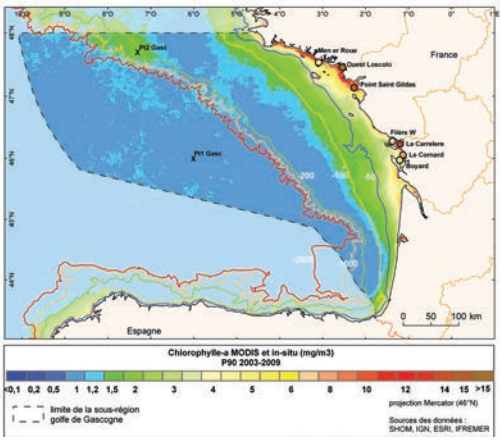

Figure 3: The percentile 90 of Chlorophyll-a over the productive period 2003-2009 (March to October) in the Bay of Biscay

Chlorophyll-a is also monitored from space as it is an indicator of the eutrophication risk in coastal waters. Fig. 3 shows the percentile 90 of Chlorophyll-a over a 6-year period from satellite and in-situ data (Gohin et al., 2010).

2 - Some specific events of natural origin in coastal waters

Together with the routine long-term surveillance, strong phytoplankton blooms may occur episodically. Some of these may occur at high level of chlorophyll with a strong signature in the satellite imagery. Fig.4 shows a Harmful algal bloom of Karenia mikimotoi in the Western English Channel (WEC) in July 2003. These blooms often occur at the beginning of summer in the frontal region between the stratified waters of the Atlantic and the mixed waters of the WEC.

Figure 4: A Karenia mikimotoi bloom observed in situ and from space in July 2003

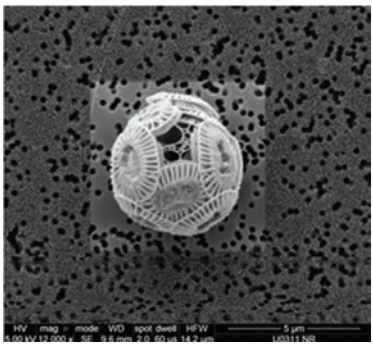

Figure 5: A typical bloom of coccolithophore occurring in June on the margin of the continental shelf (MODIS image in RGB source NASA). An observation by electronic microscopy of a cell of Emiliania huxleyi (source Ifremer) is shown on the right

Blooms of coccolithophores, giving a whitish coloration to the surface waters are also highly visible from space from March to August, initially in the southern Bay of Biscay and appearing northwards through the spring and summer

3 - Conclusion

Many events, from mineral origin, as resuspension of sediment after storms or in relation with the tidal cycle, and from biological origin, as strong phytoplankton blooms of coccolithophores, affect the colours of the surface waters observed from space. These phenomena can make the identification of oil slick more difficult. However, they are generally well understood and don't occur without a physical or biological cause that we have learnt to know. The experience acquired since the launch of the SeaWiFS sensor in August 1997, followed by MODIS, MERIS, VIIRS, and Sentinel-3 in February 2016, can help us to identify most of these events.

References

Gohin, F., Bryère, P., Griffiths, J.W. (2015) The exceptional surface turbidity of the North-West European shelf seas during the stormy 2013-2014 winter: consequences for the initiation of the phytoplankton blooms? Journal of Marine Systems, 148, Pages 70–85.Open Access version: http://archimer.ifremer.fr/doc/00252/36303/

Gohin, F. (2011) Annual cycles of chlorophyll-a, non-algal suspended particulate matter, and turbidity observed from space and in-situ in coastal waters. Ocean Sci., 7, 705-732, doi:10.5194/os-7-705-2011.

Gohin, F, Saulquin, B., Bryere, P?, (2010) Atlas de la Température, de la concentration en Chlorophylle et de la Turbidité de surface du plateau continental français et de ses abords de l'Ouest européen. Ifremer. Open Access version : http://archimer.ifremer.fr/doc/00057/16840/

Le Traon, P.-Y., D. Antoine, A. Bentamy, H. Bonekamp, L.A. Breivik, B. Chapron, G. Corlett, G. Dibarboure, P. DiGiacomo, C. Donlon, Y. Faugère, J. Font, F. Girard-Ardhuin, F. Gohin, J.A. Johannessen, M. Kamachi, G. Lagerloef, J. Lambin, G. Larnicol, P. Le Borgne, E. Leuliette, E. Lindstrom, M.J. Martin, E. Maturi, L. Miller, L. Mingsen, R. Morrow, N. Reul, M.H. Rio, H. Roquet, R. Santoleri & J. Wilkin (2015) Use of satellite observations for operational oceanography: recent achievements and future prospects, Journal of Operational Oceanography, 8:sup1, s12-s27, DOI:10.1080/1755876X.2015.1022050


3

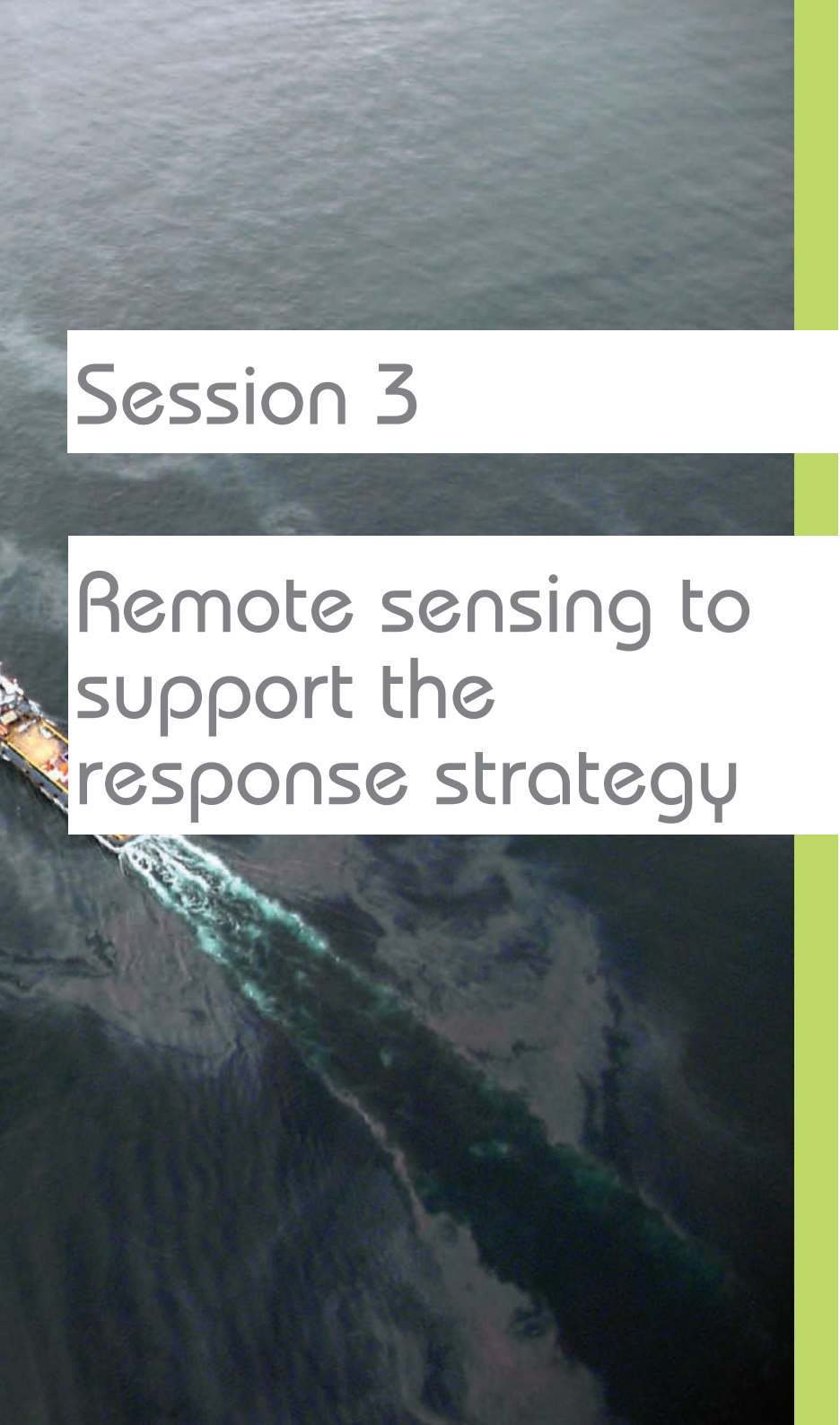

Session 3

Remote sensing to support the response strategy

VIGISAT ground receiving station and EMSA CleanSeaNet services

G. Hajduch, CLS, France

Introduction

The European Maritime Safety Agency (EMSA) has developed the CleanSeaNet service to support the EU Member States in their activities to monitor the marine oil spills, caused by the maritime traffic, in the European EEZs. The CleanSeaNet service is designed in a way to improve the efficiency of national inspections at sea, by delivering rapid oil spill alerts as soon as the radar satellite images reveal the presence of oil at sea. The Member States have a responsibility to dispatch their marine patrol assets, verify the spills, and when possible, control polluter ships in application of the MARPOL convention which restricts the discharge of mineral oil at sea.

The timeliness of the data flow, from image acquisition to delivery in compact formats to EMSA and the Member States is of highest importance. The oil spill warnings are today delivered in less than 20 minutes. Further investigation such as detection of ships surrounding the spill and identification by external means (AIS) is made in 30 minutes from the image.

After 8 years of operation, the CleanSeaNet has demonstrated its added value as an operational, not only for oil spill surveillance, but also for surveillance of the maritime traffic. Once integrated into a more powerful data management system such as IMDate, with appropriate data fusion and behavior analysis functions, the observations from satellite radar images may also serve other applications. The CleanSeaNet service may now serve applications such as:

- The detection of oil spill activities produced from ships in transit, the original CSN mission;
- The detection of pollutions produced by the oil platforms, caused by accidental damages (explosion, wrong manipulation, storm) like the accident of Deepwater Horizon in the Gulf of Mexico;
- Maritime activities surveillance in support to EFCA for detection of fishing vessels. The correlation of echoes with positions given by mandatory Vessel Monitoring Systems should allow detection of suspicious fishing vessels;
- Maritime activities surveillance in support to Frontex for illegal transborder activities (immigration, smuggling etc).

For the past 15 years, several scientific organizations and operational services have used Synthetic Aperture Radar (SAR) satellites to detect oil spills on the sea surface. The concept gradually evolved from R&D to pilot projects and operational systems. Oil spill detection now represents one of the most current applications of SAR satellites.

After the setup phase (June 2010 - March 2011), the operations of the CleanSeaNet 2nd Generation started in February 2010 with ENVISAT segments. RADARSAT-1 and RADARSAT-2 segments were progressively incorporated in operations. Since the loss of ENVISAT in April 2012 and RADARSAT-1 in March 2013, the service is based on RADARSAT-2 mission. The 3rd phase of CleanSeaNet service will be running from 2014

until 2018. The service is mostly based on the European SAR satellites, the Sentinel-1 mission (two spacecraft: Sentinel-1A and Sentinel-1B).

1 - VIGISAT ground receiving station and detection of pollution in Near Real Time

Figure 1: Tasking Areas of CleanSeaNet 3rd Generation

CLS has provided reception and analysis of Envisat, Radarsat-2 and Sentinel-1 scenes throughout the CleanSeaNet service. The SAR scenes are received in VIGISAT in Brest, their analysis performed by experienced personnel, and the reports are delivered to EMSA with oil spill positions, date/time, oil spill dimensions and characterization, and metadata related to the sensors settings. The whole process should be performed within maximum 30 minutes. The oil spill reports are designed to be of immediate use for client web-based browsers or in clients' software applications (typically to be ingested in a GIS or Vessel Traffic System).

The echoes produced by ships in the image are also extracted as individual features (Vessel Detection Reports). If resolution allows, the length and heading of the ship is measured.

From the same SAR satellite scene, the sea surface roughness is processed and converted into a wind field. These products from the SAR scene are:

- Oil spill detection reports
- Vessel detection reports
- Wind detection reports

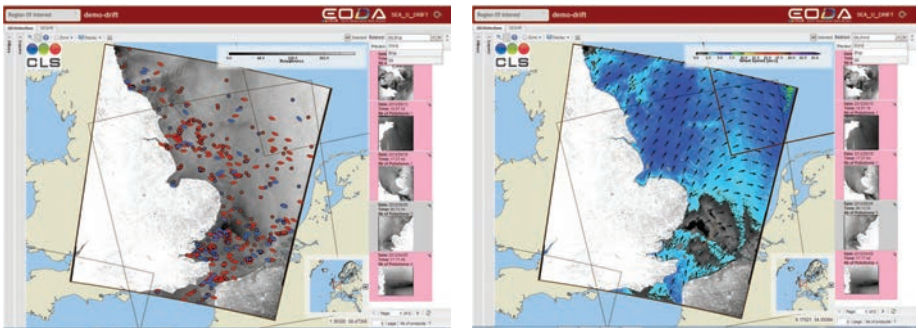

Figure 2: (Left) Vessel detection reports with two classes of confidence and (Right) SAR derived wind fields

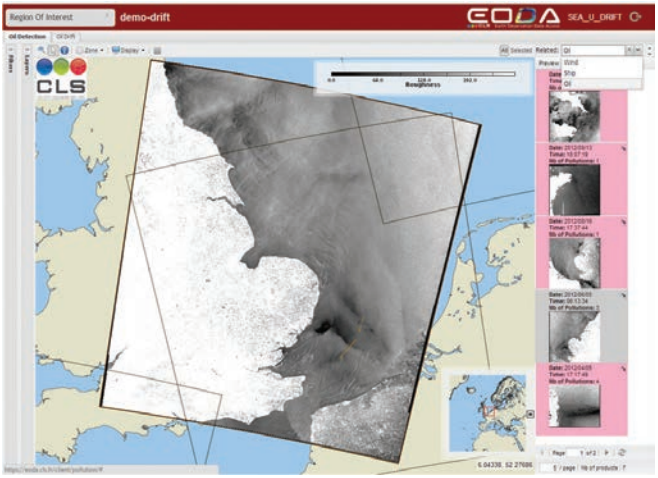

Figure 3: Sea surface roughness and oil spill

The above products displayed in CLS ©Maestro portal are all produced from the same scene.

- Sea surface roughness and a linear oil spill contoured in orange (south east of England)
- Vessel detection reports from the SAR scene (two classes)
- Wind measurement from SAR image

2 - Polluter identification with AIS data flows and drift modelling

A further evolution of the service includes the identification of polluters using the AIS messages received from ships in the region of the spill. The AIS data are supplied by EMSA from the SafeSeaNet system which gathers all AIS positions received along the European coastlines through terrestrial receiving antennas.

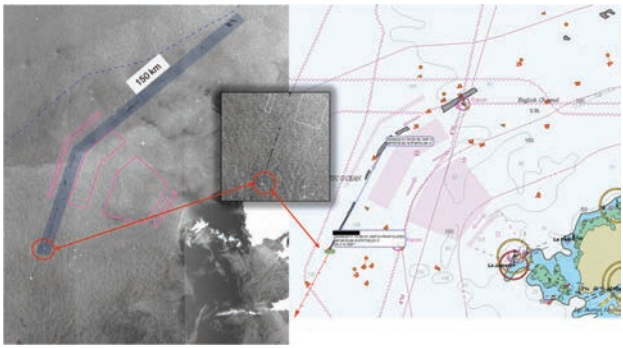

Figure 4: Oil pollution and ship connected to the spill, with AIS identification in THEMIS GIS Envisat scene ©ESA

The methodology for oil spill detection and association with a list of potential polluter identifiers is now mature. It was demonstrated in February 2012 during the MAERSK Kiera pollution report off the Scilly Islands. The ship was detected causing pollution

within the 12-nautical mile zone from the coast. The press related the investigation based on an investigation by the Maritime Coastguard Agency in charge of the EEZ. The satellite image was sufficiently explicit to lead the shipping company admit its responsibility.

“The unique trial at Truro Magistrates Court has been highlighted as the first time satellite footage has been used by the Maritime and Coastguard Agency in the prosecution of a company for dumping waste illegally in the UK.”

Read more: http://www.westernmorningnews.co.uk/Tanker-spied-space-polluting-seas-Cornwall/story-19889142-detail/story.html#ixzz2ikkh7nLY

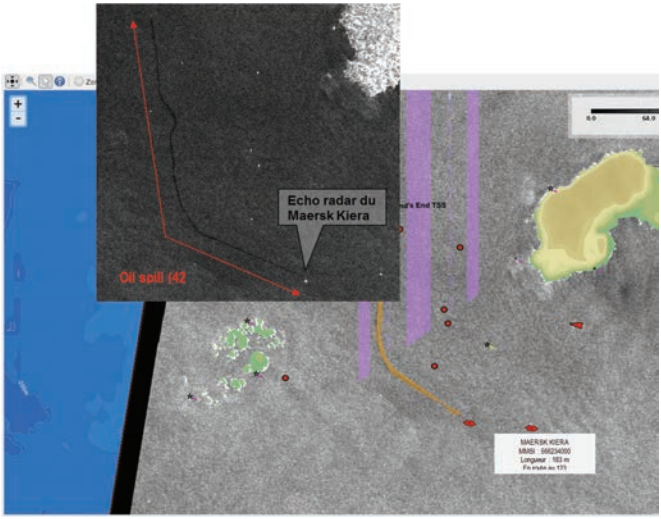

Figure 5: Oil pollution and ship connected to the spill for the case of MAERSK Kiera in February 2012

Recently, CLS updated its operational services chain to integrate the drift component when analyzing AIS and detected oil spill. There exist two possible ways to estimate the pollution source with drift modelling: the backward and the forward approaches.

- When using the backward approach, the detected SAR-based oil spill is propagated in the past and the pollution source is the target whose route intersects in an optimally manner the backward propagated pollution.
- In the forward approach, all the vessels are assumed to be a source of pollution: they pollute along their routes. The pollution source corresponds to the forward simulated pollution with the best agreement with the SAR-based detected oil spill.

The pros and cons of each methodology are outlined below:

- Pros of the backward approach: Easiest approach in terms of algorithms and CPU time consumption as only the detected oil spill is drifted in the past
- Cons of the backward approach: The analyst would need to find the best spatial agreement while tuning the time scale in the past. No simple quantitative criteria can be implemented to assess the likely polluter. Analysis may be complex with spatial and temporal consideration.

- Pros of the forward approach: the overall situation is 'frozen' at one single time step, the SAR acquisition time. The analyst only performs a spatial analysis with distance-shape criteria between simulated and detected oil spill. Possibility in fine to assess quantitatively the likely polluter.
- Cons of the forward approach: Potentially time consuming since it implies to simulate the drift for all the vessels potentially in the vicinity of the oil spill from its release until the SAR acquisition time. However, drift computation can be carried out before the SAR image acquisition, and as such is not a limiting factor for NRT operational services.

Currently, CLS has successfully implemented the forward approach.

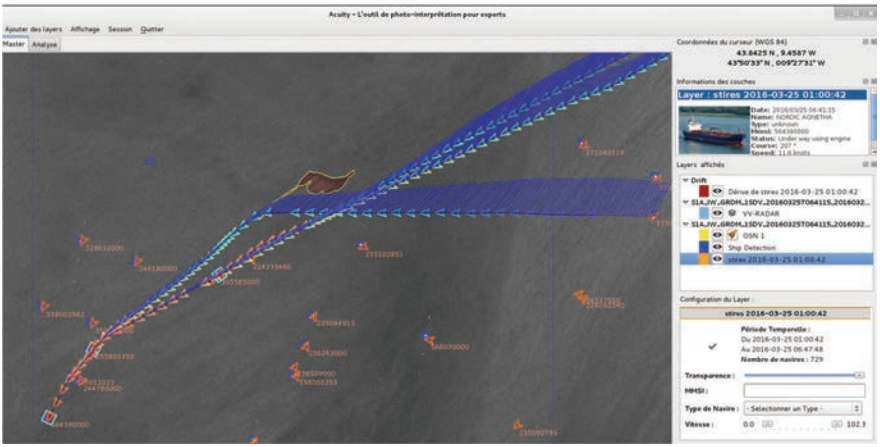

Figure 6: Integration of drift modelling for polluter identification in the CLS ©ACUITY platform

System-to-system interface between the EMSA CleanSeaNet service and OSERIT: the potential synergies between remote sensing and modelling in case of marine pollution

S. Legrand (a) and R. Schallier (b)

(a) Belgian Marine Forecasting Centre (MFC), Operational Directorate Natural Environment, Royal Belgian Institute of Natural Sciences, Brussels, Belgium.

(b) Aerial Surveillance Team (SURV), Management Unit of the North Sea Mathematical Model, Operational Directorate Natural Environment, Royal Belgian Institute of Natural Sciences, Brussels, Belgium.

Abstract

The European Maritime Safety Agency (EMSA) and the Royal Belgian Institute of Natural Sciences (RBINS) develop and operate together a system-to-system interface between the EMSA's CleanSeaNet service and OSERIT, the Belgian Oil Spill Evaluation and Response Integrated Tool. This interface is meant to provide CleanSeaNet users with a support tool for early and automatic oil drift and fate simulation results of any satellite-detected oil spills reported by the CleanSeaNet service in the North Sea and the English Channel. In view of the automatic forecast and backtrack simulations results, CleanSeaNet users have the possibility to further refine this early risk assessment either by activating their own national decision support system or by requesting new, advanced simulations through the CleanSeaNet GIS viewer.

This interface is currently passing the final acceptance tests. However, the system has already been used by RBINS for the oil pollution event subsequent to the *Flinterstar* sinking at 8km off the port of Zeebrugge on the 6th of October 2015. This event perfectly illustrates the potential synergies of remote sensing and modelling in case of marine pollution and their integration in risk assessments that must be performed for any significant pollution of the marine system.

1 - Introduction

Marine pollution is a global environmental problem. If large accidental oil pollution and their dramatic environmental impacts receive a lot of public attention, the marine environment also suffers from chronic operational oil pollution discharge of oil sludge, oily ballast from fuel tanks, machinery space bilges and oil cargo residues. To protect the marine environment from these discharges, a series of more and more stringent regulations have been being successfully implemented from the 1950's onwards at global (OILPOL 1954/1962, MARPOL 73/78…), continental (EU directives 2000/59/EC or Directive 2008/56/EC…), regional (e.g. Bonn Agreement 1969/1983/1989…) and national levels (Lagring et al., 2012).

Surveillance plays a key role in this global strategy of marine pollution reduction. For instance, the Bonn Agreement was amended in 1989, committing North Sea Coastal States to carry out regular surveillance activities in their zone of responsibility.

At national level, this surveillance primarily relies on airborne platforms (airplanes, helicopters and drones) on which can be mounted various remote sensors such as trained operators' eyes, side looking airborne radar (SLAR), visible-band cameras, infrared-band cameras or other night vision devices and in some cases multi-spectral or hyper-spectral cameras. In addition, since the mid 2000s, the airborne surveillance programs are completed with satellite-based synthetic aperture radar (SAR) surveillance services such as the EMSA CleanSeaNet service.

Airborne and satellite-based remote sensing are complementary tools, each having their pros and cons:

- The pixel brightness of a radar image (SLAR or SAR) is actually a measurement of the local sea surface radar backscattering. Since surface slicks significantly dampen the amplitude of the wind-generated short gravity-capillary waves, they appear on radar images as well-contrasted and well-defined dark shapes. However, many other phenomena can decrease the sea surface radar backscattering so that any radar detection should be confirmed by a direct observation. If SLAR detections can easily be confirmed by the operators of airborne surveillance flights, false-positive detections remain a problematic issue for satellite-based surveillance.
- Up to some extent, a trained operator of airborne surveillance flights can estimate pieces of information describing a marine pollution such as the probable type of contaminant, the slick thickness, the spilt volume or the weathering state. Although radar images provide accurate information on the position and extension of a potential slick, the above mentioned characteristics cannot be retrieved from radar images.
- Airborne surveillance is extremely flexible. In a couple of hours, a surveillance flight can be activated. Its flight plan can also be adjusted according to observations. Satellite surveillance is by far less flexible as it is constrained by the satellite orbits.
- Satellite-based SAR images cover a very large area as they are acquired in segments of up to 1,400km and swaths of up to 500km.
- While airborne surveillance flights can be cancelled in case of strong wind gusts, low cloud ceiling or bad visibility, SAR satellite imagery is almost not affected by bad weather conditions. At the opposite, since a minimal wind speed of 2-3 m/s is needed to get enough brightness and contrast in the radar images, too calm weather conditions negatively impact satellite-based surveillance.

The airborne and remote sensing surveillance programs naturally aim at detecting marine pollution and monitoring their evolution. However, they mainly provide snapshots of a pollution event and must therefore be further analysed and interpreted by coastguard operators or other national responsible authorities to get a full and comprehensive understanding of the pollution and its consequences. In particular, in case of a significant pollution, one of the priorities is to assess the risk posed by this pollution (1) to the public and responder safety, (2) to the marine environment and (3) to the socioeconomic assets upon which a state or coastal community depend.

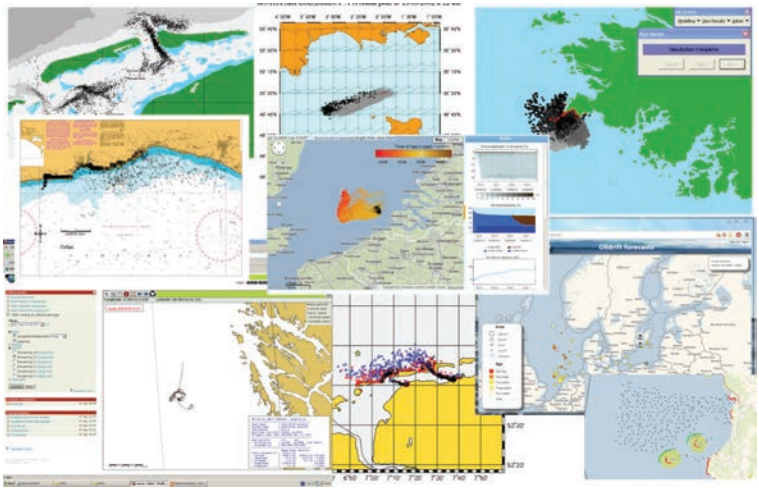

Figure 1: Snapshots of the main decision support systems used in North Sea by public authorities, including OSERIT, Oilmap, SeaTrackWeb, Mothy, OD3D, BSHmod.L and OilTrans. cf. Bonn Agreement (2016) for the most recent exhaustive overview of the decision support systems used in case of marine pollution (Image courtesy: RBINS, met.no, Meteo-France, BSH, FCOO, Deltares, Marine Institute and CEFAS, 2013)

While 10 years ago these assessments were mainly an 'expert judgment matter', they presently more and more rely on decision support systems that integrate at least a spill drift and fate model (Figure 1). The most advanced systems allow their operators within a couple of clicks

- to describe the pollution;
- to perform forward or backward spill drift and fate simulations forced the most recent and reliable met-ocean forecasts;
- to access and visualize the resulting relevant information such as spill drift trajectory, the maximal pollutant concentration in sensitive areas, time residency of pollutant concentration above given thresholds, beaching risk and pollutant mass balance, i.e. the time evolution of the evaporated, floating, naturally dispersed, chemically dispersed, dissolved and sunk mass fractions of the contaminant;
- to interpret them along with other information such as socio-economic and environmental sensitivity maps, AIS vessels track or pollutant descriptions stored in database;
- to update previously done analyses by integrating the latest available observations or factual elements of information.

Concretely, these systems allow or facilitate the quantification of the risk associated to the different listed sensitive resources; an estimation -as objectively as possible- of the efficiency of the different possible response strategies; the guidance of surveillance teams towards spills observed a few hours ago; the identification of potential polluters; the delimitation of safety and/or exclusion areas; the design of the (post-) crisis environmental monitoring program. In addition, their graphical outputs are in-

creasingly used by crisis managers for communication purposes.

In order to provide faster and easier access to information for operational decision-making for oil spill surveillance, potential polluter identification and spill response, the European Maritime Safety Agency (EMSA) implements a system-to-system interface between the CleanSeaNet service and several leading European oil spill drift and fate model service providers. Two interfaces are being implemented for the Baltic Sea and the North Sea, respectively, while two other demonstration cases are envisaged for the Portuguese Atlantic Region and the Mediterranean Sea.

The purpose of this article is to present the North Sea region-wide implementation of the system-to-system interface between the EMSA CleanSeaNet service and the Belgian operational oil spill drift and fate model OSERIT. The article is organised as follows. First, both the CleanSeaNet and the OSERIT systems will be shortly described. Then, the philosophy of the system-to-system interface will be explained. Finally, the potential synergies between remote sensing and modelling will be illustrated using the oil pollution event subsequent to the Flinterstar sinking at ~8 km off the port of Zeebruges on the 6th of October 2015.

2 - The EMSA CleanSeaNet service

EMSA helps to identify, trace and track illegal oil discharges and polluters through the satellite image-based service CleanSeaNet. Synthetic aperture radar images are used to detect the position and extension of potential oil slicks on the sea surface and adjacent vessels. This monitoring service supports coastal states and the European Commission and offers a solid basis on which to expand illegal discharge-related measures and to support response operations to accidental pollution.

In addition to Radarsat-2, the synthetic aperture radar satellites and sensors now in use include Sentinel-1 and the TerraSar-X and Tandem—X constellation. Optical imagery from a wide range of satellites is also available. Coastal states define their service coverage requirements. In cooperation with the users, EMSA plans and orders satellite images to meet these requirements. Accordingly satellite data are acquired via a network of receiving stations.

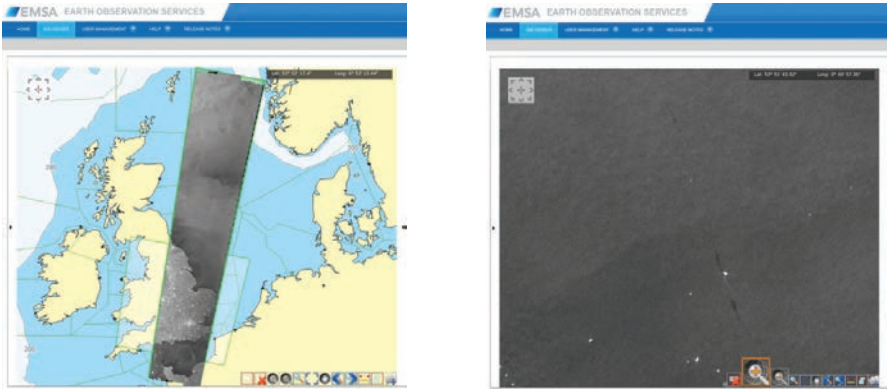

Figure 2: Example of a SAR image made available to CleanSeaNet users through CleanSeaNet GIS viewer and a close-up view of potential spills detections at 20 km off England coastlines

Operators assess the images, together with supporting meteorological, oceanographic and ancillary information (AIS, vessel detection) where available, to identify possible polluters, to determine the likelihood of the presence of oil on the sea surface and to assist in identifying the source of the pollution. If a potential spill is detected (Figure 3), it is of utmost importance that coastal state administrations are immediately alerted by phone and email with the aim of increasing the likelihood of catching a polluter red-handed.

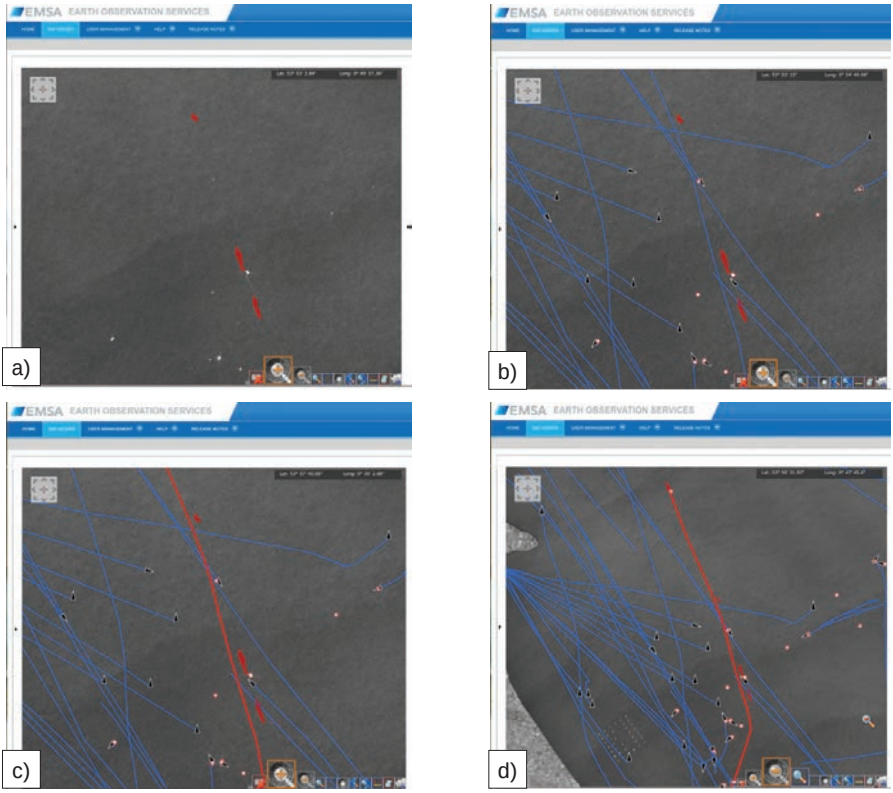

Figure 3: In case possible slicks are detected, coastal state administrations receives a report within 30 minutes after the SAR image acquisition time. In order to help catching a polluter red-handed, the coastal state operator can log in the CleanSeaNet web-based GIS viewer in order to better visualise the slicks (a.) and all the vessels present in the scene as well as their AIS track if available (b.). On basis of these observations, the operator can identified a subset of potential polluters (c.) who are not necessarily the vessels located the closest to the slicks (d.).

As time is critical for confirming a possible spill and catching polluters in the act, the shortest possible delay between satellite detection and alert is essential for a rapid response by coastal states. CleanSeaNet is a near real time service. Detection results are reported to the affected coastal state approximately 30 minutes after satellite image acquisition (the exact time varies according to the size of the image).

In addition to the regular monitoring service, the Agency also provides assistance to member states during emergency situations. This is usually requested by member

states through the Monitoring and Information Centre of the European Commission in Brussels, which coordinates assistance to member states during emergencies. In relation to CleanSeaNet, assistance usually takes the form of additional services over an area where an incident or accident has occurred, in order to monitor the extent of a spill and changes over time (e.g. direction of drift).

CleanSeaNet quality monitoring and user support form part of the EMSA's day-to-day activities to keep up a high level of service performance. This, together with end user training provided by the Agency, is of fundamental importance to ensure the efficient use and integration of the CleanSeaNet service into national operations.

As CleanSeaNet is linked to national and regional response chains, interaction with user communities in the coastal states is important for ensuring the best use of the service and identifying improvements to be made. To that effect CleanSeaNet User Group meetings are organised regularly by EMSA. These events are an opportunity to foster better communication with authorities using CleanSeaNet in the coastal states and get feedback on the user requirements, and on weaknesses and strengths of the service from their perspective.

The first three years of operations have demonstrated that CleanSeaNet is efficient for the detection of oil spills. During the period 16 April 2007 – 31 December 2009, 5816 images have been successfully delivered to the 26 coastal states using the service. Within these images 7193 possible spills were detected by CleanSeaNet. 1997 were verified on site by the member states and 542 were confirmed as being mineral oil. The overall rate of confirmation is better than 50% if the spill is checked by aircraft no later than 3 hours after satellite acquisition.

In 2015 3,052 satellite images were delivered (2,635 to coastal EU Member States, Turkey and Montenegro under the regular CleanSeaNet service, as well as 262 for Greenland, 4 for the Dutch Caribbean, and 151 for Safemed and Traceca) and a total of 2,423 possible oil spills were detected.

3 - OSERIT

OSERIT is the Belgian Oil Spill Evaluation and Response Integrated Tool, a 24/7 accessible support decision system for evaluation of an oil spill reported in North Sea and English Channel. It is made of a 3D Oil drift and fate model and a user-friendly web-based decision support system restricted to registered users mainly coast guard operators from Belgium and its surrounding countries.

3.1 - The OSERIT Oil Spill Model

The OSERIT model has been designed trying to balance the state-of-the art in oil spill modelling with the reality of the field and operational needs, i.e. mainly the short time window for intervention and the common lack of information on the spill itself.

The OSERIT model is a kinetic model based on empirical data and parameterizations that simulates the 3D drift and fate of oil at the sea surface and in the water column using the usual Lagrangian particle tracking approach (Figure 4).

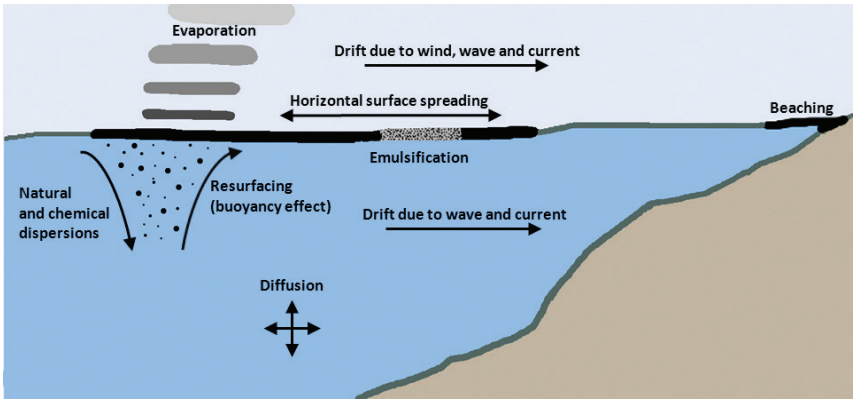

Figure 4: Physical processes included in the OSERIT oil spill model

Advection at the sea surface is computed as a result of the combined effect of winds (leeway drift), surface water currents and waves (Stokes drift). Within the water column, particles move under the action of water currents, waves and buoyancy effect. The horizontal and vertical turbulent diffusive transport is expressed using the random walk technique following Wang et al. (2008). Particles can move from the surface into the water column through the process of vertical natural dispersion. Surface oil is then split into smaller droplets that are propelled into the water column. The oil natural dispersion follows the kinetic approach of Tkalich and Chan (2002) but its rate can also be defined by the user. Two different parameterizations have been implemented in OSERIT to simulate the horizontal surface spreading of oil over the water surface mainly due to the combine effect of gravity, inertia, interfacial tension and viscosity. The first method is based on Fay (1971) and approaches the spreading due to gravity-viscous forces by computing random velocities in the range of velocities that are assumed proportional to the diffusion coefficients (Garcia et al. 1999). The second method, also based on Fay (1971), considers the oil slick as an ellipse which elongates along the wind direction (Lehr et al, 1984). The surface horizontal spreading stops when the terminal thickness is reached based on data from McAuliffe (1987), as done in French (2003). Beaching is included.

Oil weathering processes and their effects on oil characteristics can also be computed by the model. Emulsification is computed as a function of oil characteristics and significant wave height as in Scory (2005). Oil evaporation can be computed following one of the two following approaches: the pseudo-component approach of Jones et al. (1997) that divides the oil into a number of pseudo-components, computes the evaporation rate for each component, and combines them to get the total evaporation rate, and the analytical approach of Fingas (1996; 1997; 2011) that treats the oil as one single substance.

Finally, the model is able to compute the drift of chemically dispersed oil. However, the user has to define the dispersant efficiency (i.e. the percentage of oil affected by the chemical dispersant).

Biodegradation is not included in the model since it is a slower process with relatively little impact on the oil behaviour during the very first days. Due to the lack of infor-

mation relative to oil sedimentation in the North Sea, no such parameterization has been implemented yet in the OSERIT model.

The model can be run forward in time to provide forecast of the oil spill drift and fate or backward in time to provide a backtracking of oil spill. For a maximum flexibility, each process implemented in the model can be activated (or deactivated) by designated model switches.

The complete description of the model equation can be found in Dulière et al. (2013a).

It is important to note that oil slicks drift away under the influence of winds, waves and ocean currents. As a result, the accuracy of the simulation depends to a large extent on the reliability of the wind, waves and current data used. The oil drift model allows performing a large range of simulations; from 2D drift-only simulations to 3D simulations that include horizontal surface spreading, natural vertical dispersion, buoyancy, weathering, etc. Some of these last processes strongly depend on oil type. As a result, the simulation accuracy relies on oil characteristics given by the user.

3.2 - OSERIT visualisation tool

To enable a 24/7 accessibility by all Belgian Coast Guard Agencies, a web-based interface has been developed: http://oserit.mumm.ac.be/. This interface was designed to be as user-friendly as possible. It offers two main functionalities: a simulation manager and a visualisation tool.

The simulation manager allows users to manage existing model simulations and to request new ones. To this end, they must define the simulation setup by filling in a setup form. Basic inputs consist in initial time and location of the slick and simulation type (forward or backward in time). Advanced options can include oil characteristics, oil release and spill scenarios, oil physical processes to be taken into account, and the possible use of chemical dispersant.

The visualisation tool can provide users with marine forecast and various diagnostics derived from the drift simulation such as probability maps, oil impacted areas, oil concentrations and exposure times through geographical overlays. Part of the interface is based on Google Maps and allows superimposing model results with other environmental and economic GIS layers. Time series of oil vertical distribution, volume balance and oil characteristics can also be displayed. Results are available for download from the visualisation tool (Figure 5).

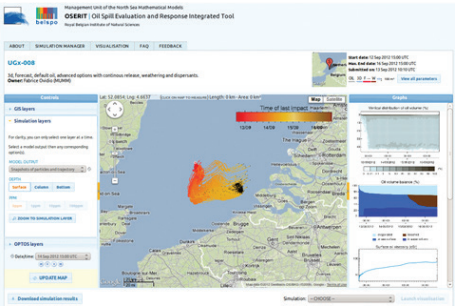

Figure 5: Screenshot of OSERIT web-based visualisation tool

3.3 - OSERIT domain

The domain of the OSERIT model is presented in Figure 6. It covers the English Channel from 4°W and the southern North Sea up to 57°N. During model simulations, any oil that is pushed out of the domain covered by OSERIT is considered as 'lost' and can therefore not come back in. This is a problem for spills that occur close to the OSERIT boundaries.

Figure 6: The domain covered by OSERIT. The inner blue rectangle shows the area where high resolution hydrodynamic forcing is available

3.4 - OSERIT met-ocean forcing

OSERIT met-ocean forcing is produced from three different state-of-the-art operational forecasting systems:

- Atmospheric forcing (i.e. air temperature and wind at 10 meters above water surface) are forecast from the global Numerical Weather Prediction system of the UK Met Office;
- Hydrodynamic forcing are forecast from the RBINS operational hydrodynamic models OPTOS-NOS and OPTOS-BCZ (including 3D current, sea surface elevation and turbulent vertical diffusivity). Their horizontal resolutions are of 5 km and 750m, respectively.
- Sea state (including wave period, direction and significant height) are forecast from the RBINS operational implementation of the WAM model.

3.4 - OSERIT oil data base

Some oil processes implemented in the OSERIT model (such as evaporation, horizontal surface spreading, natural vertical dispersion, emulsification and buoyancy) strongly depend on oil properties. It is therefore crucial to provide the right oil characteristics to the model. To help with the lack of information on oil characteristics in most cases of marine pollution by oil, the OSERIT model was built with an oil database. This database was kept intentionally short for ease of use and includes a wide range of oil

types that are likely to cross the Southern part of the North Sea (Figure 7). Oil types go from light, medium, heavy and very heavy crude to main fuel types. Characteristics of oil involved in the *Erika* and the *Prestige* incidents are also available. The complete list of available oil is given in Figure 8. The OSERIT database is based on oil characteristics provided in ADIOS, Jokuty (1999) and Fingas (2011) and by the Cedre.

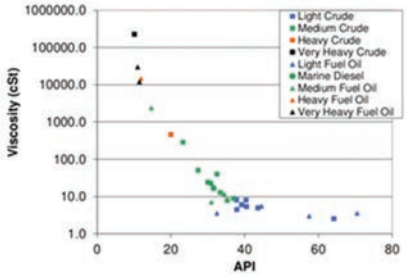

Figure 7: Scatter plot between viscosity and API for each oil type of the OSERIT database. Viscosity is given in cSt at 15°C (from Dulière et al., 2013a)

Oil type selection

- Light crude
  - Brent blend
  - Algerian condensate
  - Brega
  - Ekofisk
  - Forties blend
  - Saharan blend
  - Statjord
- Medium crude
  - Arabian
  - Arabian extra light
  - Arabian heavy
  - Arabian light
  - Arabian medium
  - Iranian heavy
  - Alamo
  - Oseberg
- Heavy crude
  - Alba
- Very heavy crude
  - Boscan
- Light fuel oil
  - Unleaded Interm Gasoline
  - Fuel oil N°1 (Avjet A)
  - Gasoline blending stock (Alkylate)
  - Gasoline blending stock (Reformate)
- Marine diesel
  - Marine diesel
- Medium fuel oil
  - Fuel oil N°2 (diesel)
  - Fuel oil N°2 (Ho/diesel)
  - Intermediate fuel oil 180
- Heavy fuel oil
  - Intermediate fuel oil 360
- Very heavy fuel oil
  - Erika
  - Prestige

Figure 8: Oil type list available within the OSERIT oil database (from Dulière et al., 2013a)

4 - A system-to-system interface between CleanSeaNet and OSERIT

Since oil spill modelling provides valuable information which could assist in the identification of vessels responsible for the illegal discharge (spill backtracking) and in the prediction of spill drift and fate (spill forecasting) to support decision making for pollution response activities, EMSA has implemented a generic system-to-system interface between the CleanSeaNet Data Centre and a generic 'Model Service Provider' in order to perform the following actions in a fluent and fully automatized way:

1. Submission of a simulation request package to the model service provider through a dedicated sftp box and/or an OGC Web Processing Service.
2. [Execution of the simulation request by the model service provider]
3. Uploading in a dedicated sftp box of an output package that includes the simulations results in a file format that can be directly ingested in the CleanSeaNet Data Centre.
4. Visualisation of the simulation results in the CleanSeaNet GIS viewer.

The request package is made of

- One "package information XML file" that describes the content of the package.
- One "Oil Spill feature GML file", i.e. a file format routinely used by the CleanSeaNet Data Centre to store the characteristic of any possible oil spill detections. This includes the geometry of the spill (a polygon that describes the external contour of the slick, as well as data about its length, width and area) and ancillary data such as the CleanSeaNet spill identifier, the scene acquisition time and if available the oil type, the weathering status (in days adrift), the oil thickness, viscosity and density. These last 5 elements of information are only available for the confirmed spills.
- One "process request XML file", i.e. a file that fully describes the requested model set up. This includes at least the start time of the simulation and its duration; the number of Lagrangian particles, the output time step and the simulation type (forward or backward in time). In specific cases, the file can also include or supersede the exact oil type, thickness, density and viscosity, total spill volume, discharge duration.

The output package is made of

- One "package information XML file" that describes the content of the package.
- One "model output description file" that provides a model output summary, including the trajectory of the centre of mass of the spill.
- A series of "Oil Spill feature GML file" (one file per model output time step) that can be directly inserted in the CleanSeaNet Data Centre to describe the simulated time evolution of the surface slick characteristics: external contour(s) and surface oil thickness, viscosity and density.
- Optionally, a "netcfd file" describing the oil concentration in the water column.

EMSA and RBINS have jointly implemented, tested and fine-tuned this system-to-system interface between CleanSeaNet and OSERIT for the North Sea and the English Channel. Four different use-case scenarios have been identified, namely:

- the automatically triggered forecast and backtrack scenarios that are generic scenarios to be applied to every satellite-detected oil slicks reported by CleanSeaNet on the OSERIT domain and
- the manually triggered forecast and backtrack scenarios that allow CleanSeaNet users to refine the results provided by the automatically triggered scenarios.

4.1 - Scenario 1: Automatically triggered forecast

The automatically triggered forecast scenario consists of an instantaneous release of 1000 Lagrangian particles that are randomly scattered at the sea surface within the given closed polygon provided in the 'process request package'. The 3D drift simulation takes into account the drift due to current, wind and waves (stokes drift), oil endogenous spreading at the sea surface, natural vertical dispersion and horizontal turbulent diffusion if the oil Lagrangian particle is within the water column.

Because no reliable information on the oil type and initial oil weathering is available from the satellite image, oil weathering is not computed in this scenario (i.e. no oil evaporation, emulsification and time evolution of the oil density and oil viscosity at the sea surface). However, oil spreading and natural dispersion are computed assuming that the spilt oil closely behaves like a fresh marine diesel.

The simulation length is set to 72 hours.

4.2 - Scenario 2: Automatically triggered backtrack

The automatically triggered backtrack scenario will consist in an instantaneous release of 1000 Lagrangian particles that are randomly scattered at the sea surface within the given closed polygon provided in the 'process request package'. The 2D surface backtracking takes into account the drift due to current, wind and waves as well as horizontal diffusion at the sea surface. The horizontal diffusion aims at providing some confidence interval for identifying potential polluters.

In this automatically triggered backtrack scenario, oil spreading, oil weathering and natural vertical dispersion and resurfacing processes cannot be computed.

The backtrack simulation length is set to 24 hours.

4.3 - Scenario 3: Manually triggered forecast

The manually triggered forecast scenario aims at offering CleanSeaNet users the possibility to refine the automatically triggered forecast scenario.

In comparison with the automatically triggered forecast scenario, the CleanSeaNet users are able to

- specify the number of Lagrangian particles to be used (with a maximum of 2500 particles);
- specify the starting time, the duration of the leak, the depth of the release and the oil discharge in case of a continuous release;
- specify the oil type;

- supersede the initial oil viscosity [in cSt at 15°C] and density [in kg/m^3 at 15°C];
- compute the oil weathering with the limitation that the initial weathering state is fresh oil.

4.4 - Scenario 4: Manually triggered backtrack

The manually triggered backtrack scenario aims at offering CleanSeaNet users the possibility to refine the automatically triggered backtrack scenario, provided the possibilities and limitations offered by the 'process request file'. Taking into account the fact that OSERIT limits backtracking simulations to 2D surface drift, this means:

- Specifying the number of Lagrangian particles to be used (with a maximum of 2500 particles);
- Specifying the starting time, the duration of the leak, the depth of the release and the oil discharge in case of a continuous release.

4.5 - Performance of the system-to-system interface

The interface is currently passing its final acceptance tests. The tests show that the automatically triggered forecast and backtrack simulation results are made available in the CleanSeaNet GIS viewer within 15 minutes after the spill alert (Figure 9).

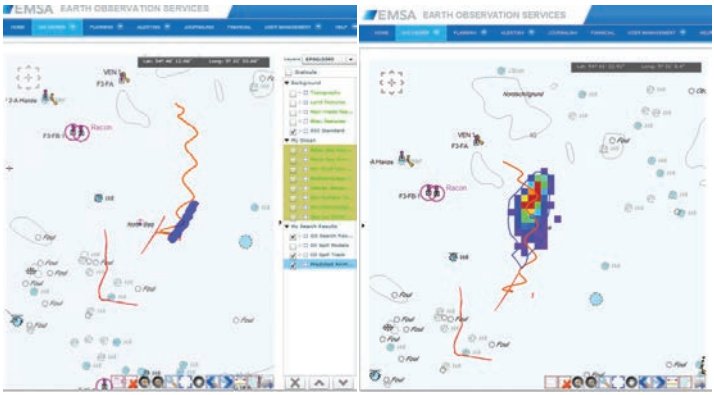

Figure 9: OSERIT forecast simulation results as presented in the CleanSeaNet GIS viewer 15 minutes after the spill alert. Are shown, the detected oil spill (in red, left and right), the trajectory of the centre of mass of spill (in red, left and right), snapshot of the slick contour (in blue, left) and snapshot of the oil concentration (multicolour, right). A control panel (not shown) allows an easy navigation in time

5 - The Flinterstar incident

5.1 - The incident

At 04:10 CET on Oct. 6th 2015, the LNG tanker *Al Oraiq* entered into a collision with the general cargo vessel *Flinterstar* in the coastal shipping lane 'Scheur' located in the Belgian Territorial Sea nearby the port of Zeebrugge (Figure 10). The *Al Oraiq* remained stable, suffering limited hull damage at its bow, and did not release any oil or other harmful substances; the tanker soon sailed to the port of Zeebrugge for inspection. The *Flinterstar* however was severely damaged in its mid-section, and

the vessel was pushed on a very shallow (-10 m) coastal sandbank named 'Wandelaar' where it sank as a 'total loss' at position 51°24.007'N – 003°03.717'E, at merely 8 km NW of the port of Zeebrugge.

Figure 10: Location of the *Flinterstar* wreck

There was an almost continuous release of fuel oil from the wreck of the Flinterstar, from the start of the incident on Oct. 6th until the end of the fuel removal operations on Nov. 2nd 2015, requesting the activation of 3 oil recovery vessels with sweeping arms (Figure 11). It is worth noting that booms and skimmers activated on the first day of the pollution and deployed in a U-configuration were unable to contain the HFO, probably due to the strong tidal currents in the area and the strange behaviour of the apparently quite fluid HFO which got mixed with gasoil. Furthermore, it was observed that the spilt HFO sometimes had a tendency to disappear from the sea surface and to drift sub-surface: thicker oil films consisting of true oil colour were mainly observed nearby the wreck site, although the observed oiled (sheen) area often amounted to several km². Moreover, in calmer wind conditions, the previously submerged HFO sometimes tended to reappear at the surface. This "yo-yo" effect puzzled the experts for 2 weeks until the physical-chemical analysis of a weathered oil sample taken at sea showed that the weathered oil has a density (1.011) comparable to the seawater density near Zeebrugge (1.02 at temperature of 14°C and salinity of 30) (Table 1; Anonymous, 2016).

Figure 11: Oil spill response at sea during the *Flinterstar*: (a.) ARCA; (b.) INTERBALLAST I; (c.) HEBOCAT 7.

	HFO tank 1	HFO tank 3	HFO tank 4	ARCA sample
Physical properties				
Viscosity @15°C (mPa.s)	1982	1496	2150	78000
Density @ 15°C	0.991	0.955	0.993	1.011
Water content (%)	0%	0%	0%	61%
Chemical composition				
Content (% wt.)				
- SARA analysis:				
- Saturates	34.7	48.5	32.8	37.3
- Aromatics	33.7	28.2	32.3	30.2
- Resins	19.8	19.5	24.9	19.9
- nC_5-asphaltenes	11.7	3.8	10.0	12.6
- Asphaltenes and waxes:				
- *nC7*-asphaltenes	8.3	1.7	9.3	11.9
- Waxes	7.1	2.6	7.0	5.5

Table 1: Physico-chemical characterisation of HFO reference samples (Ref.: Cedre RPTs L15.25 & L16.08)

Based on aerial surveillance and oil recovery data, it is estimated that ca. 200 m³ of fuel oil (mixtures of HFO and gasoil) was released in the marine environment over that 1-month period and ca. 50 m³ was mechanically recovered. More precisely, for the first week following the initial collision, an oil spill in a continuous order of magnitude of 50 – 100 m³ was observed at the sea surface (Figure 12); although fresh oil releases were continuously observed from the *Flinterstar* wreck, the volumes observed in the second week decreased drastically (with estimated volumes in the order of 1- 10 m³). At the end of the second week however, cargo suddenly started shifting during the oil removal operations resulting in a pierced fuel tank and new significant releases of oil from the *Flinterstar* wreck, leading to observed oil volumes in the order of 50 m³ or more. Thereafter, only minor oil releases (order of 1 m³ or less) were observed until the end of pumping operations on Nov. 2nd 2015.

5.2 - Monitoring and surveillance of the oil and its fate/behaviour

Given the gravity of the situation, which was not catastrophic but severe (total loss

of a vessel; significant maritime safety and environmental impact risks; oil spill of >100 m³), Belgium's national contingency plan for the North Sea – the so-called General Emergency and Intervention Plan North Sea - was immediately activated. The environmental monitoring and surveillance programs involved in-situ sampling (oil and seabed), remote sensing observations and modelling.

For instance, in the period between 06 Oct. – 02 Nov.2015, 40 consecutive flights, or 55 "on task" flight hours were performed by the remote sensing aircraft for aerial monitoring of the oil pollution and aerial assistance of response units. Further airborne assets that were deployed for aerial monitoring of the spill and incident site consisted of a helicopter and UAVs. 4 CleanSeaNet satellite images were received on a regular basis offering valuable snapshots of the overall extent of the accidental oil pollution, and resulted in a total of 9 probable oil spill detection alerts that were received through CleanSeaNet and were verified and confirmed as mineral oil in the field by the Belgian authorities.

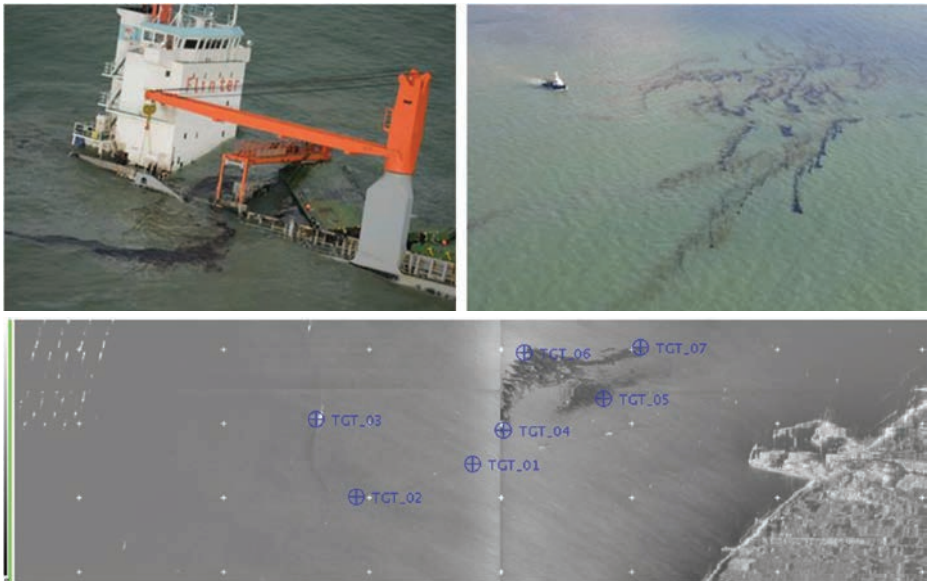

Figure 12: Illustrations of *Flinterstar* wreck and the significant initial oil releases on Oct.6th 2015: SLAR image + photos taken from surveillance aircraft

Oil samples were taken in the field throughout the incident period. Reference samples of the HFO were first obtained from the ARCA (sample of recovered HFO taken o/b ARCA); later on during the oil removal operations reference samples were also obtained from the different HFO fuel tanks. The fingerprinting analyses performed on these samples by the RBINS chemical lab in accordance with the CEN methodology could positively match the field samples taken at sea and on the beaches with the reference samples, demonstrating a clear causal link. The fingerprinting analysis performed on the reference samples also indicated that at least part of the HFO that was pumped out the wreck a couple of weeks after the start of the incident had already

weathered to a certain degree inside the wreck. Reference samples were also sent to Cedre for a detailed physico-chemical characterisation of the HFO present on board the *Flinterstar* to obtain a better understanding of the strange behaviour of the heavy fuel when released into the sea and to improve released oil volume estimations.

Since the incident took place in very shallow and vulnerable coastal waters and the spilt oil posed an immediate risk for the nearby Belgian and Dutch shores, OSERIT was activated to evaluate and predict the drift and behaviour of the spilt oil as good as possible. Based on factual data (known location of the wreck and information contained in the *Flinterstar*'s last bunker sheet), a series of 3D simulations have initially been performed assuming continuous release from a partially immerged ship wreck of fresh HFO-300 and MDO (marine diesel) and validated against the daily pollution observation reports from the various surveillance platforms (Figure 13).

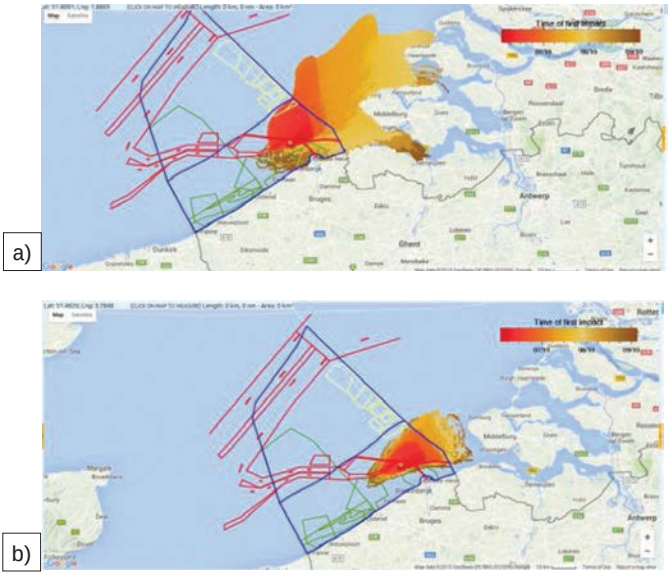

Figure 13: OSERIT 3-day oil drift model simulation for the period 06 Oct. – 09 Oct. 2015 of 75 m³ of fresh HFO-300: (a.) area impacted by surface slick(s); (b.) area impacted by naturally dispersed oil.

Although they were already providing useful information for the response planning, this first series of simulation were not able to simulate and explain the observed "yo-yo" effect, what lead to overestimation of the oil fraction remaining at the sea surface; an overestimation of the sea surface area impacted by the surface oil slicks and in case of North-East wind, an overestimation of the beaching risk (i.e. false alert for the civil protection in charge of the beach cleaning operations). Although dozens of calibration simulations were performed to try to adjust the discharge rate at the breach, the natural-dispersion rate and the oil distribution size droplets, the simulations were not totally satisfying until it was demonstrated, through oil sample analyses, that the HFO had already started weathering in some fuel tanks and that the

density of the oil samples taken at sea was much higher than expected. Once the HFO density value was set to the observed value, OSERIT started to simulate the observed yo-yo effect, leading to much more accurate oil spill drift and predictions.

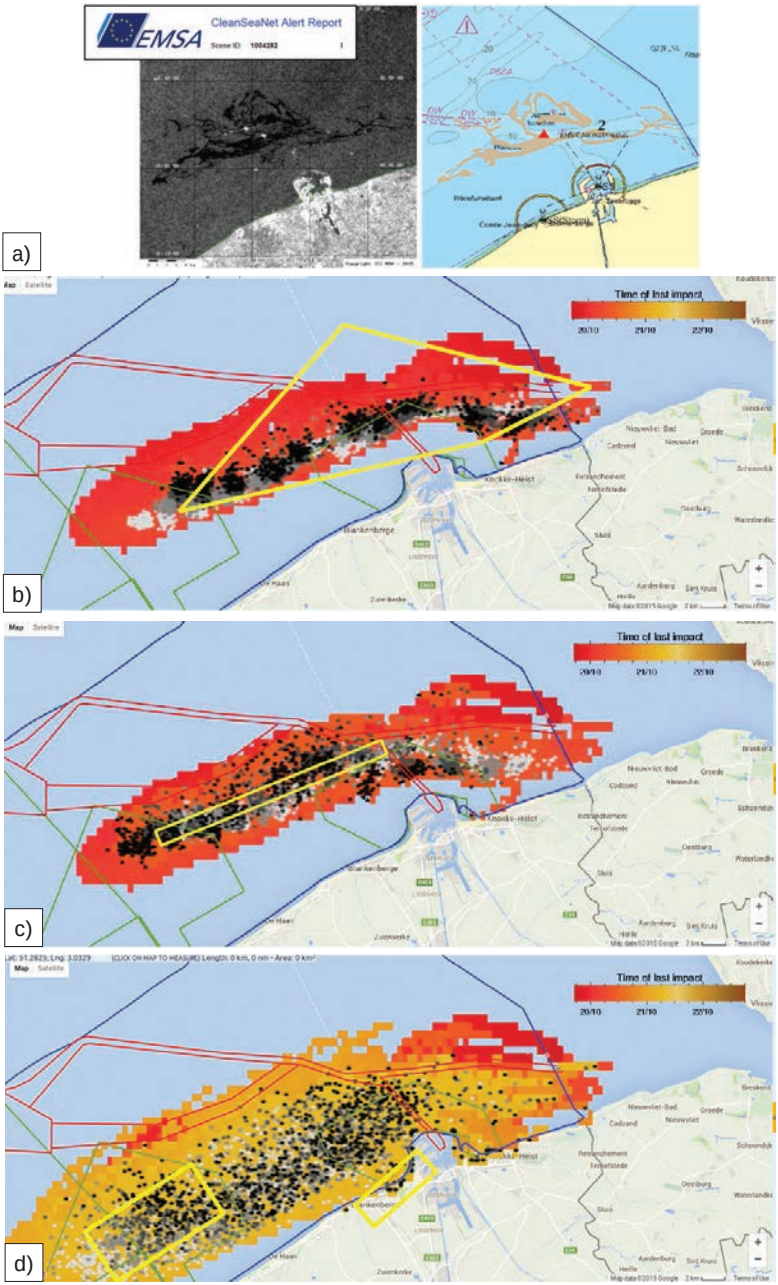

Figure 14: Example of a manually triggered simulation results of the system-to-system interface between CleanSeaNet and OSERIT for CleanSeaNet scene ID 1004282 (19 Oct, 17:30 UTC) at time steps for which aerial observations were available (yellow rectangle): (b.) for flight 15179 (20 Oct. 07:00), (c.) flight 15181 (20 Oct, 12:30 UTC) and (d.) flight 15182 (21 Oct 6:30 UTC). Black dots show the simulated position of the Lagrangian particles at the sea surface at the specified time; dark grey dots one hour earlier and light grey dots two hours earlier.

Although the system-to-system interface was not operational yet at that time, a preliminary version of the interface has been applied on the CleanSeaNet scene ID 1004282 (19 Oct., 17:30 UTC) (Figure 14a). The simulation corresponds to a manually triggered simulation in which the oil density has been set to 1.011. The simulation results perfectly matched the aerial observations made during surveillance flights 15179 (20 Oct, 7:00 UTC), 157981 (20 Oct, 12:30 UTC) and 15182 (21 Oct, 6:30 UTC) and could partially explain the minor stranding of tar balls at the west of Zeebrugge between Blankenberge and Zeebrugge at the early morning of the 21 Oct (between 2:00 and 4:00 UTC). The simulation also forecasted some risk of stranding at the East of Zeebruges on the 21 Oct, but these did not occur.

6 - Conclusions

In order to further improve the chances of identifying potential oil spill polluters and also to automatically provide CleanSeaNet users with a preliminary risk assessment for any satellite-based oil slick detection in the North Sea and the English Channel, a system-2-system interface between EMSA's CleanSeaNet and the Belgian advanced 3D oil spill drift and fate model OSERIT has been implemented. Four different use-case scenarios have been identified, namely

- the automatically triggered forecast and backtrack scenarios that are generic scenarios to be applied to every satellite-detected oil slicks reported by CleanSeaNet on the OSERIT domain and
- the manually triggered forecast and backtrack scenarios that allow CleanSeaNet users to refine the results provided by the automatically triggered scenarios.

Although CleanSeaNet users will have access to this new system from early 2017 onwards, the preliminary and tests results have already demonstrated the usefulness of the system-to-system interface. During the *Flinterstar* incident in 2015, SAR images have been successfully used, in combination with other aerial observations at the time of the incident, to validate the OSERIT model simulations and demonstrate their accuracy.

6 - Acknowledgements

The implementation of the system-to-system interface between CleanSeaNet and OSERIT has been financed by the contract EMSA/NEG/69/2013. Sébastien Legrand warmly acknowledges Anne Mari e Hayes, Gianluca Luraschi and Jose Matos from the "European Maritime Safety Agency's Unit C – Operations" as well as Nino Pace from "Advanced Computer Systems" for their active collaborations.

References

Anonymous (2016) The Flinterstar incident. Report OTSOPA 16/8/Info.1 (L) submitted by Belgium and presented at OTSOPA 16, 24 – 26 May 2016, Scheveningen (The Netherlands), 11 pp.

Bonn Agreement (2016) Chapter 20 – Inventory of assessment tools (computer models), Bonn Agreement counter-pollution manual, technical report.

V. Dulière, F. Ovidio and S. Legrand (2013a) Development of an Integrated Software for Forecasting the Impacts of Accidental Oil Pollution- OSERIT. Final Report. Brussels: Belgian Science Policy Office 2013 – 65 p. (Research Programme Science for a Sustainable Development)

Lagring, R., Degraer, S., de Montpellier, G., Jacques, T., Van Roy, W. and Schallier, R. (2012) Twenty years of Belgian North Sea aerial surveillance: A quantitative analysis of results confirms effectiveness of international oil pollution legislation. Marine Pollution Bulletin, 64, 644-652. Doi:10.1016/j.marpolbul.2011.11.029

Fay, J. A. (1971) Physical processes in the spread of oil on a water surface. Proc. Joint Conf. Prevention and Control of Oil Spills, Washington, DC.

Fingas, M. (1996) The evaporation of oil spills: variation with temperature and correlation with distillation data. In: Proceedings of the 9th Arctic Marine Oil Spill Program (AMOP), technical seminar, Canada. Environment Canada, Ottawa, Quebec, Canada, pp. 29-72.

Fingas, M. (1997) The evaporation of oil spill: prediction of equations using distillation data. Proceedings of the 20th Arctic and Marine Oil Spill Program (AMOP), Technical seminar. Environment Canada, pp. 1-20.

Fingas, M. (2011) Oil spill science and technology. Edited by M. Fingas, Elsevier/Gulf Professional Publishing, Boston, MA, ISBN-13: 978-1856179430, 1192 pp.

French McCay, D. (2003) Development and application of damage assessment modeling: example assessment for the North Cape oil spill. Marine Pollution Bulletin, 47, pp. 341-359.

Garcia-Matinez, R. and H. Flores-Tovar (1999) Computer Modeling of Oil Spill Trajectories with a high Accuracy Method. Spill Science & Technology Bulletin, 5 (5/6), pp. 323-330.

Jones, R.K. (1997) A simplified pseudo-component oil evaporation model. In: Proceedings of the 20th Arctic and Marine Oil Spill Program (AMOP) Technical seminar. Environment Canada, pp. 43-61.

Lehr, W.J., R.J. Fraga, M.S. Belen, and H.M. Cekirge (1984) A new technique to estimate initial spill size using a modified Fay-type spreading formula. Marine Pollution Bulletin, 15, pp. 326-329.

McAuliffe, C.D. (1987) Organism exposure to volatile/soluble hydrocarbons from crude oil spills – a field and laboratory comparison. Proceedings, 1987 Oil Spill Conference, Baltimore, Maryland, USA, pp. 275-288.

Scory, S., 2005. The use of mathematical models for estimating oil pollution damage at sea, in: Maes, F. Ed. Marine resource damage assessment: liability and compensation for environmental damage. pp. 211-252.

Tkalich, P., and E.S. Chan, 2002. Vertical mixing of oil droplets by breaking waves. Marine Pollution Bulletin, 44, pp. 1219-1229.

Wang, S.D., Y.M. Shen, Y.K. Guo, and J. Tang, 2008: Three-dimensional numerical simulation for transport of oil spills in seas. Ocean Engineering, 35, pp. 503-510.

Remote sensing for oil spill response: operational aspects

M. Januszewska and S. Hall, OSRL, United Kingdom

Content

- About Oil Spill Response Ltd (OSRL)
- OSRL - Remote sensing by satellite
- Satellite JIP recommendations
- Satellite remote sensing in preparedness
- OSRL – Remote sensing by aircraft
- Global Response Network remote sensing team
- Emerging technology i.e. tethered balloons, Unmanned Aerial Vehicles (UAVs)

1 - About OSRL

Oil Spill Response Limited (OSRL) is the largest international industry-funded cooperative which exists to respond to oil spills wherever in the world they may occur, by providing preparedness, response and intervention services. OSRL is wholly owned by most of the environmentally responsible oil and gas companies, and membership represents the majority of global oil production. OSRL currently employ 300 people across 9 locations around the world.

Figure 1: OSRL membership

2 - OSRL - Remote sensing by satellite

2.1 - Satellite Service

OSRL has a contract with (MacDonald, Dettwiler and Associates Ltd (MDA) Geospatial Services to provide satellite imagery in an oil spill incident using synthetic aperture radar (SAR) and optical sensors. MDA have a profile of what OSRL expects in an incident which ensures we receive standard outputs that our members can clearly understand. OSRL can also specify the area of interest (AOI) and the acquisition frequency. Oil analysis is completed in near real time, the aim being four hours from receipt of the radarsat imagery at the Canadian data processing facility (when using the satellite RADARSAT-2) but typically imagery is interpreted and delivered in less than one hour. Post processing of the data by an MDA analyst mark oil spill targets (polygon overlays with comments and coloured confidence categories) onto the satellite image report.

2.2 - Satellite Joint Industry Project (JIP) recommendations

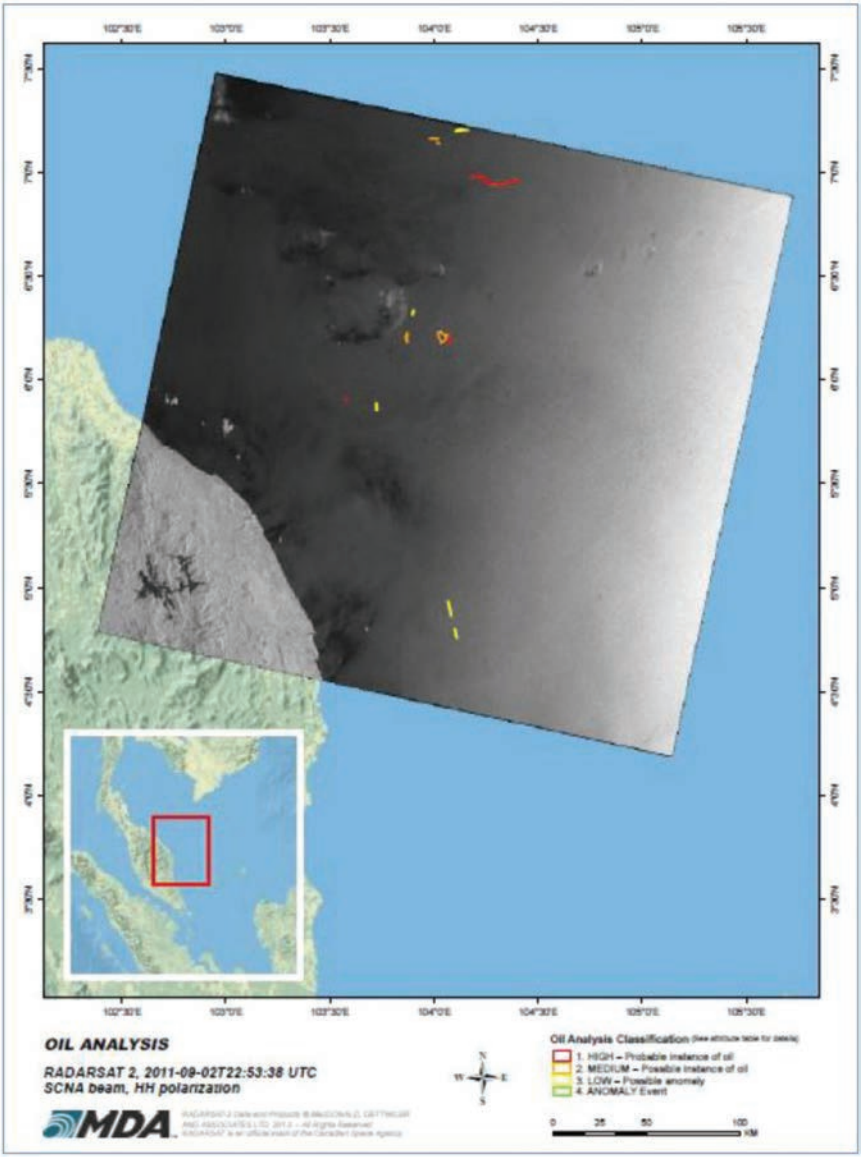

Figure 2: OSRL satellite service

The OSR-JIP represents the oil industry's consensus view on good practices related to oil spill preparedness and response. Under the category Surveillance, Modelling and Visualisation (SMV) there is a report published on the JIP website titled 'An Assessment of Surface Surveillance Capabilities for Oil Spill Response using Satellite Remote Sensing'. Within the report are a number of recommendations including using satellite

imagery in exercises, training on a regular basis, ensuring delivery of imagery is within 2-3 hours from data acquisition and implementing satellite monitoring programmes.

2.3 - Satellite remote sensing in preparedness

There are a number of satellite preparedness services that can be provided to industry including;

- Shoreline habitat mapping within oil spill contingency plans (OSCPs)
- Tactical response plans within OSCPs
- Change detection (seasonal environmental analysis)
- Bathymetric mapping (vessel depth surveys)
- Ice tracking (density pathways)
- Satellite response plans (OSCPs)
- Offshore monitoring
- Exercises
- Shoreline pre-spill analysis (OSCPs)

3 - OSRL – Remote sensing by aircraft

3.1 - Regionally dedicated aircraft

UK

- Aerial surveillance only
- Dedicated to the UKCS region
- Aircraft: Navajo PA-31
- Turret with visual, IR, UV
- Operated by 2excel
- Based in Doncaster
- 1hr mobilisation in daylight hours
- Low flying rate

West and Central Africa (WACAF)

- Surveillance + tier 2 dispersant
- Dedicated to West and Central Africa
- Bandeirante aircraft
- Cover from the western boundary of Côte d'Ivoire in the NW - southern boundary of Angola + adjoining sea for a distance of 150 miles from the coast
- Dispersant stockpiles
    - o Cote D'Ivoire
    - o Equatorial Guinea
    - o Angola
    - o Ghana
    - o Gabon

3.2 - Global Response Network (GRN) remote sensing team

The GRN exists to share information improve spill response performance and provide centres of excellence in spill preparedness, response and recovery techniques. It is primarily for oil spill response organisations to improve their individual performance and effectiveness by fostering collaborative relationships amongst industry and establishing functional teams to exchange operating information and share good practice. There are six operational teams in the GRN which 'remote sensing' is one.

Figure 3: GRN remote sensing team

3.3 - Emerging technology: tethered balloons, unmanned aerial vehicles (UAVs)

OSRL is focusing on two areas (tactical support, short range)

- Improve efficiency of the shoreline/inland survey teams
- Improve encounter rates offshore (traditionally spotter aircraft)

UAVs on the shoreline

Figure 4: Shoreline survey with UAVs

In 2016 OSRL completed a proof of concept demonstration on the shoreline using UAVs to support a shoreline response team. The proof of concept assessed how UAVs

could be used for quick surveying (instead of by foot or helicopter) and to gain access (surveying coastline not accessible or difficult to access by foot), instead of using a helicopter i.e. sensitive sites, rocky shores.

The conclusion (without testing on a spill…) is that UAVs are:

- a very useful tool in the toolbox
- are very spill specific – need to assess the scenario at the time (other methods of surveying will sometimes be preferable i.e. helicopter, foot)
- Most likely to be most useful
  - o Sensitive sites i.e. saltmarsh, mudflats, mangroves
  - o Difficult access sites
  - o Spills where a helo cannot be sourced (poor infrastructure)
- Need to manage the expectations of when UAVs could be used – will not replace foot or helo surveys

Tethered balloons offshore

Figure 5: Offshore survey using tethered balloons

What's the problem with offshore containment and recovery operations?

- Even with the most efficient and effective boom and skimmer systems unless vessels can be directed to the thickest parts of the oil recovery rates will still be low
- We need to improve encounter rates by targeting the thickness patches of oil and improving skimmer effectiveness/efficiency and debris handling

Traditionally spotter aircraft are used but now technology allows an alternative surveillance platform to carry out the task of tactically supporting containment and recovery operations. This technology can also be used to target vessel dispersant spraying and carry out shoreline monitoring i.e. site overview and equipment and personnel tracking.

Advantages

- Real time tactical information, besides visual spotting (a tactical tool!)

- Tracking moving oil (visual spotting)
- Classification of oil targets as recoverable or non-recoverable (i.e. sheen vs. true colour)
- Staying in the recoverable oil as it moves
- Expanding the operating window to low-light conditions
- Eliminating false positives i.e. red tide plankton bloom
- Platform gives height of eye i.e. a 'birds eye view' (usable visual range of the cameras is 1-4nm)
- Multiple sensors (Visual/IR)
- Allows a 'constant stare' through the days operations i.e. up to 12hrs 'hang time'
- System is compact, easily transportable
- Compensates for a lack of dedicated surveillance aircraft or aircraft of opportunity
- Can provide a "feed" to the members Common Operating Picture (COP)

Optimizing the use of aerial surveillance assets in oil spill response operations: the case for using SUAS as a force multiplier in spill response coordination

Lt C.-H. Thouaille, CEPPOL (French Navy counter pollution expertise & response unit), French Navy, France

Abstract

Offshore oil spill response operations, and more generally any maritime operation requiring a high level of situational awareness, often rely on the use of aerial assets to continually monitor the scene. The near constant presence of aircraft on scene presents both opportunities (including but not limited to the ability to continuously monitor the situation as it develops, update the on scene coordinator (OSC: officer in charge of the coordination of units tasked with spill remediation operations at sea), and evaluate the effectiveness of operations on an ongoing basis) and challenges. While there are costs associated with the use of aircraft (both pecuniary and human), the main challenge is of a logistical nature. The availability of aircraft for such operations, the supply train that they rely on, and the relative priority of other concurrent operations also factor in the frequency of their overflights, thus potentially limiting the "refresh rate" available to the OSC. This "refresh rate" has obvious effects on their ability to provide a bird's eye view of operations that can, in turn, have severe consequences on the ability of an OSC to effectively manage oil spill response operations. The wholesale development in availability, at a fraction of the cost previously associated with such systems, of small unmanned aircraft systems (SUAS) in tandem with the advent of cheaper, miniaturized high definition visual and multispectral sensors renders the use of SUAS as a supplementary source of airborne surveillance a very attractive proposition indeed. In order to evaluate the benefits of SUAS in oil spill response operations at sea, CEPPOL has been running a campaign of tests since November 2015.

1 - Introduction

Extensive research efforts have been under way for a decade on the use of unmanned aircraft systems (UAS) in the oil spill response sector. This research, while focusing mostly on military grade UAS, supports the thesis that UAS use in OSR operations provides "value added".

"If a suspect oil leak is detected, the UAS can be [...] vectored to the suspect sight where it can loiter and video record the situation with the side-mounted color or IR camera, providing direct GPS position and visual information to the field control station [...]. A single trained operator of a two man team is all that is required to review and asses the real time information displayed." (Allen & Walsh, 2008)

Our ambition in undertaking this experimental campaign is not to compete with the pre-existing body of research on the topic, but rather to build on what has already been widely acknowledged : namely that "UAS show promise as a tool in oil spill response observation and spotting [...] can provide command and control with additional real-time situational awareness" (Parscal, Ziska, & Williams, 2014) and test whether

these conclusions hold true when transposed to commercially available (off the shelf) consumer oriented SUAS.

With the advent of cheap, mass produced, consumer oriented "drones", the availability of relatively easy to use aerial sensor systems has exploded. Their small size, ease of use and ability to carry light payload (such as high definition video cameras) for up to 25 minutes while streaming back high quality video signals in real time means that with little training, most people are able to operate airborne sensors.

In a field where situational awareness is the only way to ensure the effectiveness of operations, having such sensor systems at one's disposal seems a comparatively cheap way to complete airborne surveillance operations when other, more advanced aircraft (such as specialized helicopters or airplanes) are not available.

While on a purely theoretical basis, the characteristics of commercially available SUAS, as announced by their manufacturers, seem promising, an in situ experimentation protocol seems necessary in order to determine the fitness for use of "off the shelf" systems.

2 - Assumptions & working hypotheses

The following table outlines the assumptions at the core of the working hypothesis used in our experimental protocol:

The experimental protocol currently under way at CEPPOL is designed to test the working hypotheses by testing the validity of each core assumption through the step by step validation of each one of their corollaries.

A1: Core assumption	A1: Off the shelf SUAS offer value added in offshore and near shore oil spill response operations.
A 1: Corollary assumption	A1(i): Flight time & operational radius are sufficient for close range scouting and reconnaissance missions.
	A1(ii): Payload available will successfully be able to detect slicks and stream visual data in real time to the SUAS operator.
	A1(iii): As close range, supplementary sensors, SUAS will better enable on scene commanders situational awareness.
A2: Core assumption	A2: Off the shelf SUAS are deployable at sea, with sufficient ease that the potential disruption they may cause on normal operations (cost) is far outweighed by the added situational awareness (benefit).
A 2: Corollary assumption	A2(i): SUAS operations are compatible with oil spill response operations as carried out onboard OSR vessels.
	A2(ii): Deployment and recovery are sufficiently easy to execute that pilots require minimal training (low investment/high yield) and training time required in order to operate SUAS effectively is reasonably short.

A 2: Corollary assumption	A2(iii): Training and associated costs are reasonably low.
	A2(iv): The extant legal framework allows the use of SUAS in operational scenarios compatible with their intended use.
A3: Secondary assumption	A3: Off the shelf sensors, compatible with SUAS use, provide a human operator the source material to reliably identify, qualify and quantify oil spills remotely.
A3: Corollary assumption	A3(i): Visible spectrum cameras commercially available off the shelf are fit for this purpose.
	A3(ii): Multispectral sensors commercially available off the shelf are fit for this purpose.
	A2(iii): Thermal infrared sensors commercially available off the shelf are fit for this purpose.
Core hypothesis:	Off the shelf SUAS are able to successfully detect slicks at sea as close range airborne surveillance systems while their ease of use ensures that the cost benefit analysis remains firmly on the positive side of the balance.
Secondary hypothesis:	Off the shelf miniaturized imaging sensors (visible and invisible spectrum) can be used in conjunction with SUAS to provide OSCs with better situational awareness.

3 - Experimental protocol: testing the primary hypothesis

Prior to the decision to pursue a campaign of in situ tests with a view to determine the usefulness of SUAS in oil spill response operations, it was necessary to start with a literature review. Research sources cited in the bibliography were reviewed in parallel with information available from recreational "drone" manufacturers and retailers.

3.1 - Technical specifications

On the basis of the technical review, CEPPOL defined the following technical specifications that appeared best suited for compatibility with the current operational framework and standard operating procedures.

Flight parameters	Image	Others
P1: Assisted flight modes (automatic management of stability, attitude, altitude, speed).	P1: Ability to stream back high quality video to operator for slick detection.	P3: Waterproof
		P2: Flight parameters and telemetry available remotely in real time
P1: Automatic stationary flight mode (GPS enabled).	P1: HD video recording.	P1: Does not necessitate a license in order to operate.
P1: Autonomy (18 + minutes).	P1: HD photography.	P1: Available off the shelf for under 5,000 €

P1: Operational altitude: >150m.	P1: Stabilized image (gimbal or software stabilization).	P2: Able to embark additional payload.
P1: Max distance from operator >1000m.	P2: Can be customized (upgrade camera / change sensors).	P1: Ground station, drone & spare parts fit in a backpack.
P: Wind resistance: >20kts	P2: Images can be geotagged.	P2: Ability to track SUAS position (GPS coordinates) in real time.
P2: Operating temperature range: -10°C +40°C		
P2: Ability to return to operator GPS coordinates.		

3.2 - Operational requirements

For SUAS to be of use, they must be compatible with the existing standard operation procedures (SOP) of the organization that will be using them. If not, the adaptations of said SOPs must be minimal. For instance, in order for CEPPOL to find an a priori interest in SUAS as a supplementary airborne surveillance capacity, the following minimum operational requirement have to be met:

- Ability to operate SUAS without embarking additional personnel when conducting spill response operations;
- Ability to deploy and recover the SUAS from a cluttered deck onboard a seagoing vessel;
- Ability to operate SUAS in weather conditions compatible with spill recovery operations (up to sea state 3-4 / winds up to 30kts max);
- Deployment and recovery of SUAS do not interfere with spill cleanup operations;
- SUAS operations do not constitute an additional hazard for personnel involved in ship conduct or spill cleanup operations.

These criteria echo some of the difficulties outlined in (Parscal, Ziska, & Williams, 2014), where it was found that operating SUAS from sea going vessels is possible, but the nature of OSR vessels and the equipment they carry present both opportunities (deck space) and pitfalls (large amount of equipment occupying the space). With a view to facilitate operations, we decided to start our investigations with vertical takeoff and landing (VTOL) capable SUAS. Leading us to begin our investigations with quadcopters.

3.3 - Choice of SUAS

The technical specifications and operational requirements listed in the previous paragraphs served to narrow the field of commercially available systems. A number of contenders were available at the time of purchase, but none that would fit all criteria listed above were then available off the shelf. The technical specifications were further prioritized and CEPPOL acquired a 3DR Solo (see appendix 1) in order to proceed

with the in situ experimentation phase. This particular model met all P1 technical specification except the minimum range of 1000m with live HD video streamed back to the pilot. Given the expected conditions of use (close range slick repositioning, assessment of the effectiveness of spill response operations, increased situational awareness to aid OSC in coordinating vessels…), a distance of 800m from the operator while maintaining live video stream was judged sufficient. Appendix 2 provides an overview of the technical specifications deemed: essential (P1), recommended (P2), and desirable (P3) and matches them against Solo's specifications.

Figure 1: CEPPOL SUAS (3DR Solo & Gopro 3+Black)

3.4 - Systematic testing of assumptions

In order to determine the validity of the core hypothesis formulated during the review process, namely that:

Off the shelf SUAS are able to successfully detect slicks at sea as close range airborne surveillance systems while their ease of use ensures that the cost benefit analysis remains firmly on the positive side of the balance.

Both core assumptions and their corollaries were tested in turn. For the most part, these tests were carried out during oil spill training deployments (half day to a day at sea where various types of equipment are deployed in order to maintain personnel and equipment readiness levels). However, three large scale national oil spill response exercises provided an excellent opportunity to test some of the assumptions in a realistic scenario where SUAS operations had to "fit in" the operational response or be abandoned. These exercises showed, as a preliminary conclusion, that the use of off the shelf SUAS was compatible with the current SOPs and concept of operations without major evolutions.

To this date, all tests performed in determining the fitness for purpose of SUAS as a supplementary airborne sensor to be used in oil spill response operations have been carried out using simulants (rice husks and fluorescein) to model oil slicks. In the absence of actual spills during the various tests, the airborne sensors that equip CEP-

POL's SUAS have not been tested with real oil. Nevertheless, the preliminary conclusions that will be drawn from these tests can then be assessed against a wide body of data available following oil spill response operations worldwide.

Evaluating core assumption 1

Since acquisition, CEPPOL's SUAS has been deployed at sea on 6 occasions to test

A1: Core assumption	A1: Off the shelf SUAS offer value added in offshore and near shore oil spill response operations.
A 1: Corollary assumption	A1(i): Flight time & operational radius are sufficient for close range scouting and reconnaissance missions.
	A1(ii): Payload available will successfully be able to detect slicks and stream visual data in real time to the SUAS operator.
	A1(iii): As close range, supplementary sensors, SUAS will better enable on scene commanders situational awareness.

the validity of the assumptions that support our core hypothesis. Three of these deployments were short training exercises and three of these were large scale national exercises.

Assumption A1 rests on the corollaries listed in the table above. Flight time and operational radius have proved sufficient to successfully survey the area of operations at close range around the OSC's oil spill response vessel (OSRV) and other units deployed to combat simulated oil spills.

The payload available at the time enabled the OSC to verify that the assets he had tasked were indeed deployed in accordance with the operation plan and that they were deployed as effectively as possible. One of the reasons airborne surveillance assets are necessary when dealing with oil spills is the difficulty for crews on a vessel's bridge, to accurately see a slick. When close to sea level, a slick's exact location and size is difficult to identify with any degree of precision. SUAS allow the on scene coordinator a bird's eye view, thus enabling him to see whether the assets at his disposal are in or next to the slick they are tasked with recovering.

Further testing with real oil, and upcoming tests with different payloads (including multispectral and thermal infrared sensors) are expected to further support this preliminary finding. A wide body of evidence exists to back up the part of our core hypothesis that relies on off the shelf optical sensors being able to distinguish oil spills from the air. Technical findings that stem from similar research conducted with different types of UAS also support this hypothesis. In their 2014 paper, Parscal and Ziska provide clear evidence that visual spectrum sensors carried onboard "regular" UAS can and do detect oil slicks (Parscal, Ziska, & Williams, 2014). While the UAS they used in their research and CEPPOL's 3DR Solo differ in size and form, their payload and flight parameters are sufficiently close that we posit that their UAS' ability to detect oil provides sufficient evidence to support corollary A1(ii).

Despite not having been able to test our SUAS against real oil slicks, we consider that

the existing research proves this assumption to be sound.

Corollaries A1(i) through A1(iii) are thus deemed correct. Furthermore, during the maritime prefecture for the Channel and North sea's annual oil spill response exercise, a dense fog covered the entire area of offshore operations. No manned aircraft was permitted to operate due to security concerns. CEPPOL's SUAS suffered no such constraints; it was successfully deployed and recovered after two consecutive missions, providing the OSC with valuable information (including nearby slick positioning) further proving that the use of SUAS in oil spill response operations could provide added value.

Figure 2: Visual detection of rice husk from 100m altitude (SUAS: 3DR Solo & Gopro 3+Black)

Evaluating core assumption 2

A2: Core assumption	A2: Off the shelf SUAS are deployable at sea, with sufficient ease that the potential disruption they may cause on normal operations (cost) is far outweighed by the added situational awareness (benefit).
A 2: Corollary assumption	A2(i): SUAS operations are compatible with oil spill response operations as carried out onboard OSR vessels.
	A2(ii): Deployment and recovery are sufficiently easy to execute that pilots require minimal training (low investment/high yield) and training time required in order to operate SUAS effectively is reasonably short.
	A2(iii): Training and associated costs are reasonably low.
	A2(iv): The extant legal framework allows the use of SUAS in operational scenarios compatible with their intended use.

Core assumption 2 has been less extensively tested. While corollaries (i) – (iii) have been proven correct in the course of our various tests, the constant evolution of the

French legal framework dealing with the use of SUAS proves more elusive.

As evidenced by the repeated use of the SUAS in national exercises, SUAS operations are compatible with spill response operations carried out on specialized vessels. The space available for deployment and recovery is sufficient, these operations do not disrupt the normal operations that take place on deck or on the bridge, and while rough weather conditions can make recovery of the SUAS challenging at times, most responders with regular practice should successfully be able to deploy and recover SUAS. Thus far, only one pilot has carried out live deployments at sea, but all CEPPOL technical staff have had opportunities to practice flying in challenging conditions ashore.

Training an operator to operational standards (ability to deploy and recover the SUAS, ability to perform basic search patterns) can be achieved in a matter of weeks. Anyone can successfully perform basic search patterns at close range. However, recent evolutions in the French legal framework make official training practically unavoidable for personnel likely to operate SUAS at sea in oil spill response operations.

At this stage, SUAS deployment and recovery operations have only been conducted up to winds of 20-25kts. The maximum wind conditions have not been tested thus far. Unpredictable variations in wind force can have a marked impact on the trajectory of SUAS during deployment and recovery where the environment of an OSRV rear platform (largely occupied by spill response equipment) increases the chance of a crash or loss of the SUAS. Operator confidence levels and regularity of training must therefore be considered before deploying in less clement conditions. While corollary A2(ii) is considered proven correct, deployment and recovery operations, at sea, from a vessel equipped with the necessary equipment for oil spill response operations are highly technical and necessitate some practice. The relative difficulty of those operations must not be underestimated.

The financial cost of training is a known quantity. If an operator needs to obtain a professional license, the cost associated with training varies but the mean price of a week-long one on one course represents an expenditure of approximately 2500€. Given the additional freedom afforded to formally trained and recognized operators under French law, such a course is not deemed to be overpriced. Corollary A2(iv) is thus deemed provisionally proven.

Preliminary findings

Tests carried out to this day support the validity of the core assumptions.

Off the shelf SUAS are able to successfully detect slicks at sea as close range airborne surveillance systems while their ease of use ensures that the cost benefit analysis remains firmly on the positive side of the balance.

The core hypothesis recalled above therefore appears to be supported by the evidence collected in the course of CEPPOL's experimentation. Further experimentation will be necessary to determine the exact place of SUAS in oil spill response operations and what, if any, limitations appear when dealing with real oil.

4 - Experimental protocol: underlying assumptions & testing of secondary hypothesis

The secondary hypothesis (recalled below) rests on much the same core assumptions as the primary hypothesis. In fact, it takes as a given the validity of the core hypothesis. Indeed, if our core hypothesis had proven unfounded, the secondary hypothesis would be null and void. Only three additional assumptions are made in reaching our secondary hypothesis. Those are recalled below as well.

A3: Secondary assumption	A3: Off the shelf sensors, compatible with SUAS use, provide a human operator the source material to reliably identify, qualify and quantify oil spills remotely.
A3: Corollary assumption	A3(i): Visible spectrum cameras commercially available off the shelf are fit for this purpose.
	A3(ii): Multispectral sensors commercially available off the shelf are fit for this purpose.
	A2(iii): Thermal infrared sensors commercially available off the shelf are fit for this purpose.
Secondary hypothesis:	Off the shelf miniaturized imaging sensors (visible and invisible spectrum) can be used in conjunction with SUAS to provide OSCs with better situational awareness.

Taking as a given that SUAS can successfully be used to detect slicks at close range, once their compatibility with oil spill response operations has been established, is not a farfetched assumption.

This assumption is supported by the findings of multiple studies - see (Parscal, Ziska, & Williams, 2014), (Allen & Walsh, 2008) & (DeMicco, Nedwed, & Palandro, 2015) for instance. In order to further substantiate this claim, two types of simulants were used. In July 2016, a field test involving the use of both rice husks and fluorescein were performed at sea. The SUAS (3DR Solo & Gopro 3+Black) successfully detected both simulants.

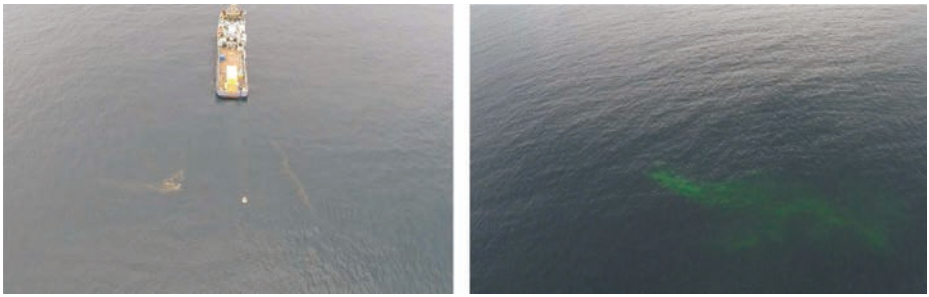

Figure 3: Rice husks (left) and fluorescein (right) detection field tests (alt. 100m), July 2016

Organizations such as the Bonn Agreement rely on visual spectrum observation to detect, characterize and evaluate (quantify) oil spills (Bonn Agreement, 2008). It is worth noting that the Bonn Agreement appearance code (BOAC) is used internationally for

classifying pollutions and quantifying the oil present in a slick. Other leading organizations such as "Cedre" and "Oil Spill Response Limited" also rely on the Bonn Agreement appearance code for this purpose (Cedre, 2004), (Oil Spill Response, 2011).

Given that qualification and quantification of pollutions on the basis of the BOAC is conducted both in situ by observers, and ex situ on the basis of recorded images, and that UAS bearing similar equipment (visible spectrum camera sensors) have successfully been proven to be well suited for oil spill detection, we consider that our field trials, despite the limitation of having been carried out without real oil, support corollary assumption A1(i).

A partnership with French drone maker "Parrot" will allow further testing of assumption A3 in the multispectral band. A multispectral sensor, initially developed for agricultural use, has been added to CEPPOL's SUAS and initial tests of the device seem promising, however at this stage, the first flights performed at the end of July 2016 have only served to validate the viability (flight worthiness, maneuverability…) of this addition to the SUAS.

The setup that we have devised will allow both regular color (visible) video to be streamed back in real time to the operator, as well as access to high resolution multispectral stills to a second operator. One factor that will limit the usefulness of this device is its inability to stream video in real time. Nonetheless, its ability to take pictures at a given rate (at a time interval defined by the operator) and to stream these back to a computer, will mitigate this shortcoming. This has been tested in the course of our experimental protocol.

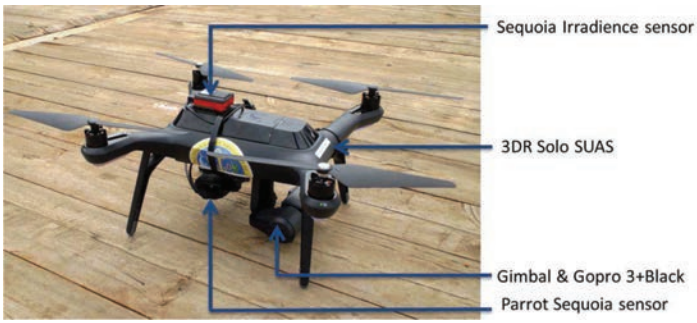

Figure 4: CEPPOL SUAS experimental visible & multispectral bands.

As yet, the fitness for purpose of the Sequoia sensor obtained in partnership with "Parrot drones" has not been tested. Based on the characteristics of the product as announced by the manufacturer, Sequoia operates in the following bands: full RGB spectrum; 550nm wavelength / 40nm bandwidth (green); 660nm / 40nm (Red); 735nm/10nm (Red edge) and 790nm/40nm (Near infrared). It is the last two bands (Red Edge and Near infrared) that the next field trials will be conducted. However, these will need to be conducted in a controlled environment with real oil in order to be conclusive. Literature available on the subject of oil spill detection and classification in these bands (Adamo, De Carolis, De Pasquale, & Pasquariello, 2009) suggests that our future tests with Parrot's agricultural multispectral sensor should be

successful. While further testing of corollary A3(ii) is necessary, we expect it to be successfully proven.

Our last corollary has not been tested yet. Thermal infrared imaging is known to be a highly effective tool in detecting oil spills (Parscal, Ziska, & Williams, 2014) and is widely used by coastguards to detect and monitor spills offshore (Nand Jha, Levy, & Gao, 2008). As such, commercially available sensors such as the small and lightweight FLIR Vue (thermal infrared camera) that can be adapted onto SUAS for a minimal cost (preliminary assesments indicate that adding thermal IR capabilities to CEPPOL's SUAS would cost approximately 2700€) are expected to perform well and succesfully prove corollary assumption A3(iii) thus providing the necessary evidence to prove our secondary hypothesis that "Off the shelf miniaturized imaging sensors (visible and invisible spectrum) can be used in conjunction with SUAS to provide OSCs better situational awareness".

5 - Conclusion: the case for using SUAS as a force multiplier in spill response coordination

The findings outlined throughout this article support the hypothesis that SUAS are not only compatible with oil spill response operations, but also bring added value at a comparatively low price (under 5,000€). Given the relative scarcity of specialized aircraft and therefore their availability for an OSC to be able to supplement the airborne surveillance data made available to him by those aircraft with SUAS at his immediate command appears highly desirable.

The view that to a large extent, oil spill response operations depend on the ability to identify and describe the characteristics of an oil spill and ultimately direct [and coordinate] the necessary resources for cleanup, and that this ability depends, in turn, on the presence and availability of trained personnel in manned aircraft, is shared by many in the oil spill response field (Parscal, Ziska, & Williams, 2014).

The ability afforded by SUAS to frequently update the location of oil patches, track their displacement over time (and confront it with drift models), and review, in real time the effectiveness of spill response operations as posited by Allen and Walsh (Allen & Walsh, 2008) is supported by our findings.

SUAS cannot replace regular surveillance assets as such. Their reach and endurance (among other things) do not permit long term observation of the area of operations. Nevertheless, as a supplementary asset, capable of accelerating the rate at which information is refreshed and made available to OSCs, they seem to have a choice place in oil spill response operations.

As a tool for close range situational awareness augmentation, SUAS do seem to constitute a force multiplier. By accelerating the refresh rate, they bring heightened situational awareness to the on scene coordinator that can review the situation where previously impossible, assess the efficacy and effectiveness of his operations, and thus better coordinate the assets made available to him.

The force multiplier effect is contingent on the good integration of SUAS operations in the wider OSR operations. Sea to air and air to air coordination is paramount so as to

not run the risk of mid-air collision and optimize the use of resources. SUAS could therefore be made available to on scene coordinators as an additional tool, but only be deployed in the absence of other airborne surveillance assets. The extensive testing conducted during large scale exercises also supports this claim.

Appendix 1

Abridged technical data sheet for CEPPOL SUAS

CEPPOL

Type of equipment : SUAS	Version: 01 24/11/2015	N°: 1
Designation: SOLO-CEPPOL-01	Manufacturer : 3D Robotics	

Description
SUAS to be tested for deployment from oil spill response vessel in typical conditions (up to sea state 3-4 / wind < 30kts). **Additional equipment necessary** : GoPro Hero 3+Black (or compatible), tablet (IOS or Android), additional battery, ground station, battery charger, memory cards.

Operational limits		
Maximum wind : 30kts Rain.	Technical data : • 20 minutes autonomy • Max dist. from pilot : 800m • Max altitude (legal) : 150m	Technical data (continued) : • Max speed : 40kts • Resolution : 12MP • Video 1080p at 60fps / 2.7k at 30fps

Characteristics
• Live HD video streamed to pilot ground station / remote control. • Flight data & parameters (technical and geographic) logged and stored after each flight.

Transport	Weight	Dimensions	Misc.
Backpack	1.8 kg	Length / Width: 46cm Height : 25cm	All necessary equipment in transport bag.

Appendix 2

Comparison of initial technical specifications identified vs capabilities of 3DR Solo

Flight parameters	Image	Others
P1: Assisted flight modes (automatic management of stability, attitude, altitude, speed).	P1: Ability to stream back high quality video to operator for slick detection.	P3: Waterproof **Not waterproof. Tested successfully in dense fog conditions.**
P1: Automatic stationary flight mode (GPS enabled).	P1: HD video recording.	P2: Flight parameters and telemetry available remotely in real time. **Via a secondary interface only.**
P1: Autonomy (18 + minutes).	P1: HD photography.	
P1: Operational altitude: >150m.	P1: Stabilized image (gimbal or software stabilization).	P1: Does not necessitate a license in order to operate.
P1: Max distance from operator >1000m. **Actual distance announced and tested up to 800m.**	P2: Can be customized (upgrade camera / change sensors).	P1: Available off the shelf for under 5K €
P1: Wind resistance: >20kts	P2: Images can be geotagged.	P2: Able to embark additional payload.
P2: Operating temperature range: -10°C +40°C		P1: Ground station, drone & spare parts fit in a backpack.
P2: Ability to return to operator GPS coordinates. **Only capable of automatic return to takeoff location.**		P2: Ability to track SUAS position (GPS coordinates) in real time. **Via a secondary interface only.**

- White cells: specifications coherent with the initial specifications list.
- Yellow cells: specifications approaching initial requirements.
- Orange cell: initial specification not met but partly mitigated.

References

3D Robotics. (2015). Solo user manual. Berkley: 3D Robotics.

Adamo, M., De Carolis, G., De Pasquale, V., & Pasquariello, G. (2009). Detection and tracking of oil slicks on sun glittered visible and near infrared satellite imagery. International Journal of Remote Sensing, 6403-6427.

Allen, J., & Walsh, B. (2008). Enhanced Oil Spill Surveillance, Detection and Monitoring through the Applied Technology of Unmanned Air Systems. International Oil Spill Conference, (pp. 113-120).

Bonn Agreement. (2008). The Bonn Agreement Oil Appearance Code. Bonn Agreement Aerial Operations Handbook.

Cedre. (2004). L'observation aérienne des pollutions pétrolières en mer. Brest: Centre de Documentation, de Recherche et d'Expérimentation sur les Pollutions Accidentelles des Eaux.

DeMicco, E. D., Nedwed, T., & Palandro, D. (2015). Small Unmanned Aerial Systems to Determine Slick Thickness. Interspill.

Engelhardt, F. R. (1999). Remote sensing for oil spill detection and Response. Pure Applied Chemistry, 71(1), 103-111.

Fingas, M., & Brown, C. E. (1997). Review of Oil Spill Remote Sensing Technologies. Spill Science & Technology Bulletin.

Laurent, M. (s.d.). Fixed detection devices for oil slick. (Cedre, Éd.) Brest.

Long, M. D. (s.d.). Remote Sensing for Offshore Marine Oil Spill Emergency Management, Security and Pollution Control. Presentation white paper. Aerial Surveillance Systems.

Nand Jha, M., Levy, J., & Gao, Y. (2008). Advances in Remote Sensing for Oil Spill Disaster Management: State-of-the-Art Sensors Technology for Oil Spill Surveillance. Sensors, 8, 236-255.

Oil Spill Response. (2011). Aerial Surveillance Field Guide (éd. 2). Southampton: OSRL.

Parrot drones. (2016). Parrot Sequoia user guide. Parrot.

Parscal, B., Ziska, M., & Williams, J. (2014). A field evaluation of Unmanned Aircraft Systems for Oil Spill Response. International Oil Spill Conference, (pp. 373-387).


4

Session 4

Remote sensing for exploration

Potential of imaging UAVs for coastal monitoring

M. Jaud[a], C. Delacourt[a], N. Le Dantec[a,b], J. Ammann[a], P. Grandjean[c], P. Allemand[c], L. Cocquempot[a]

a) Laboratoire Domaines Océaniques - UMR 6538, Université de Bretagne Occidentale, IUEM, Plouzané, France.

b) Cerema - Centre d'Etudes et d'expertise sur les Risques, l'Environnement, la Mobilité et l'Aménagement, Plouzané, France.

c) Laboratoire de Géologie de Lyon : Terre, Planètes, Environnement - UMR CNRS 5276, Université Claude Bernard Lyon 1, Villeurbanne, France.

Introduction

Metropolitan France has nearly 5,500 km of coastline. This coastal area comprises many environmental issues (great variety of geological features, flora, fauna, diversity of habitats, etc.) and societal issues (housing, transport, tourism, fishing, industrial, energy, etc.). But this coastal area has a strong and varied sediment dynamics, characterized by changes in the coastline, especially under the action of complex hydrodynamic and morphodynamic mechanisms. The National Observation Service DYNALIT (DYNAmics of LITtoral and coastline) was set up by CNRS (Centre National de Recherche Scientifique) to further understand the dynamics of coastal areas. This service aims to acquire, collect and bring coherence to the metrological data for the long term. With this aim in mind, 29 study sites were chosen (Figure 1). These sites are spread all along the French coastlines (metropolitan and overseas) and are representative of the different coastal contexts (sandy coasts, cliffs, estuaries). The objective is to understand the processes involved in the coastal dynamics. The parameters measured in this perspective are the topography, the bathymetry and the sea states.

Figure 1: Localization of DYNALIT study sites

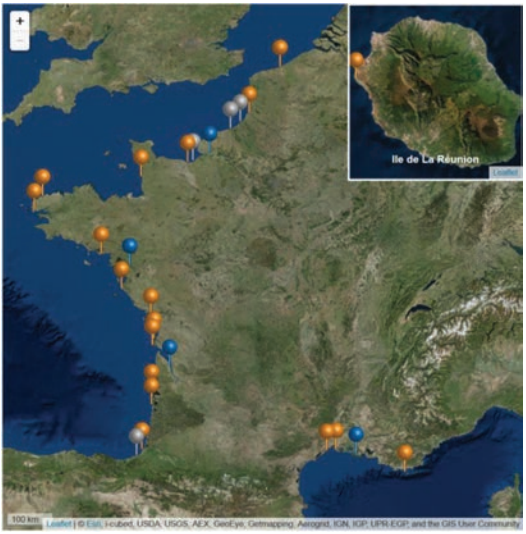

1 - Constraints on the survey

The diachronic measurement of these parameters thus calls for the development of specific tools and methods to meet specifications, which require:

- repeated acquisitions, with a frequency ranging from several days to several decades;
- flexibility in order to make surveys at key dates (tides, post-storm surveys ...) and to be able to adapt to weather constraints;
- limited acquisition time to adapt to tidal phenomena;
- ability to perform surveys on sites where access may be difficult;
- preservation of sites and respect for public space;
- equipment resisting to coastal conditions (salt air, wind, spray ...).

For many years, the measurement of these parameters was performed by on-board sensors from ships, aircrafts or satellites as well as by in-situ measurements through DGPS cross-shore profiles.

Nevertheless, the development of new miniaturized image sensors (digital cameras, thermal sensors, hyperspectral, LIDAR, etc.) and positioning systems associated with the development of new platforms such as Unmanned Aerial Vehicles (UAVs) lead to the emergence of new coastal monitoring strategies. Indeed, those combined techniques are offering a synoptic vision combined with better spatial resolution and accuracy at lower costs.

The technological improvements on platforms and miniaturization of imaging and positioning sensors can meet these challenges.

2 - Examples of UAV platforms

The laboratory Domaines Océaniques performs drone surveys of the coastline since 2006, by adapting the DRELIO system (Drone Helicopter Environment) to fit with the study issues and innovations offered by the market (Figure 2).

The first drones used for coastal monitoring were Pixy flying wings developed by IRD (Research Institute for Development) requiring large areas for takeoff and little wind. Then, therma engine helicopters with significant payload capacity were used but were difficult to pilot. Subsequently, these helicopters were equipped with autopilot. But the revolution in the sphere of drones was the arrival of electric multicopter UAVs, more stable in flight, more reliable and easier to use. However, the carrying capacity of these UAVs is limited (a few hundred grams to several kilograms depending on the model) hence the miniaturization of sensors.

Figure 2: Various models of drones implemented by the laboratory Domaines Océaniques since 2006: (a) Pixy wing, (b), (c), (d) thermal helicopters, (e) hexacopter, (f) octocopter.

For photogrammetry, DRELIO 10, the model currently used by the Laboratory Domaines Océaniques, is an electric hexacopter UAV with a diameter of 0.8 m (Figure 3). This UAV is equipped with a collapsible frame allowing easy transportation. It weighs less than 4 kg and can handle a payload of 1.6 kg. The flight autonomy of DRELIO 10 is about 20 min. It is equipped with a reflex camera Nikon D700 with a focal length of 35 mm, taking one 12 Mpix photo in intervalometer mode every 2 seconds. The camera is mounted on a tilting gyro-stabilized platform. The flight control is run by the DJI® software iOSD. Although DRELIO 10 is able to perform a semi-autonomous flight, take-off and landing, ground station software is used to control the UAV during the flight.

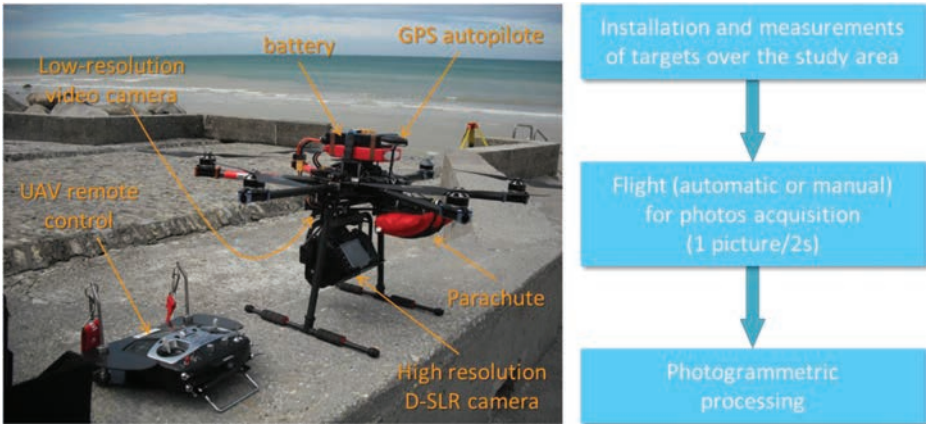

Figure 3: DRELIO 10 system configuration and main steps during a drone survey.

3 - Survey protocol

In practice, targets have to be installed over the studied area. These targets, whose position is precisely measured by RTK DGPS (Real-Time Kinematic Differential GPS), serve as control points and are used for data georeferencing as well as for improving the quality of the photogrammetric processing. The flight for photographic acquisition can be then performed. The current regulations limit the flight altitude to 150 m, but

below this limit flight altitude can be adjusted according to the study issue. Flights at lower altitudes will limit the footprint of the images and therefore the imaged area, but will improve the spatial resolution of the data. When the drone has landed, the photographs are downloaded and checked. Another flight can be conducted immediately after replacing the batteries. It takes 1 to 2 hours and three operators to conduct a complete survey of an area of 50,000 m².

4 - Data processing

The data are processed a posteriori, using dedicated software. These software solutions are based on stereophotogrammetry, a process using stereoscopy. Many software solutions are now available, including the widely used PhotoScan® Pro, an easy to handle software, developed by Agisoft© and the open-source MicMac® tools developed for many years by IGN© (National Institute of Geographic and Forestry Information).

Two types of products are generated by this photogrammetric processing (Figure 4):

- an orthophotograph or orthoimage (planimetric representation, georeferenced and geometrically corrected, which can be superimposed on a map);
- a Digital Elevation Model (DEM), representing 3-dimensional topography of the studied area.

For a flight at 100 m of altitude, the spatial resolution of the orthophoto is about 1.5 cm and the spatial resolution of the DEM is about 3 cm. The accuracy, depending on the number of targets, their spatial distribution and the quality of the GPS measurement, is of the order of 3 cm.

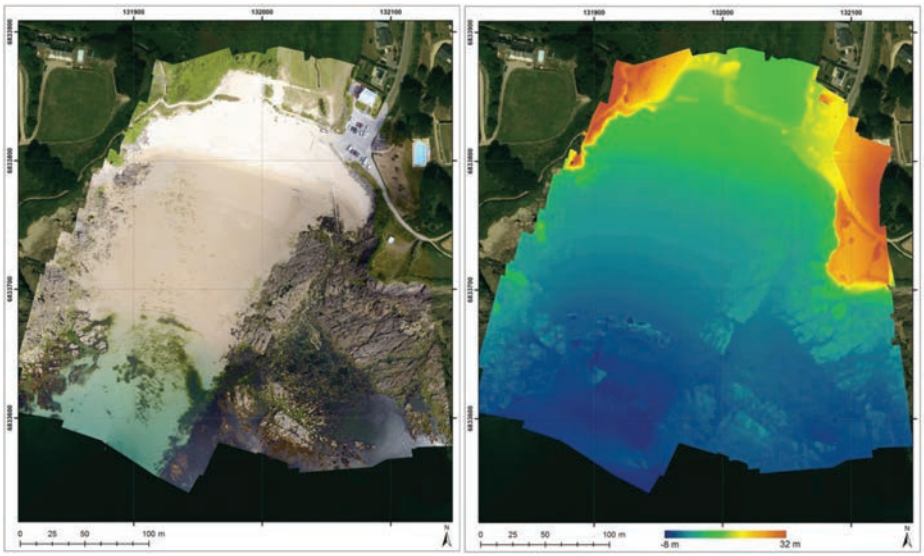

Figure 4 : Orthophotograph and Digital Elevation Model (DEM) of the beach of Porsmilin (computed from 72 photographs collected in June 2015)

5 - Examples of applications

Repeated surveys of the same study site thus enable a multi-temporal comparison of orthoimages and DEM (Figure 5). From these comparisons, it is possible to deduce the morphodynamic evolution of a site and to link this evolution with the hydrodynamic forcing, weather forcing or anthropogenic forcing affecting the site.

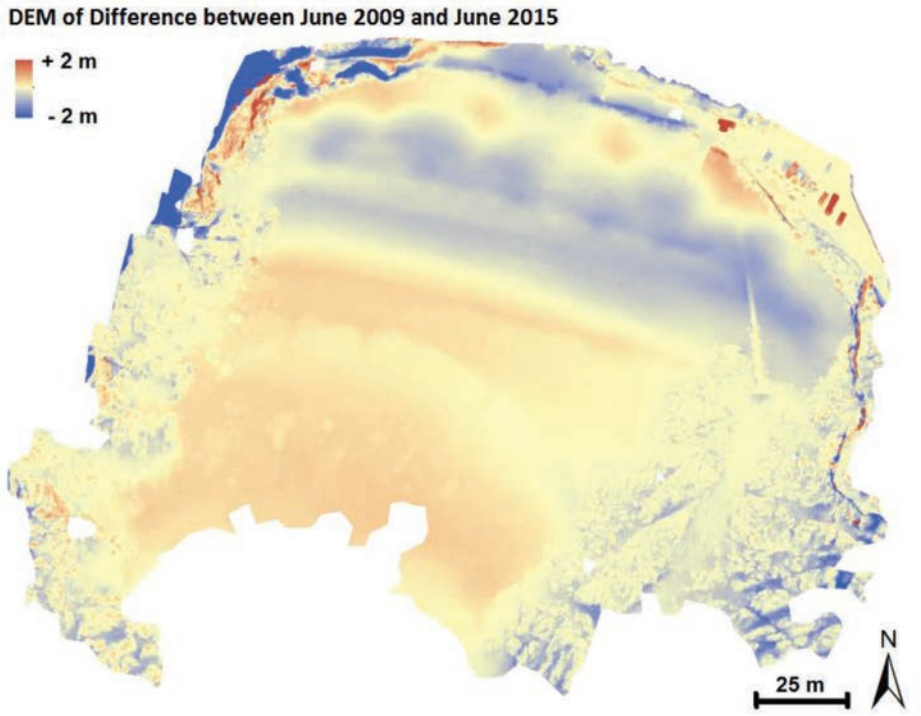

Figure 5: Example of DEM of Difference made from photogrammetric DEM representing the evolution of the beach of Porsmilin between June 2009 and June 2015

This drone has already been used in multiple coastal contexts: sandy beaches, pebble beaches (Sillon de Talbert - Pleubian), cliffs (Brittany and Normandy), estuarine mudflats at the mouth of the Seine... Each coastal environment has intrinsic constraints which sometimes require to adapt the methodology of acquisition and / or data processing. As an example, the acquisition of nadir photographs is difficult to adapt to image the vertical face of cliffs. To answer this particular issue, the orientation of the camera is changed so as to capture the cliff face with an angle of 20-30°. But this also imposes constraints on the definition of the flight plan which can no longer be managed by the autopilot. Similarly, mudflats are an extremely demanding environment. Moving over the site being extremely complex, installation and measurement of targets should be made at the minimum. Once more, changing the acquisition strategy and flight plan, the impact of the limited number of targets can be minimized.

Figure 6: Performing UAV surveys in different coastal environments: (a) estuarine mudflat, (b) pebble beach, (c) cliff, (d) sandy beach

6 - Conclusions

The booming of drones encourages the industry to miniaturize most of their sensors. In parallel, new UAV platforms are being developed, seeking to improve their payload capacity or autonomy in flight. Thus, new opportunities are offered to scientists and new kinds of measurements gradually complete photographic surveys: thermal measurements, LiDAR, etc.

Drone potential is still increasing with the development of light and compact hyperspectral cameras, which can be installed on-board UAV. Hyperspectral measurements provide access to water column parameters, bathymetry inversion, detection of pollution, benthic habitats classification, etc.

Natural escapes of oil in sedimentary basins: spaceborne recognition and pairing with seafloor and sub-seafloor features

R. Jatiault, Total

Introduction

Natural seepage of oil occurs in most of worldwide sedimentary basins, in petroliferous basins (Fig.1). Hydrocarbons are generated from both biogenic processes associated to burial diagenesis which produces light gas (methane) and thermocatalytic processes which produces heavier hydrocarbon, potentially oils.

In case of insufficient cap rock efficiency, stocked hydrocarbons among petroleum reservoirs migrate through the sedimentary series, using fault bypass systems or stratigraphic discontinuities to be subsequently naturally released from the seafloor. It is estimated that an amount of 600 000 tons of hydrocarbons are expelled each year over the world, including biogenic and thermogenic seeps, bounded by uncertainties of 200 000 tons (Wilson et al., 1973). The release of hydrocarbon from the seafloor typically expressed as pockmark erosive features, which are conical-like seafloor depressions associated with contemporary focused fluid flow (King and McLean., 1970).

Most spectacular seeping province account for the Gulf of Mexico and South Caspian Sea where hundreds of recurrent oil seeps were revealed from the analysis of space borne SAR imagery (Zatyagalova et al., 2007, Garcia-Pineda et al., 2010).

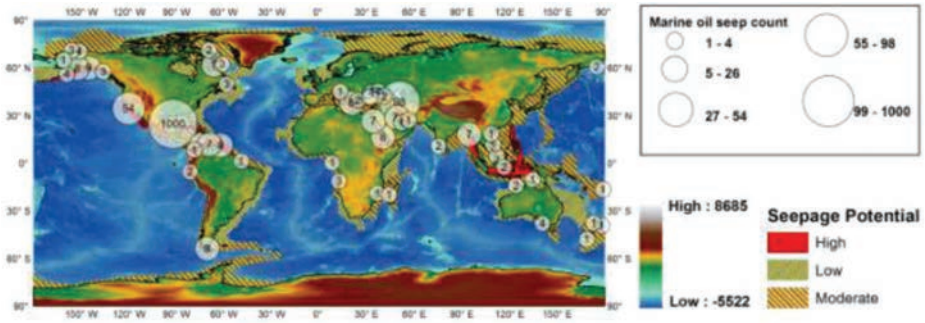

Figure 1: Inventory of published locations of natural occurrence of oil seeps. Superimposed with seepage potential estimated from geological context (Wilson et al., 1973); in dashed yellow are low potential provinces and in dashed orange and red are moderate to high potential seepage provinces

In complement to these areas, the Congo Delta is considered as an active petroleum province where geophysical investigations of the seafloor allowed the recognition of high density fluid flow features (Gay et al., 2003; Andresen et al., 2011; Andresen and Huuse, 2011) with a probable thermogenic origin (Andresen 2012; Anka et al., 2013).

In the case of oil escapes, buoyant hydrocarbons migrate through the water column towards the sea surface while heavier matter remains stocked on the seafloor (Va-

lentine et al.,2010; Keller et al., 2010). Depending on surface current strength, oil droplets are horizontally deflected toward their surfacing impact area at the sea surface while rising through the water column. Understanding the pathways of oil droplets is compulsory to identify the seafloor origin of leaking oils.

The objectives of this presentation are to show the efficiency of SAR data to understand seepage situation in the Lower Congo Basin, to present the methodology used to identify recurrent oil slicks and the limitation of the technique. In addition, this paper integrates measurement of underwater currents assessed from ADCP mooring point to understand the migration pathway of oil droplet and the behavior of oil plume when rising through the water column. Finally, the integration of surface slicks, current measurements and seafloor expression of fluid flow will allow pairing seafloor seeps to sea surface oil slicks.

1 - -Datasets and methods

1.1 - Data

Spaceborne tools to detect seeping hydrocarbons

Synthetic Aperture Radar (SAR) is sensitive to capillary waves of cm scale induced by the local wind at the sea surface (Franceschetti et al., 2002; McCandless and Jackson, 2003). Oil surfactants smooth the sea surface and significantly reduce capillary waves which triggers a contrast in roughness between oily covered areas and free water. Sea surface dampening may be induced by a large inventory of look-alike seep features, for instance bioturbation threadlike films (Gade et al., 1998; Espedal and Johannessen., 2000) or low wind conditions (Espedal and Wahl., 1999). Petroleum platforms or boats spills induce significant pitfalls (Johannessen et al., 2000; Trivero and Biamino., 2010; Leifer et al., 2012). Anthropogenic activities were discarded from the location of boats or platforms as they appear as shinny diffracting points on SAR data.

We used a large collection of overlapping SAR scenes in order to identify the location of recurrent oil seeps. Archive data acquired from 1994 to 2012 were used to detect recurrent oil slicks and afterward to identify the sea surface location of natural oil seepage. The dataset is mainly composed of Envisat ASAR (Advanced Synthetic Aperture Radar) scenes acquired between 2002 and 2012 by 3 the European Space Agency. Envisat ASAR operates in C-Band with an Image Mode Precision (IMP) and a Wide Swath Mode (WSM) (Table 1). We complemented our dataset with both C-band Radarsat, ERS (1 and 2) data and X-band Cosmo-Skymed (2009 - 2014) data. Once stacked, the coverage density of the SAR data reached about 150 scenes (Fig.2).

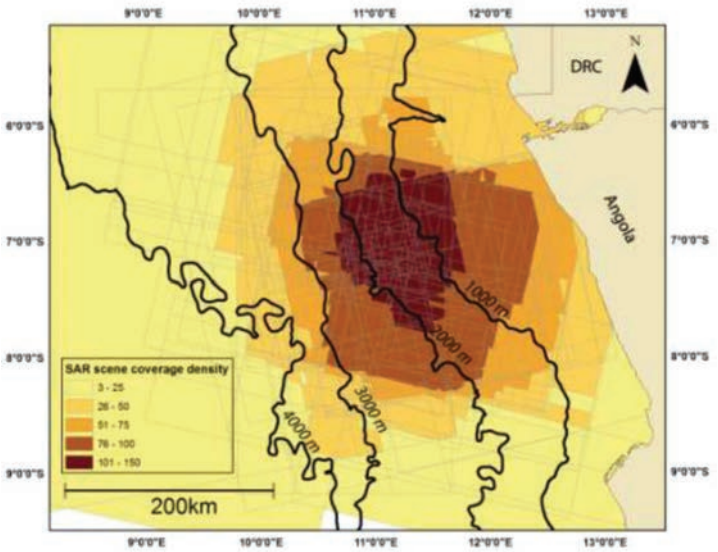

Figure 2: Stack of SAR data coverage used to identify recurrent natural seepage slicks

Assessment of current velocity across the water column

The current velocity was measured from ADCP (Acoustic Doppler Current Velocity) tools which use particle displacement to determine current speed (Rowe and Yound 1979, Gordon and RDI, 1996). The data were collected during 6 months of mooring between January 2009 and July 2009 and provide measurements of current orientation and velocity along a mooring line from a series of 62 sensors across the water column. The water depth of the seafloor is about 1800m below sea level.

Imaging sedimentary series using petroleum exploration data

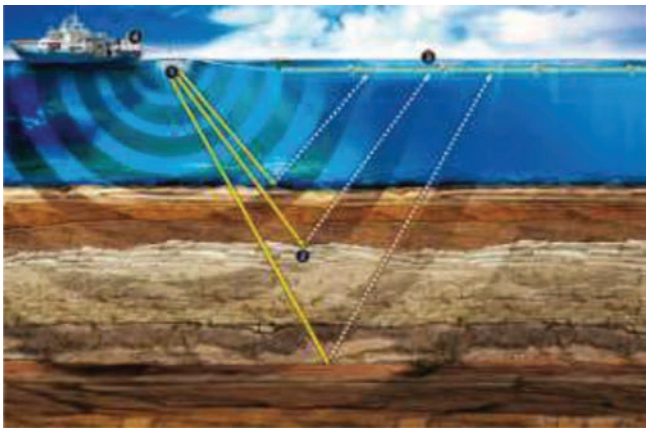

Figure 3: Principle of acoustic wave propagation for imaging sedimentary series in the marine environment (extracted from www.sercel.com)

Seismic data are widely used in petroleum companies in both onshore and offshore domains. In the marine environment, air guns send acoustic waves from the sea surface that propagate through the water column and sedimentary series. Stratigraphic unconformities trigger a contrast in impedance which reflects acoustic waves towards the sea surface. Geophysical sensors are deployed at the sea surface along streamers and record propagation times of reflected waves to estimate the vertical distance of stratigraphic reflectors (Fig.3). The method was developed during the 19s by Schlumberger and is now extensively used as an exploration tool for petroleum companies as it provides a remote imaging technique of seafloor and sub-seafloor conditions.

1.2 - Methods

Because of its sensitivity to centimeter wavelengths of the surface roughness (e.g., MacCandless and Jackson, 2003), Synthetic Aperture Radar (SAR) is a remotely operated tool widely used in ocean studies for the recognition of sea surface patterns and more particularly for the detection of liquid hydrocarbons. The presence of oil surfactants dampens the sea surface and significantly reduces the amount of energy backscattered to the satellite (Fresnel specular reflection - Fig.4) compared to the surrounding free water. Sea surface covered by oil seepage appears as black streaks on SAR images (Johannessen et al., 2000; Espedal and Johannessen, 2000; Williams and Lawrence, 2002; Ivanov et al., 2007; Zatyagalova et al., 2007; Garcia-Pineda et al., 2009; Körber et al., 2014).

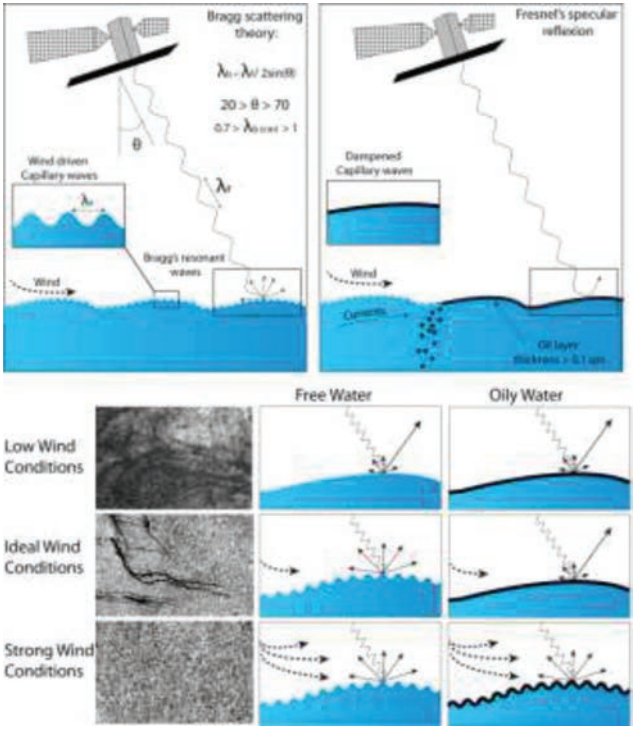

Figure 4: Identification of floating oil at the sea surface using spaceborne SAR

As the sea surface, the shape of natural oil slicks is induced by the strength and orientation of the wind and surface currents (Espedal and Wahl, 1999). Wind and surface currents induce short-term variations of the sea surface dynamics. The sinuosity of black patterns is a first order criterion to detect oil content slicks (Fig. 4). Sharp radiometric values contrast between oil-covered areas and free water corresponds to the sideward detectable edge of the slicks and can be used to identify the extent of individual seepage slicks (see examples in Fig.4).

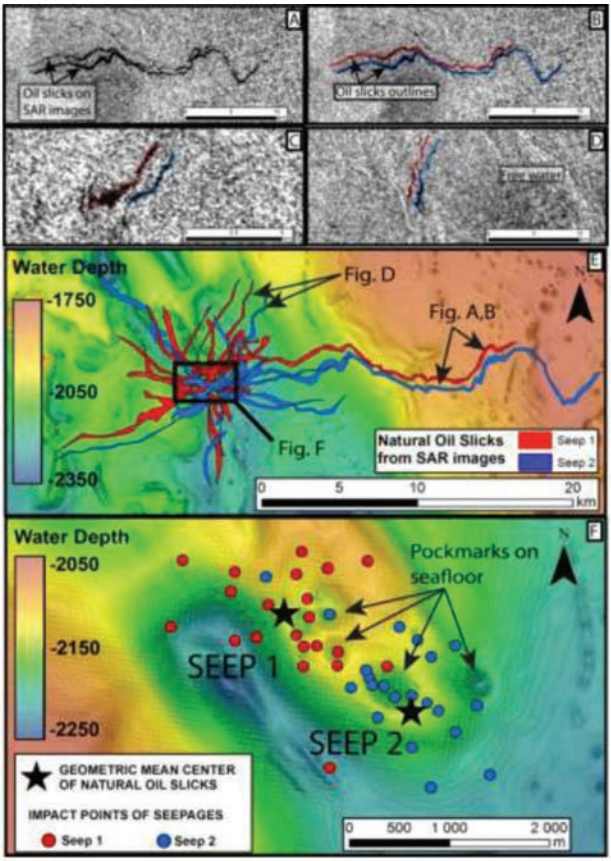

Figure 5: Extract from ASAR WSM SAR scene dated of 26/03/2012. Grey speckled background represents backscattered energy from sea surface free water. Black streaks depict the location of seepage slicks. B. Same SAR image extract complemented with manual picking. C and D. ASAR WSM SAR sub-scenes dated of respectively 25/02/2012 and 07/12/2002 superimposed with manual picking of oil slicks. The three different SAR extracts overlap at a common spatial location. Black arrows show the direction flow of surface currents during SAR scene acquisition. E. Compilation map of oil slicks outline mapped from the entire dataset, including slicks displayed in A., B., C. and D. at two major seeping sites. All scenes are provided by the European Spatial Agency (ESA). In superposition with seafloor data measured with multibeam echosounder at 12.5m resolution. F. Zoom at the location of seeping area revealing seafloor erosive features (pockmarks). Colored dots are Oil Slicks Origin (OSO – Garcia-Pineda et al., 2009). Black stars are computed from the centroid of individual OSO

Once mapped, diverging black streaks evidence active seeping areas of thermogenic fluids (Zatyagalova et al., 2007; Garcia-Pineda et al., 2014; Körber et al., 2014). The center of each diverging structure corresponds to the probable impact area of the fresher oil droplets at the sea surface.

2 - Results

2.1 - Oil slick mapping

A total of 1400 interpreted oil slicks were mapped from the analysis of the 82 SAR data over 18 years. The integration of IHS database and recognition of diffracting point associated to the boat or platform location allowed about 200 slicks associated to anthropogenic activities to be remove. The remaining 1400 seepage slicks are displayed in Fig.5 A. Among them, 1240 or 90% of the slicks are recurrent, forming diverging patterns on the compilation map. The length of the slicks varies from a few hundred meters up to 80 km. We recognized 102 active oil seep sites whose geometric mean centres are associated with active seep zones, displayed in coloured dots in Fig.5 B. The water depth of the seeping provinces ranges roughly from 1100 to 2600 m and they are 130 km to 200 km distant from the Angolan coastline. Active seep sites are distributed all along the southern part of the Congo Basin over an area of 21,000 km².

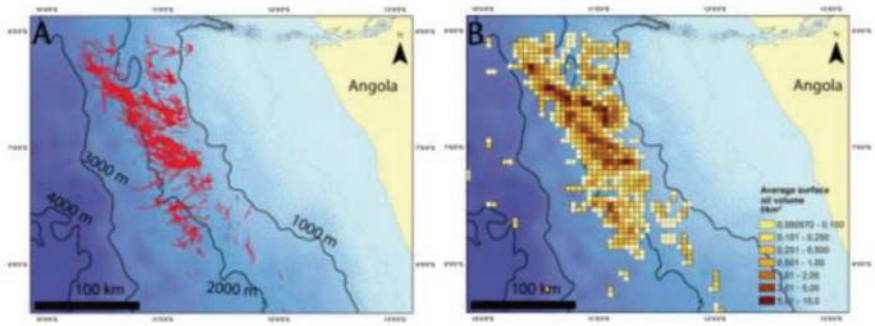

Figure 6: A. Compilation map of the outline of sea surface slicks (red polygons) mapped from the analysis of SAR scene collection. B. Average volume of sea surface oil during the long term monitoring gridded by square cells of 5 km²

The volume of oil was computed from the amount of detected oil from the analysis of overlapping scenes normalized to the coverage density of the SAR stack. The addition of each cell across the basin suggests that an average of 1625 liters of oil is currently surfacing the ocean surface. This volume was computed considering a random slick thickness of 0.145 um, estimated from in-situ measurements in the Gulf of Mexico and based on the Bonn Agreements. We estimated that the amount of expelled oil from natural seeps is about 4400 m³ each year.

2.2 - Oil migration pathways and horizontal deflection

Oil droplets are horizontally deflected from their seafloor source point towards the surfacing area while rising through the water column. The deflection value is controlled

by underwater current strength. In order to quantify the horizontal deflection during SAR acquisition we ordered SAR scenes during ADCP measurements.

The integration of ADCP data allowed interval values to be computed. The summation in direction and distance among each interval allowed the horizontal deflection during the SAR acquisition to be quantified.

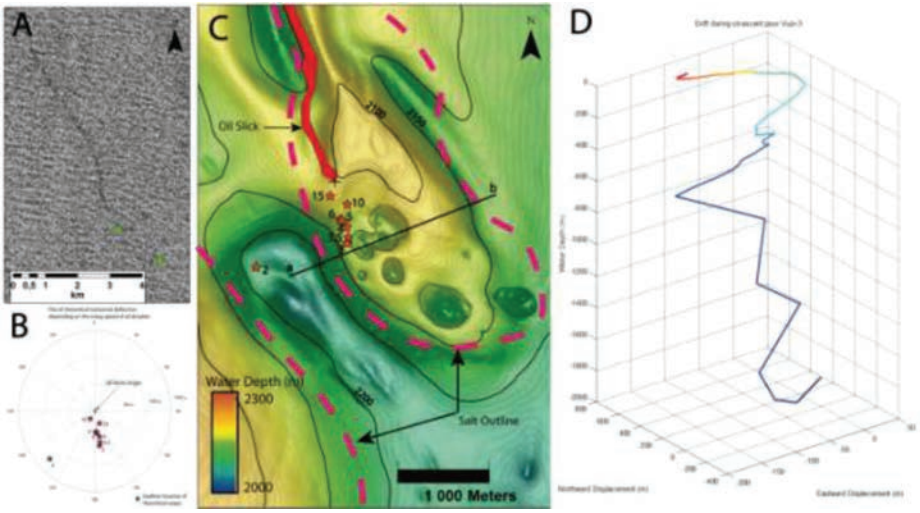

Figure 7: A. Extract of SAR scene dated from the 30/06/2009 allowing the recognition of oil surface covered areas (black patches). Green points are two centroids of OSO. B: Backward modeling of theoretical deflection (m) from sea surface OSO to seafloor seep. Computed for different rising speeds between 2 to 15 cm/s (labeled next to red stars) by integrating ADCP data measurements (15 km from seeping area). C: Seafloor map (isochron superimposed with dip map) in addition to the oil slick location (Fig. 9A), salt outline (extracted from 3D seismic) and backward deflections with different rising speeds. Best fit between seafloor pockmark location and sea surface slicks is obtained for a rising speed of 3 cm/s across the water column. D: Theoretical migration pathway of oil droplet through the water column from seafloor source to the seepage slicks surfacing point (rising speed of 3 cm/s)

The mooring area is located 15 km westward from a major seeping area recognized for the interpretation of SAR collection. We considered the location as the sea surface impact area of the seepage slick, namely the Oil Slick Origin (Garcia-Pineda et al., 2009) to preserve deflection within the water column, freely from sea surface drift. The slicks detected on 30/06/2009 (Fig.7) lie over an area previously recognized for a high seepage activity (Seep 1 in Fig.5).

First of all, Fig.7B shows that the horizontal deflection value remains low compared to the water depth. Considering a uniform rising speed across the water column, a slow rising speed of 2 cm/s produces a deflection value below 1500m.

The seafloor origin is well identifiable from seafloor and sub-seafloor data. The analysis of seafloor features reveal conical-like pockmarks typical of natural fluid seeps (Fig. 7 C).

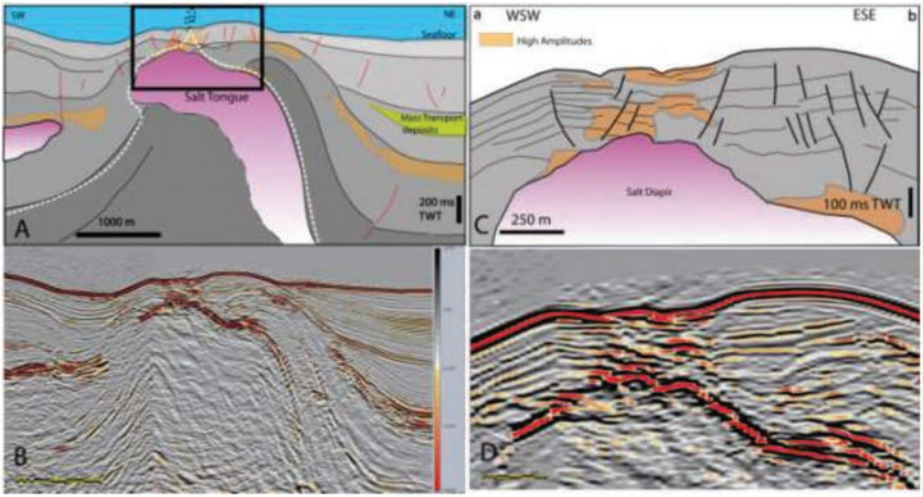

Figure 8: A, B: Line drawing and wide seismic cross section through underlying sedimentary series at the location of the seeping site. White dashed line represents the probable migration pathways. C and D: Line drawing and seismic section focus at shallower depths allowing the recognition of high amplitudes on seismic section, fault network, salt diapirs

The analysis of underlying geophysical profiles shows that the active pockmark is located at the rim of evaporitic diapirs (mainly composed of Halite, Gypsum,…), which is known to create efficient migration pathways for migrating oils towards the seafloor in the area, at the sedimentary/evaporitic interface (Gay et al., 2007, Andresen et al., 2012, Serié et al., 2016). In addition, hydrocarbon seeps are usually associated with high impedance patches close to the seafloor. The anaerobic oxidation of methane creates hardground authigenic carbonates (Hovland et al., 1987) which are reflective series on seismic section and typical of hydrocarbon seepage systems. Fig.8 shows the location of the salt diapir, seafloor pockmark and migration chimney made of carbonates. These characteristics suggest that the pockmark is obviously hydrocarbon active and the origin of expelled oil.

The theoretical deflection value computed for high rising speeds of 15 cm/s projected on the seafloor locate far for any seafloor seeps manifestations. The progressive decrease of rising speeds brings the theoretical location closer to seafloor seeps (Fig.7.C). The best correlation between the observed and computed location of fluid source gas for a rising speed of 3 cm/s for migration pathways is displayed in Fig.7.D.

The modeled migration profile suggests distinctive water mass units with reverse direction. The horizontal deflection resulting from the addition of opposite currents expressed through a low horizontal deflection.

Garcia-Pineda et al. (2009) established a linear relationship between the water column and horizontal deflection offset of oil droplets in the Gulf of Mexico. The hydrodynamics of the Lower Congo Basin might be inflected by a reverse current component which produces a restricted horizontal deflection and surfacing area of oil droplets.

3 - Conclusion

Natural oil seepage is recurrent processes whose seepage slick signal can be followed on overlapping SAR scenes. The work presented here gives a first order assessment of oil plume behavior in the water column. The association of surface slicks and seafloor pockmarks was successfully performed with the integration of current measurements across the water column. Integration of ADCP data also shows that horizontal deflection remains low compared to the great water depth value. In comparison to anthropogenic spills, natural seeps are recurrent processes which potentially allows the plume behavior to be studied over a consistent period. The integration of an extended collection of SAR data during the mooring period is necessary to validate oil droplets behavior across the water column. This should help to monitor oil seepage affected regions and understand horizontal deflection over longer periods. Studies of natural seepage complement the evaluation of oil/gas plume behavior from accidental spills and could also help regarding the emergency response.

References

Andresen, K.J., Huuse, M., Shödt., N.H., Clausen, F., Seidler, L. (2010), Hydrocarbon plumbing systems of salt minibasins offshore Angola revealed by three-dimensional seismic analysis, *AAPG Bulletin, 95*, 1039-1065, http://dx.doi.org/10.1306/12131010046

Andresen K.J., Huuse, M. (2011), 'Bulls-eye' and polygonal faulting in the Lower Congo Basin: Relative timing and implications for fluid expulsion during shallow burial, Marine Geology 279, 111-127, http://dx.doi.org/ 10.1016/j.margeo.2010.10.016

Andresen, K.J. (2012), Fluid flow features in hydrocarbon plumbing systems: What do they tell us about the basin evolution, *Marine Geology, 332-334*, 89-108, http://dx.doi.org/10.1016/j.margeo.2012.07.006

Anka, Z., Ondrak, R., Kowitz, A., Schodt, N. (2013), Identification and numerical modeling of hydrocarbon leakage in the Lower Congo Basin: Implications on the genesis ok km-wide seafloor mounded structures, Tectonophysics, 604, 153-171, http://dx.doi.org/10.1016/j.tecto.2012.11.020

Espedal, H.A., Wahl, T. (1999), Satellite SAR oil spill detection using wind history information, *International Journal of Remote Sensing, vol. 20*, 49-65

Espedal, H.A., Johannessen, O.M. (2000), Detection of oil spills near offshore installations using synthetic aperture radar (SAR), *International Journal of Remote Sensing, 21:11*, 2141-2144, http://dx.doi.org/10.1080/01431160050029468

Franceschetti, G., Iodice, A., Riccio, D., Ruello, G. Siviero, R., SAR Raw Signal Simulation of Oil Slicks in Ocean Environments, IEEE TRANSACTIONS ON GEOSCIENCE AND REMOTE SENSING, VOL. 40, NO. 9

Gade, M., Alpers, W. (1998), Imaging of biogenic and anthropogenic ocean surface films by the multifrequency/ multipolarization SIR-C/X-SAR, *Journal of Geophysical Research, 103,* 18851-18866.

Garcia-Pineda, O., Zimmer, B., Howard, M., Pichel, P., Li, X., MacDonald, I.R. (2009), Using SAR

images to delineate ocean oil slicks with a texture-classifying neural network algorithm (TCNNA), *Canadian journal of Remote Sensing, 35,* 411-421.

Garcia-Pineda, O., MacDonald, I., Zimmer, B., Shedd, B., Roberts, H., (2010), Remote-sensing evaluation of geophysical anomaly sites in the outer continental slope, northern Gulf of Mexico, *Deep-Sea research II 57,* 1859-1869, http://dx.doi.org/10.1016/j.dsr2.2010.05.005

Gay, A., Lopez, M., Cochonat, P., Sultan, N., Cauquil, E., Brigaud, F. (2003). Sinuous pockmark belt as indicator of a shallow buried turbiditic channel on the lower slope of the Congo Basin, West African Margin. In: Van Rensbergen, P., Hillis, R.R., Maltman, A.J., Morley, C.K., *Subsurface Sediment Mobilization, Geological Society of London, Special Publications, vol. 216,* 173–189.

Gordon, R. L., & Instruments, R. D. (1996). Principles of operation a practical primer. RD Instruments, San Diego.

Hovland, M., Talbot, M.R., Qvale, H., Olaussen, S., Assberg, L., (1987), Methane-related carbonate cements in pockmarks of the North Sea, *Journal of Sedimentary Petrology, 57:5,* 881 - 892

Ivanov, A.Y., Gobulov, B.N., Zatyagalova, B.B. (2007), On oil and gas seeps and underground fluid discharges in the Southern Caspian based on Space Radar Data, *Earth Exploration from Space, 2,* 62-81

Johannessen.,O. M., Sandven, M., Jenkins, A. D., Durand, D., Petterson, L. H., Espedal, H., Evensen, G., Hamre, T. (2000), Satellite earth observation in operational oceanography, *Coastal Engineering, 41,* 155-176.

Körber, J.H., Sahling, H., Pape, T., dos Santos Fereira, C., MacDonald, I., Bohrmann, G. (2014), Natural oil seepage at Kobuleti Ridge, eastern Black Sea. *Marine and Petroleum Geology, 50,* 68- 82, http://dx.doi.org/10.1016/j.marpetgeo.2013.11.007.

King, L.H., MacLean, B., Pockmark on the Scotian Shelf (1970), *Geological Society of America Bulletin,* V.81, P.3141-3148

Leifer, I., Lehr, W.J., Simecek-Beatty, D., Bradley, E., Clark, R;, Dennison, P., Hu, Y, Matheson, S., Jones, C.E., Holt, B., Reif, M., Roberts, D.A., Svejkovsky, J., Swayze, G., Wozencraft, J. (2012), State of the art satellite and airborne marine oil spill remote sensing: Application to the BP Deepwater Horizon oil spill, *Remote Sensing of Environment, 124,* 185-209, http://dx.doi.org/10.1016/j.rse.2012.03.024

McCandless,S.W., Jackson, C.R. (2003), Principles of Synthetic Aperture Radar in *Synthetic Aperture Radar Marine User's Manual, 1-24*.

Rowe, F. and J. Young (1979) An ocean current profiler using Doppler sonar, Oceans '79 Proceedings.

Serié, C., Huuse, M., Schødt, N. H., Brooks, J. M., & Williams, A. (2016). Subsurface fluid flow in the deep-water Kwanza Basin, offshore Angola. Basin Research.

Trivero, P., Biamino, W. (2010), Observing marine pollution with Synthetic Aperture Radar, Observing marine pollution with Synthetic Aperture Radar, *Geosciences and Remote Sensing, New Achievements*.

Williams, A. and Lawrence, G. (2002), The Role of Satellite Seep Detection in exploring the South Atlantic's Ultradeep Water, in Surface exploration case histories: Applications of geochemistry, magnetic, and remote sensing, , D. Shumacher and L. A. LeSchack, eds., *AAPG Studies*

in geology No. 48 and SEG Geophysical References Series No. 11, 327-344.

Wilson, R. D., Monaghan, P.H., Osanik, A., Price, L., C., Rogers, M. A. (1973), Estimate of Annual input of Petroleum to the Marine Environment from Natural Marine Seepage. *Trans. Gulf Coast Assoc. Geological Societies, 23,* 182-193.

Zatyagalova, V.V., Ivanov, A.Y., Gobulov, B.N. (2007), Application of Envisat SAR imagery for mapping and estimation of natural oil seeps in the South Caspian Sea. In *Proceedings of the Envisat Symposium 2007,* 23 – 27.

Cedre • 715 rue Alain Colas • CS 41836 • 29218 BREST CEDEX 2 • FRANCE
Tel.: +33 (0)2 98 33 10 10 • Fax: +33 (0)2 98 33 10 10
contact@cedre.fr • www.cedre.fr

ISBN
978-2-87893-124-2